Molecular and behavioral analysis of magneto-aerotaxis in *Magnetospirillum gryphiswaldense*

Dissertation zur Erlangung des Doktorgrades

der Fakultät für Biologie

der Ludwig-Maximilians-Universität München

vorgelegt von

Felix Popp

aus Wolfsburg

München, Juli 2015

1. Gutachter: Prof. Dr. Dirk Schüler (Universität Bayreuth)

2. Gutachter: Prof Dr. Heinrich Jung (Ludwig-Maximilians-Universität München)

Tag der Abgabe: 08.07.2015

Tag der mündlichen Prüfung: 22.10.2015

CONTENTS

PUBLICATIONS AND DECLARATION OF CONTRIBUTIONS

Publication 1

Popp F., Armitage J., and Schüler D.

Polarity of bacterial magnetotaxis is controlled by aerotaxis through a common sensory pathway.

Nat. Commun. 5:5398 doi: 10.1038/ncomms6398 (2014).

F.P., J.P.A. and D.S. designed research; F.P. performed research; F.P., D.S. and J.P.A. analysed data; F.P., D.S., and J.P.A. wrote the paper.

Publication 2

Borg S.*, Popp F. *, Hofmann J., Rothbauer U., Leonhardt H., and Schüler D.

An intracellular nanotrap re-directs proteins and organelles in live bacteria.

mBio 6(1):e02117-14. doi:10.1128/mBio.02117-14 (2015).

* These authors contributed equally to this study.

S.B., F.P., and D.S. designed the research; F.P., S.B. and J.H. constructed the mutant strains; S.B. and F.P. performed experiments; F.P. analysed motility behavior and conducted chemotaxis assays; S.B., F.P., and D.S. analysed the data; S.B., F.P., and D.S. wrote the paper.

I hereby confirm the above statements:

Felix Popp Dr. Sarah Borg Prof. Dirk Schüler

ABBREVIATIONS

aer $^{+/-}$	Aerotactic phenotype
B	Ambient magnetic field
$\mathbf{B_{geo}}$	Geomagnetic field
C polarity	Cellular polarity
CCW	Counterclockwise
CHAP	Chain analysis program
CheOp	Chemotaxis operon
CM	Cytoplasmic membrane
CW	Clockwise
fps	Frames per second
GBP	GFP-binding protein
GFP	Green fluorescent protein
m	Magnetic dipole moment
M polarity	Magnetic polarity
mag $^{+/-}$	Magnetic phenotype
MCP	Methyl-accepting chemotaxis protein
MMP	Multicellular magnetotactic prokaryote
MTB	Magnetotactic bacteria
NS	North-seeking
OATZ	Oxic anoxic transition zone
PB_{ind}	Polarity bias of individual cells
PB_{pop}	Mean polarity bias of the population
PCR	Polymerase chain reaction
pol $^{+/-}$	Swimminng polarity phenotype
RBP	RFP-binding protein
REC	Response regulator receiver
RFP	Red fluorescent protein
SS	South-seeking
TEM	Transmission electron microscope
WT	Wild type

SUMMARY

Magnetotactic bacteria (MTB) contain nanometer-sized crystals of a magnetic iron mineral enabling directed swimming along geomagnetic field lines. However, although this unique behavior was discovered already 40 years ago, it still has remained poorly understood at the cellular level and the molecular mechanisms responsible for sensing environmental stimuli and transducing signals to the flagellar motors have been unknown. Therefore, the major goal of this thesis was to investigate the swimming behavior of *Magnetospirillum gryphiswaldense* both at the behavioral and molecular level.

Individual motors of tethered *M. gryphiswaldense* cells were found to rotate both clockwise and counterclockwise with equal speed. Cells swam at speeds of up to 60 µm s^{-1} and commonly displayed runs of several hundred µm in length. In striking contrast to *E. coli*, which reorients the cell body between run intervals at random angles, motor switching events caused swimming reversals with reorientation angles close to 180°.

The sensory repertoire of *M. gryphiswaldense* was analyzed by classical macroscopic chemotaxis assays, and aerotaxis was found to be the dominant behavior. In addition to the strong microaerophilic response in oxygen gradients, I observed tactic bands also under anoxic conditions within gradients of the alternative electron acceptor nitrate, suggesting that aerotaxis is part of a general redox or energy taxis mechanism.

The aerotactic response of *M. gryphiswaldense* was furthermore analyzed by recording and tracking single cells under controlled atmospheric conditions in a gas perfusion chamber. Compared to other well-studied bacteria, *M. gryphiswaldense* displayed unusually low swimming reversal rates (<0.1 s^{-1}) under equilibrium conditions. Abruptly shifting oxygen levels from 2% to 0% only slightly increased reversal rates, whereas a reverse shift from 0% to 2% caused a transient threefold increase in reversal rates that was directly followed by an extraordinarily sustained smooth-swimming phase without return to pre-stimulus levels.

Apart from 56 putative genes encoding chemoreceptors that might be involved in magnetotaxis, four putative chemotaxis operons (*cheOp1-4*) were identified in the genome of *M. gryphiswaldense*, containing genes commonly involved in signal transduction from chemoreceptors to the flagellar motors. Single or combined deletions of *cheOp2-4* did not have any pronounced effect on motility or aerotaxis. In striking contrast, deletion of *cheOp1*, which comprises only the

canonical set of chemotaxis genes (*cheAWYBR*), caused individual cells to swim straight without reversing, resulting in a complete loss of aerotaxis.

When analyzed under oxic conditions, most MTB possess a clear directional preference corresponding to downward movement in their natural habitat, referred to as "polar magneto-aerotaxis". Although cultivated strains of magnetotactic spirilla were previously assumed to lack any directional preference, in this work polar swimming behavior could be restored in *M. gryphiswaldense* through repeated cultivation of cells in magnetic fields superimposed on oxygen gradients. Individual cells displayed a gradual bias of swimming runs with one of the cell poles leading that depended on ambient oxygen levels. In anoxic microdroplets, addition of 2% oxygen rapidly reversed the overall swimming direction of the entire population. However, in the absence of CheOp1 swimming polarity could be no longer selected and no reversal of swimming bias was observed. These findings for the first time show that there is a direct molecular link between aerotactic sensing and the determination of magnetotactic polarity, through the sensory pathway CheOp1.

In a joint project in the last part of this thesis, I demonstrated how magnetotactic behavior can be manipulated through artificial recruitment of polarly localized $CheW_1$-GFP fusion proteins to midcell anchors. GFP-labelled proteins were trapped by expressing GFP-binding nanobodies on the magnetosome membrane surface (referred to as "nanotrap"). By varying the expression level of the nanobody, a gradual knockdown of magneto-aerotaxis was achieved.

ZUSAMMENFASSUNG

Magnetotaktische Bakterien (MTB) enthalten wenige Nanometer große Kristalle magnetischer Eisenminerale, die ihnen die faszinierende Fähigkeit verleihen, sich entlang der Feldlinien des Erdmagnetfelds fortzubewegen. Obwohl diese besondere Form bakteriellen Schwimmverhaltens bereits vor nunmehr 4 Jahrzenten entdeckt wurde, ist das Verhalten einzelner Zellen, sowie die Mechanismen, die der Reizerkennung und Signaltransduktion zum Flagellenmotor zugrunde liegen, bis heute nur wenig erforscht. Das Ziel dieser Doktorarbeit war daher, die molekularen Grundlagen der Magnetotaxis im Modellorganismus *Magnetospirillum gryphiswaldense* zu charakterisieren und die Motilität einzelner Zellen detailliert zu untersuchen.

Im ersten Teil meiner Arbeit konnte ich zeigen, dass die Flagellenmotoren von *M. gryphiswaldense* jeweils mit gleicher Geschwindigkeit in beide Drehrichtungen rotieren und dadurch die Zellen auf bis zu 60 µm s^{-1} beschleunigen. Im Gegensatz zu *E. coli*, das während häufiger Taumelphasen seine Ausrichtung ändert, werden die oft mehrere hundert Mikrometer langen, geraden Schwimmepisoden von *M. gryphiswaldense* durch Umkehrvorgänge unterbrochen, die eine Änderung der Schwimmrichtung um ca. 180° bewirken.

Bei der Untersuchung des allgemeinen chemotaktischen Verhaltens in makroskopischen Tests zeigte sich, dass die mikroaerophile Antwort von *M. gryphiswaldense* stark dominiert. Da unter Ausschluss von Sauerstoff zudem Bandenbildung in künstlich hergestellten Nitratgradienten beobachtet wurde, kann davon ausgegangen werden, dass das dominante aerotaktische Verhalten Teil einer umfassenderen Redox- oder Energietaxis ist.

Die Aerotaxis von *M. gryphiswaldense* wurde anschließend unter kontrollierten atmosphärischen Bedingungen auf Einzelzellebene untersucht. Im Vergleich zu anderen gut erforschten Bakterien wurden unter Gleichgewichtsbedingungen nur relativ wenige Umkehrvorgänge registriert (<0.1 s^{-1}), und ein abruptes Absenken des Sauerstoffgehalts von 2% auf 0% führte zu einer lediglich geringen Zunahme der Umkehrvorgänge. Nach einer plötzlichen Anhebung des Sauerstoffgehalts von 0% auf 2% stieg dagegen die Umkehrfrequenz kurzzeitig um das Dreifache an. Im Anschluss hieran wurden jedoch bemerkenswerterweise über lange Zeiträume fast keine Umkehrvorgänge registriert und selbst nach 80 s lag die Umkehrfrequenz unter dem Ausgangswert.

In der genomischen Sequenz von *M. gryphiswaldense* wurden neben 56 Chemorezeptor-Genen insbesondere vier mutmaßliche Chemotaxisoperons (*cheOp1-4*) identifiziert. Während die Deletion von *cheOp2-4* (sowohl einzeln als auch in Kombination) keinen deutlichen Einfluss auf das Schwimmverhalten hatte, wurde nach Deletion von *cheOp1* ein komplett nicht-aerotaktischer Phänotyp beobachtet, gekennzeichnet durch lange, ununterbrochene Schwimmepisoden.

Unter sauerstoffgesättigten Bedingungen weisen die meisten MTB eine klare Richtungspräferenz auf, sogenanntes „polares Schwimmverhalten". Obwohl den in Reinkultur verfügbaren Magnetospirillen diese Fähigkeit traditionell abgesprochen wurde, konnte im Rahmen der vorliegenden Arbeit durch wiederholte Kultivierung von *M. gryphiswaldense* in Sauerstoffgradienten, die von Magnetfeldern überlagert waren, polares Verhalten erzeugt werden. Die Mehrzahl der Zellen wies eine graduelle Bevorzugung einer Schwimmrichtung auf, die sich durch Variation des Sauerstoffgehalts beeinflussen ließ. Dies wurde durch Beobachtungen an zunächst anaerobisierten Zellpopulationen untermauert, die bei Zuführung von 2% Sauerstoff kollektiv ihre Vorzugsschwimmrichtung änderten. Nach Deletion von *cheOp1* wurde im Gegensatz dazu keine Wiederherstellung der Schwimmpolarität beobachtet, was den Schluss nahe legt, dass ein direkter Zusammenhang zwischen der durch *cheOp1* kodierten Signaltransduktionskaskade und der molekularen Determination der magnetotaktischen Polarität existiert.

Im letzten Abschnitt dieser Arbeit konnte ich im Rahmen eines Kooperationsprojekt zeigen, wie durch Expression von GFP-bindenden *nanobodies* auf der Magnetosomenoberfläche die native Lokalisierung von GFP-markierten Signaltransduktionskomponenten künstlich verändert wird. Durch Variation der Kopienzahl des *nanobodies* wurde das $CheW_1$-GFP Fusionsprotein in unterschiedlichem Umfang zur Zellmitte verschoben, was einen graduellen Ausfall der Magneto-Aerotaxis bewirkte.

1 INTRODUCTION

Bacteria can sense and translate a large variety of internal and external stimuli into cellular responses, comprising not only the regulation of gene expression and developmental programs, but also the active search for environments that are favorable for their survival and growth. It has been known for a long time that many motile bacteria can move in a directed fashion within gradients of attractants and repellents, e.g. gradients of light, oxygen and substrates used as carbon or energy sources (Engelmann 1881; Gest 1995; Pfeffer 1888). More recently, it has become clear that some bacteria also orient themselves within gradients of other environmental cues (like pH, temperature, osmolarity, fluid flow, terminal electron acceptors, and redox potential), the most intriguing mode of navigation being the magnetotaxis displayed by a diverse group of aquatic bacteria.

A magnetic response of bacterial cells was first observed by the Italian scientist Salvatore Bellini in the late 1950s who realized that a fraction of bacteria from sediment samples swam along magnetic field lines (Bellini 2009b; Bellini 2009a). In 1975 Richard Blakemore independently discovered the same type of bacteria (Blakemore 1975) and coined the term magnetotaxis to describe their astonishing swimming behavior. This reflected the fact that apart from their passive alignment the analyzed cells apparently also showed directed movement parallel to the magnetic field vector. Blakemore established that magnetotactic bacteria (MTB) contain intracellular chains of membrane-enveloped iron-rich particles (Blakemore 1975), the so-called magnetosomes, and discovered that these crystal-like inclusions consist of permanently magnetic iron minerals conferring a magnetic moment on the cell (Blakemore et al. 1979; Frankel et al. 1979; Balkwill et al. 1980). This seminal discovery has attracted broad interdisciplinary interest, fostered research on biomineralization processes and even stimulated the investigation of magnetoreception in higher organisms (Kirschvink 1997; Kirschvink et al. 2001; Davila et al. 2003). However, while the mechanisms controlling the biosynthesis of magnetosomes have been broadly investigated in the last decade, there have been only few studies addressing the motility behavior of MTB at the single cell level and the molecular determinants controlling flagellar output have remained unknown. In this thesis, the intriguing aerotactic response of *Magnetospirillum gryphiswaldense* was characterized in detail. For the first time genetic determinants were identified that are essential for both aerotaxis and magnetic swimming polarity.

1.1 Cellular structure and ecology of magnetotactic bacteria

The enrichment of bacteria at the edge of a sample drop that was exposed to the magnetic field of a permanent magnet led to the unexpected discovery of MTB. The underlying alignment of cells to the ambient magnetic field (**B**) is caused by magnetosomes (Fig. 1-1), which are intracellular ferromagnetic iron mineral inclusions that are surrounded by a lipid bilayer derived from the cytoplasmic membrane through invagination (Bazylinski & Frankel 2004; Greene & Komeili 2012). Magnetosomes therefore are viewed as prominent example of a true prokaryotic organelle that is homologous to subcellular compartments found in eukaryotic cells.

Magnetosome nano-crystals consist of either magnetite (Fe_3O_4) or greigite (Fe_3S_4) and the crystal shape can vary significantly between species: besides cuboctahedral crystals mostly found in alphaproteobacteria, elongated prismatic and bullet-shaped crystals can be distinguished, and the occurrence of particles with a particular geometry correlates with the phylogenetic affiliation of the respective bacterium (Lefèvre et al. 2013; Bazylinski & Frankel 2004). The average size of magnetosome crystals (30-120 nm) falls in the range of stable single domain magnetic particles, thereby maximizing the magnetic remanence per crystal volume being mineralized, since smaller crystals lack a stable magnetic moment and bigger crystals harbor multiple interfering magnetic domains. Today it is known that magnetosomes are aligned along an actin-like cytoskeletal filament (Fig. 1-1) and arranged in one or multiple chains along the long axis of the cell body (Jogler & Schüler 2009; Komeili 2012). The spacing between particles in the chain is such that due to magnetic interactions the dipole moments of individual crystals are oriented in parallel. This arrangement enhances the resulting magnetic dipole moment (m) of the entire cell, which is the sum of all individual magnetic moments and is strong enough to align MTB to the geomagnetic field lines like microscopic compass needles (Frankel et al. 2006).

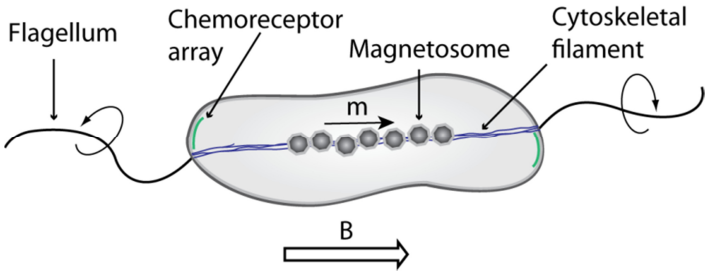

Fig. 1-1 Schematic diagram of a model cell illustrating general cellular characteristics of MTB. Magnetosomes are arranged in a chain along an actin-like cytoskeletal filament (blue). The net magnetic dipole (m) of the magnetosome chain is oriented parallel to the ambient magnetic field (**B**). Chemoreceptors form large supramolecular arrays (green) that are mainly located at the cell poles.

MTB represent a phylogenetically diverse group of bacteria. Although many representatives are notoriously challenging to cultivate, probably due to their complex lifestyle in their natural gradient habitats which are complicated to duplicate in a lab setting, increasing numbers of species have been isolated in axenic culture and many different cell morphologies have been described to date (Lefèvre & Bazylinski 2013). Among them are cocci, vibrios, rods, spirilla and even multicellular aggregations, so-called magnetotactic multicellular prokaryotes (MMPs) (Bazylinski & Frankel 2004). All representatives identified to date are affiliated with the *Alpha*-, *Gamma*- and *Deltaproteobacteria*, the Nitrospira phylum and the candidate division OP3 (Lefèvre & Bazylinski 2013). Horizontal gene transfer of a genomic island encoding all known genes that are essential to the formation of magnetosomes has been suggested as one possible explanation for the wide phylogenetic distribution of magnetotaxis (Jogler et al. 2009). Recently, the transfer of the complete set of essential operons needed for magnetosome biosynthesis to a foreign host has demonstrated the plausibility of such a theory (Kolinko et al. 2014). However, based on congruent phylogenetic divergence of magnetosome genes compared to housekeeping and 16S rRNA genes, the general trait of magnetosome formation alternatively could be derived from a common evolutionary origin indicating that the last common ancestor of all proteobacteria possibly might have been an MTB (Lefèvre et al. 2013).

Although most MTB have been isolated from freshwater, brackish or marine habitats, recently they have also been found to thrive in more extreme environments (Bazylinski & Lefèvre 2013). They are gradient organisms typically found at or just below the oxic-anoxic transition zone (OATZ) that commonly is located closely above or within the first millimeters of stratified sediments where opposing redox gradients established by oxygen and reduced inorganic compounds like e.g. H_2S are very steep (Flies, Jonkers, et al. 2005). The lifestyle and efficient navigation of MTB within gradient systems is reflected by formation of sharp chemotactic bands when cells are grown in gradient tubes e.g. within opposing oxygen-sulfide gradients (Flies, Peplies, et al. 2005; Lefèvre, Bernadac, et al. 2009; Schüler et al. 1999). Virtually all cultivated MTB are non-fermenting bacteria that metabolize short-chained organic acids (but no carbohydrates) and generally require microoxic or anoxic conditions (Lefèvre & Bazylinski 2013; Bazylinski & Williams 2007). While the majority of MTB grows heterotrophically respiring either oxygen, nitrate or sulfate, facultative chemolithoautotrophy also is a common trait using reduced sulfur compounds as energy source (Lefèvre & Bazylinski 2013; Geelhoed et al. 2010).

The model organism Magnetospirillum gryphiswaldense

The microaerophilic freshwater alphaproteobacterium *Magnetospirillum gryphiswaldense* was isolated from the sediment of the river Ryck near Greifswald (Schleifer et al. 1991; Schüler & Köhler 1992). Since it is one of the only few MTB that is genetically amenable, it served as a model in many recent studies on magnetosome biosynthesis. *M. gryphiswaldense* biomineralizes on average 35-45 cuboctahedral magnetosomes and is propelled by a single flagellum at each of its cell poles (Fig. 1-2) (Katzmann et al. 2013; Lohße et al. 2011; Schultheiss et al. 2004).

Fig. 1-2 Transmission electron micrograph of a representative *M. gryphiswaldense* cell (micrograph by E. Katzmann). Electron-dense particles (arrow) are magnetite crystals that are arranged in a chain at mid-cell. *M. gryphiswaldense* possesses a single flagellum (open arrowheads) at each of its cell poles.

When cultivated in oxygen gradients, *M. gryphiswaldense* shows microaerophilic behavior and forms sharp aerotactic bands that are well-defined against more oxygenated zones. It possesses a purely respiratory type of metabolism and is not able to grow by fermentation. Metabolizing primary fermentation products (such as lactate, acetate or succinate), *M. gryphiswaldense* grows heterotrophically at comparable cell yields over a wide range of different oxygen tensions (Heyen & Schüler 2003). Magnetite formation, however, is limited to anoxic and microoxic conditions. While the cells' magnetic response is maximum under anaerobiosis, magnetosome crystals become fewer and less regular with increasing oxygen levels, and no magnetic response is observed at concentrations higher than 2% O_2 in oxystat cultures (Heyen & Schüler 2003; Katzmann et al. 2013). Adding to the metabolic repertoire of *M. gryphiswaldense*, in the absence of free carbon or fixed nitrogen sources it is capable of facultative autotrophic growth and nitrogen gas fixation, respectively (Geelhoed et al. 2010; Bazylinski et al. 2000). Under fully anoxic conditions *M. gryphiswaldense* was furthermore shown to grow exclusively by dissimilatory nitrate reduction. Interestingly, the periplasmic nitrate reductase Nap, which is essential for denitrification, was also found to be putatively involved in redox control of magnetosome synthesis (Li et al. 2012).

1.2 Chemotactic signal transduction in bacteria

Motile bacteria actively search for environments that are optimal for their survival and growth. For this purpose they monitor temporal changes of a variety of external and internal parameters by means of chemotaxis systems (Fig. 1-3). Chemotactic signal transduction is based on specialized two-component systems that convert chemical or physical stimuli into controlled output of the rotary flagellar motor. Activation of chemoreceptors triggers autophosphorylation of the histidine kinase CheA, which is followed by subsequent phosphotransfer to a conserved aspartate residue of CheY, a diffusible response regulator protein (Wadhams & Armitage 2004). Phosphorylated CheY is then able to bind directly to the flagellar motor and modulate its output. While CheY binding leads to motor reversal in the enteric model organism *E. coli*, whose signaling pathway has served as a general paradigm since the early days of molecular chemotaxis research, in other organisms CheY binding causes motor stopping or modulation of rotational speed (Krell et al. 2011). Furthermore, in recent years it has become increasingly evident that a multitude of bacteria, particularly environmental strains, deviate from the *E. coli* paradigm and possess more complex signaling networks with additional regulatory proteins, exceptionally high numbers of different chemoreceptors and two or more distinct chemotaxis systems (Porter et al. 2011; Wuichet & Zhulin 2010). For instance, the chemotactic response in *E. coli* is terminated through action of the CheY~P phosphatase CheZ, while other organisms use alternative phosphatases (CheC or FliY) or additional CheY homologs that function as phosphate sinks (Porter et al. 2011; Schmitt 2002).

Most chemoreceptors contain transmembrane domains and are inserted in the cytoplasmic membrane. They form trimers-of-dimers that are densely packed in hexagonal arrays together with CheA and CheW proteins (Briegel et al. 2009). The core signaling complex, which represents the smallest independent signaling unit that is capable of kinase activation and adaptation, consists of two receptor trimers-of-dimers, a central CheA homodimer and two CheW molecules (Liu et al. 2012). The dense packing of signaling complexes is thought to mediate cooperativity between neighboring complexes via multiple hydrophobic contacts (Parkinson et al. 2015). Supramolecular chemoreceptor arrays are commonly localized to polar or subpolar sites, but in *R. spharoides* and in *Vibrio cholerae* recently also cytoplasmic clusters have been described (Briegel, Ladinsky, et al. 2014).

Chemotaxis systems possess remarkable sensitivity over a wide range of concentrations. This trait is mainly due to the adaptation system constituted by the dedicated methyltransferase CheR and the cognate methylesterase CheB (Vladimirov & Sourjik 2009). CheR constantly methylates chemoreceptors at several conserved glutamic acid residues in a cytoplasmic methylation domain (hence they are commonly known as methyl-accepting chemotaxis proteins

(MCPs)). While binding of attractant to MCPs shifts the kinase to the Off-state, increased methylation through CheR, however, gradually shifts the kinase back to the On-state. On the other hand, excess methylation and thus activation of the kinase is prevented through a negative feedback loop by the methylesterase CheB. The activated kinase not only transfers phosphoryl groups to CheY, but also to CheB, which drastically enhances its methylesterase activity resulting in a gradual shift of the kinase back to the Off-state. In this way the chemotaxis signal transduction system reaches an equilibrium state and quickly returns to its pre-stimulus output over a wide range of different attractant and repellent stimuli levels (Parkinson et al. 2015).

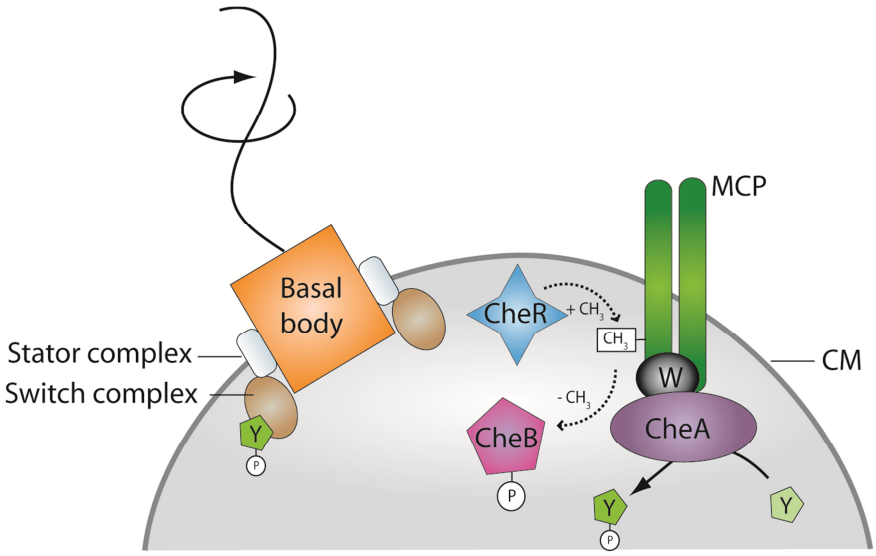

Fig. 1-3 General model of a simple chemotaxis system showing core components present in virtually every chemotactic bacterium (Wuichet & Zhulin 2010). The coupling protein CheW (black) stabilizes interactions between chemoreceptors, so-called methyl-accepting chemotaxis proteins (MCPs), and the histidine kinase CheA. The activated kinase phosphorylates the response regulator CheY (light green) which is then able to bind to the motor switch complex and modulate motor output. The methyltransferase CheR constantly methylates MCPs, while the cognate methylesterase CheB reduces methylation levels after being activated through phosphorylation by CheA. For simplicity reasons only the cytoplasmic membrane (CM) is depicted.

The periplasmic sensory domains of MCPs can bind to a large variety of compounds, e.g. amino acids, carbohydrates or potentially harmful substances like alcohols or fatty acids. Instead of directly sensing individual substances that are important for the bacterium's metabolism, there is an alternative way of reacting to general changes in cellular energy levels, either by detecting changes in the proton gradient across the cytoplasmic membrane or in the redox state of the quinone pool. Such a behavior is called "energy taxis" and has been found in a multitude of bacteria (Schweinitzer & Josenhans 2010; Alexandre et al. 2004).

1.3 Molecular mechanism and cellular patterns of swimming motility

In contrast to the whip-like beating of flagella observed in eukaryotic cells, bacteria are propelled by flagellar filaments that are driven by rotary motors which are powered by the flux of protons or sodium ions across the cytoplasmic membrane (Morimoto & Minamino 2014). These fascinating molecular machines consist of several different parts: The central part of the motor is called "basal body" and is made up of 4 ring-like structures, 3 of which are embedded in the outer membrane (L ring), the peptidoglycan layer (P ring) and the cytoplasmic membrane (MS ring), respectively. The fourth ring extends into the cytoplasm (C ring) and serves a dual function. On the one hand it represents the major part of the rotor and contains the site of torque generation that interacts with stator units, on the other it harbors the switch complex that is essential for motor reversal in response to binding of CheY~P (Sowa & Berry 2008; Minamino & Imada 2015). The C ring is made up of the proteins FliG, FliM and FliN and rotors were found to make 26 steps of 14° each symmetrically in both directions, corresponding to the number of FliG units in the rotor (Nakamura et al. 2010).

Chemotactic sensing enables bacteria to regulate the length of swimming episodes in chemical gradients, so that motion towards attractants is prolonged, while presence of repellents promotes more frequent motor reversals and thus directional changes (Vladimirov & Sourjik 2009). Different forms of flagellation and differences of motor proteins at the molecular level result in a large variety of distinct motility patterns. Enteric bacteria possess peritrichous flagella, i.e. multiple flagella inserted all over the cell body and projecting in different directions. *E. coli* swims smoothly when the motors of its 4-8 flagella turn counterclockwise (CCW) and filaments form a bundle pushing the cell forward. Single or multiple motors switching to clockwise (CW) rotation due to binding of CheY~P cause the bundle to fly apart stopping forward motion and reorienting the cell body in a so-called "tumble" (Turner et al. 2000).

Other bacteria clearly deviate from the *E. coli* paradigm. For instance, many aquatic bacteria with polar flagella do not tumble between swimming phases but instead swim in a typical run-and-reverse pattern (Thar & Fenchel 2005; Mitchell 2006; Mitchell 1991). Reverse motion does not depend on bipolar flagellation but is also observed in monotrichous bacteria. *Azospirillum brasilense* for instance possesses only a single polar flagellum and CCW rotation propels the cell forward (Zhulin & Armitage 1993). Motor reversals cause short backward excursions during which the filament is not pushing but pulling the cell. *Vibrio alginolyticus* has a related but very distinctive motility pattern described as run-reverse-flick (Xie et al. 2011). The single motor of *V. alginolyticus* turns CCW when pushing the cell forward, while CW rotation pulls the cell backwards. Motor reversals from CCW to CW rotation generally cause changes in swimming direction at angles peaking around 180 degrees and switching motors to the reverse gear as such

does not correspond to stochastic directional changes as in *E. coli*, but produces a recurring output. However, the peculiar, mostly perpendicular reorientation of cells that is triggered by a characteristic flick of the flagellum after returning to forward motion has a randomizing effect comparable to tumbles in *E. coli*. The motors of still other bacteria do not reverse direction, e.g. in the case of *R. sphaeroides* and *S. meliloti*, and reorientation in these bacteria is caused by CheY~P-mediated motor stopping or modulation of rotational speed of individual motors (Attmannspacher et al. 2005; Pilizota et al. 2009). CCW rotation is furthermore not the default rotational sense in all bacteria. In *B. subtilis*, for example, CW rotation is the default state and binding of CheY~P to the switch complex causes motor switching to CCW rotation (Szurmant & Ordal 2004). Since as in *E. coli* smooth swimming is a consequence of CCW intervals (Rao et al. 2008), phosphorylation of CheY is differently regulated in *B. subtilis*. So far, it is unclear what determines the default rotational state and the different effects of CheY~P on flagellar motors at the molecular level (Porter et al. 2011). Taking into account that all known rotor and stator proteins are well conserved and share a high degree of similarity, at the moment there are no simple explanations for the observed variations of a general theme.

1.4 Previous work on magnetotactic swimming behavior

The classical experiment used to characterize magnetotactic swimming behavior is to observe cells in the way they were first discovered by performing an aerobic hanging drop assay (Fig. 1-4b). After applying a strong magnetic field, MTB are not simply pulled by the magnetic field, as illustrated by the observation that dead or non-motile cells also align to **B** but do not aggregate at the drop edges. MTB also do not actively swim up or down magnetic field gradients, as the term “magnetotactic” might suggest. However, motile MTB accumulate at the northern- or southernmost edge of a hanging drop due to their persistent swimming either anti-parallel or parallel to **B** and subpopulations on either side can be compared in a semi-quantitative fashion. (To avoid any confusion, directions given in lower case letters specify the orientation of **B**, whereas those given in upper case letters specify geographical directions.)

In the early years of magnetotaxis research it was found that cells isolated from Northern hemisphere habitats swam parallel to **B** and accumulated at the southernmost edge in hanging drop assays (Blakemore 1982; Blakemore 1975). This swimming direction corresponded to the North-pointing end of a compass needle. Therefore, the term North-seeking (NS) was coined to describe their apparently unidirectional mode of navigation (Fig. 1-4c). (NB In a physical sense the North Magnetic Pole located close to the Geographic North Pole actually is a magnetic south pole!). Since the field vector of the geomagnetic field is inclined downwards on the Northern hemisphere and initially no cells were detected above sediments in surface waters, NS bacteria

were supposed to be directed persistently downwards in natural environments until reaching their preferred micro- or suboxic sediment habitat (Frankel et al. 2006). Subsequently, MTB isolated from the Southern hemisphere were shown to be South-seeking (SS), i.e. to swim constantly anti-parallel to **B**, and populations from locations close to the equator were found to consist of equal proportions of NS and SS bacteria (Blakemore et al. 1980; Frankel et al. 1981). This indicated that the pole-seeking behavior was selected by the inclination of the geomagnetic field, in this way simplifying the movement towards low oxygen levels from a three-dimensional to a one-dimensional search.

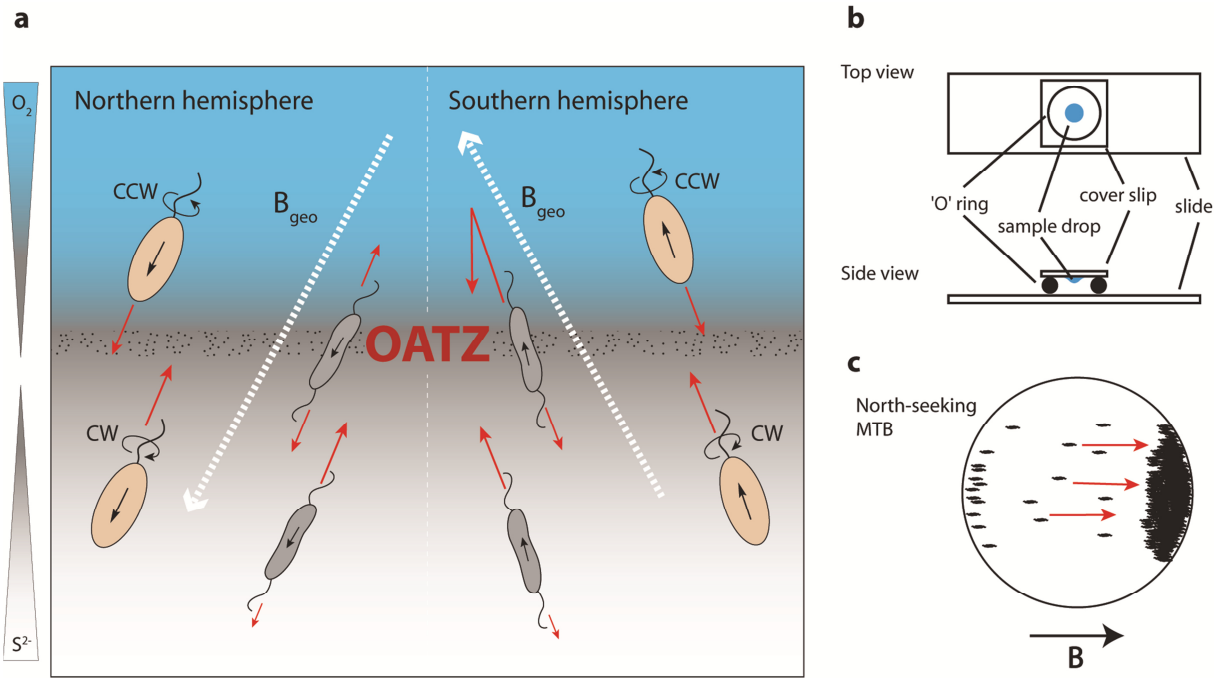

Fig. 1-4 Conventional model of magneto-aerotaxis. (a) Illustration of polar swimming behavior observed in magnetotactic cocci and of axial behavior observed in magnetotactic spirilla. Bacteria navigate within opposing gradients of oxygen and sulfide in natural environments to reach their preferred habitat close to the oxic-anoxic transition zone (OATZ). The cells' magnetic dipole moment (black arrow within cell body) rotates them into alignment with the geomagnetic field ($\mathbf{B_{geo}}$). Under oxic conditions polar cocci presumably swim unidirectionally towards anoxic sediments (red arrows) by turning their flagella CCW. However, under anoxic conditions they reverse motion by switching their flagella to CW rotation. In contrast, axial spirilla are supposed to constitutively swim bidirectionally and reach the OATZ by employing a classical temporal sensing mechanism. (b) Schematic top and side view of the classical aerobic hanging drop assay. (c) Illustration of an idealized population of North-seeking MTB observed in a hanging drop assay. Cells swim parallel to the magnetic field (**B**) under oxic conditions and accumulate at the southernmost edge of the sample drop.

However, even at equatorial sampling sites MTB were isolated from sediments, although at this latitude the geomagnetic field has virtually no vertical component (Frankel et al. 1981). Furthermore, in certain stratified, marine habitats substantial numbers of NS cocci were discovered above the sediment in the water column, close to the OATZ at these sites (Frankel et al. 1997). These findings suggested that MTB use magnetic orientation in conjunction with other navigational responses like aero- or chemotaxis (Blakemore 1982; Frankel et al. 1997). Indeed, MTB

were shown to be capable of bidirectional swimming along **B** instead of persistent unidirectional motility, and axenic cultures were found to grow as microaerophilic bands in oxygen gradients rather than at the bottom of semi-solid agar tubes (Spormann & Wolfe 1984; Frankel et al. 1997).

To highlight the prominent role of oxygen sensing in magnetotactic behavior, a revised model of magneto-aerotaxis was developed including the distinction between two different sub-types of magneto-aerotactic behavior (Fig. 1-4a)(Frankel et al. 1997; Bazylinski & Frankel 2004; Frankel et al. 2006):

- The behavior of magnetotactic cocci, which display bidirectional swimming in aerotactic bands, but persistent unidirectional swimming without adaptation in the hanging drop assay, was defined as "polar" (Frankel et al. 1997). In this motility regime the magnetic field provides not only an axis for more efficient movement, but also embodies vectorial information with respect to the orientation of the ambient oxygen gradient relative to **B**. The magnetotactic polarity of monopolarly flagellated cocci was postulated to depend only on the relative orientation of the cellular dipole with respect to the flagellated cell pole (Bazylinski & Frankel 2004). In contrast to a normal temporal sensing mechanism, cells were hypothesized to be "locked" in either of two directional states depending on oxygen (or redox) levels, until reaching a threshold concentration that switches the flagellar motor to the opposite rotational sense. Such a threshold sensing mechanism might explain several intriguing observations, e.g. aerotactic band formation occurring only at one open end of a flat capillary and band dispersal after reversal of **B** (Frankel et al. 1997). Furthermore, polar magnetotaxis could have the great advantage of efficiently orienting cells even in the absence of local gradients.
- In contrast to polar MTB, cultivated magnetic spirilla were found to display frequent spontaneous swimming reversals (Spormann & Wolfe 1984; Frankel et al. 1997). Their generally bidirectional, so-called "axial" magneto-aerotactic behavior was predicted to be a combination of passive magnetic alignment and temporal sensing. Employing a sensory mechanism equivalent to that of other chemotactic bacteria, axial bacteria supposedly reverse flagellar rotation stochastically under equilibrium conditions and bias their run lengths under gradient conditions according to relative stimuli level changes detected in the recent past.

However, there are some deviations from this broadly accepted model, and particularly the presence of SS bacteria in the anoxic zone of a Northern hemisphere habitat (Simmons et al. 2006) has questioned the general validity of the current magneto-aerotaxis model. A similar

observation of SS behavior in the hanging drop assay was made with multicellular magnetotactic prokaryotes (MMPs) from a New England salt marsh (Shapiro et al. 2011). Still, in their natural habitat neither the MMPs nor the bacteria described by Simmons and co-workers migrated upwards to more oxygenated water layers but were collected from suboxic zones.

The swimming bias of SS MMPs could be switched to NS behavior by exposing cells to UV light (Shapiro et al. 2011). In addition, some marine and freshwater spirilla were reported to react to light stimulation (Chen et al. 2010; Zhu et al. 2010) and in polar magnetococci light exposure also triggered NS behavior (Frankel et al. 1997). Short-wavelength light therefore might induce a phobic response similar to that elicited by high oxygen levels and guide phototactic MTB back to their preferred habitat.

Some indications even for magnetoreceptive behavior (i.e. sensing of the magnetic field strength) came from another uncultivated MMP, which performs an unusual back-and-forth ("ping-pong") motion in higher than geomagnetic fields. The analyzed cells responded to increases in magnetic field strength by altering their swimming behavior, i.e. an elevated frequency of ping-pong movements and shortened outward excursions (Greenberg et al. 2005).

Finally, although generally assumed to lack any polar preference, magnetotactic spirilla freshly isolated from environmental samples were found to display polar swimming behavior (Schüler et al. 1999; Frankel et al. 2006). Furthermore, axenic cultures of other MTB apparently show gradual intermediate swimming polarity phenotypes depending on several parameters including cultivation conditions and growth phase (Zhu et al. 2010; Bazylinski et al. 2013).

In summary, it has to be concluded that magnetotaxis under environmental conditions apparently is much more complex than in the simplified setting of a hanging drop, because a multitude of chemical and physical gradients needs to be integrated by MTB in their natural habitat. The observations listed above therefore call for or an extension or modification of the current magnetotaxis model.

Molecular sensing mechanism of MTB

Although the unique swimming behavior of MTB was discovered many years ago, the mechanism and interplay of magnetotaxis with other tactic responses have remained poorly understood. Currently there is a limited knowledge about the overall chemotactic repertoire of MTB, and it is not known how environmental signals are sensed, transduced, and transformed into tactic responses executed by the flagellar motors of MTB.

More than 50% of all sequenced bacterial genomes, particularly those of environmental bacteria encode multiple chemotaxis gene clusters often comprising modifications of the basic pathway (Wuichet & Zhulin 2010; Porter et al. 2011). For example, the genomes of different *Azospirillum* species encode 4-6 different chemotaxis operons (Wisniewski-Dyé et al. 2011), while *R. sphaeroides* forms a membrane-bound and a cytoplasmic signaling cluster that control the same Fla1 flagellum (Porter et al. 2011). It is known from several analyses that the genomes of MTB also contain exceptionally high numbers of chemotaxis and motility related genes, which indicates the presence of extraordinarily versatile signal transduction pathways that might reflect an adaptation to chemically highly complex natural habitats (Alexandre et al. 2004; Ji et al. 2013; Xie et al. 2010; Matsunaga et al. 2005; Hamer et al. 2010). Apart from approximately 60 different chemoreceptors found in genomes of *Magnetospirillum* species, 30 or more hemerythrin-like genes have been detected that might play a role in oxygen-sensing (Frankel et al. 2006). Furthermore, the two-state sensory mechanism postulated to be at the basis of polar magnetotaxis involves some kind of oxygen threshold sensing. As possible explanation for such a mechanism a putative FNR-like sensing protein has been proposed (Spring & Bazylinski 2006).

There is an ongoing debate about how the degree of magnetic alignment with **B** might influence magnetotactic sensing or even be a major input of the chemotaxis system (Philippe & Wu 2010; Smith et al. 2006; Zhu et al. 2010; Zhu et al. 2014). In a recent study it was even claimed that MTB might be capable of sensing magnetic field gradients (González et al. 2014). Hypothetical mechanisms for such a "magnetoreceptive" behavior feature the cytoskeletal magnetosome filament which provides a measure of the relative alignment of the cell body to **B**. The filament is supposed to transduce magnetic torque to either a mechanically activated transmembrane ion channel (Kirschvink et al. 2001; Greenberg et al. 2005) (a mechanism speculated to occur similarly in animal magnetoreception (Kirschvink et al. 2010)), or towards polar chemoreceptors to control flagellar rotation (Philippe & Wu 2010; Zhu et al. 2014).

In conclusion, it can be stated that, although there is an increasing body of literature addressing putative factors encoded in the genomes of MTB controlling magnetotactic behavior, prior to this thesis the experimental characterization of any of these candidates was still missing. This work therefore is the first to define the molecular principles and mechanistic details of the magneto-aerotactic signal transduction chain.

1.5 Scope of this work

The major goal of this thesis was to gain better understanding of the magnetotactic swimming behavior observed in *M. gryphiswaldense*. Multiple approaches were taken in parallel to reach this goal. First, cells were analyzed in classical macroscopic chemotaxis assays to characterize their overall chemotactic repertoire in response to different carbon sources and electron acceptors. To investigate motility and aerotaxis at the single cell level, a microscopy setup was established that was suited to analyze magnetotactic swimming behavior under defined atmospheric conditions. This set-up included a modified version of the "magnetodrome" (perpendicular pairs of Helmholtz coils) to apply homogenous magnetic fields, and a gas perfusion chamber together with a dedicated gas mixer to equilibrate cell suspensions with defined oxygen concentrations. Furthermore, in collaboration with *Wimasis GmbH* a custom-made tracking software was developed. Using this set-up, motility parameters of *M. gryphiswaldense* cells, such as swimming speed and frequency of reversals, were determined under various equilibrium conditions and after abrupt shifts in oxygen concentration. Additionally, tethered cells were recorded to study the rotational pattern of individual motors.

In the second part of this work, the available genomic data of *M. gryphiswaldense* was screened for candidate genes that might be involved in chemotactic signal transduction. Most importantly, four putative chemotaxis operons were identified and characterized through construction of single and combined deletion mutants.

Another aim of this thesis was to restore magnetotactic swimming polarity in *M. gryphiswaldense* and to study the underlying mechanism at the behavioral and molecular level. Swimming polarity could be selected by repeated subcultivation in magnetic fields superimposed on vertical oxygen gradients. As yet, magnetic swimming behavior was analyzed under undefined or gradient conditions, probably subjecting cells to regular random changes in atmospheric composition. To dissect magnetotactic behavior under more defined conditions, the swimming bias of selected individuals and cell populations was investigated in the gas perfusion chamber.

In the last part of this work, molecular components that were shown be involved in aerotactic signal transduction were artificially targeted to the magnetosome membrane through expression of specific nanobodies. The resulting effects on aerotactic responses and magnetic alignment were tested in microscopic analyses.

2 Publications

2.1 Publication 1:

Polarity of bacterial magnetotaxis is controlled

by aerotaxis through a common sensory pathway.

Popp F., Armitage J., and Schüler D.

Nat. Commun. 5:5398 doi: 10.1038/ncomms6398 (2014).

nature COMMUNICATIONS

ARTICLE

Received 30 Apr 2014 | Accepted 26 Sep 2014 | Published 14 Nov 2014

DOI: 10.1038/ncomms6398

Polarity of bacterial magnetotaxis is controlled by aerotaxis through a common sensory pathway

Felix Popp[1], Judith P. Armitage[2,3] & Dirk Schüler[1]

Most motile bacteria navigate within gradients of external chemical stimuli by regulating the length of randomly oriented swimming episodes. Magnetotactic bacteria are characterized by chains of intracellular ferromagnetic nanoparticles and their ability to sense the geomagnetic field, which is believed to facilitate directed motion, but is not well understood at the behavioural and molecular level. Here, we show that cells of *Magnetospirillum gryphiswaldense* unexpectedly display swimming polarity that depends on aerotactic signal transduction through one of its four chemotaxis operons (*cheOp1*). Growth of cells in magnetic fields superimposed on oxygen gradients results in a gradual inherited bias of swimming runs with one of the cell poles leading, such that the resulting overall swimming direction of entire populations can be reversed by changes in oxygen concentration. These findings clearly show that there is a direct molecular link between aerotactic sensing and the determination of magnetotactic polarity, through the sensory pathway, CheOp1.

[1] Division of Microbiology, Faculty of Biology, Ludwig Maximilians University of Munich, Großhaderner Strasse 2-4, 82152 Martinsried, Germany. [2] Oxford Centre for Integrative Systems Biology, Oxford OX1 3QU, UK. [3] Department of Biochemistry, University of Oxford, South Parks Road, Oxford OX1 3QU, UK. Correspondence and requests for materials should be addressed to D.S. (email: dirk.schueler@uni-bayreuth.de).

One of the most intriguing examples of magnetic navigation in living organisms is magnetotaxis exhibited by certain aquatic bacteria, which synthesize nano-sized intracellular ferrimagnetic crystals of magnetite (Fe_3O_4) or greigite (Fe_3O_4), enclosed in the membrane-enveloped magnetosomes[1]. The chain-like arrangement of magnetosome particles generates a magnetic dipole that passively rotates the bacterium into alignment with the ambient magnetic field (**B**) as it swims actively by means of flagella[1]. Magnetotaxis is assumed to reduce the biased three-dimensional swimming pattern shown by most motile bacteria to linear movement along the geomagnetic field lines, which is believed to facilitate navigation to growth-favouring zones close to the oxic–anoxic transition in chemically stratified aquatic environments[2]. However, the biological mechanisms governing magnetotaxis have remained poorly understood[3]. In the classical aerobic hanging drop assay, most naturally occurring magnetotactic bacteria (MTB) exhibit a uniform, polar swimming pattern (defined as swimming polarity), that is, they persistently migrate either parallel or antiparallel to **B**, which is equivalent to movement towards or away, respectively, from the magnetic south pole of a bar magnet (that is, the pole that attracts the North-pointing end of a magnetic compass needle). Migration parallel or antiparallel to **B** is called North-seeking (NS) or South-seeking (SS) swimming polarity, respectively. Swimming polarity (either NS or SS) of individual cells results from the magnetic polarity (M polarity) of the magnetosome chain with respect to the cellular polarity (C polarity) caused by some sort of cellular asymmetry such as, for instance, monopolar flagellation. In the original model of magnetotaxis only a small fraction of cells was assumed to reverse M polarity in each generation[4] and cells were suggested to display only unidirectional motion[5]. This seemed to be consistent with the predominance of NS and SS MTB collected from environments in the northern and southern hemisphere[2], respectively, which would guide MTB downwards along the opposing inclinations of the geomagnetic field in the two hemispheres to reach their microhabitat at the bottom of natural waters. More recently it was shown, however, that monopolarly flagellated MTB such as *Magnetococcus marinus* MC-1 reverse their swimming direction to alternate between upper and lower oxygen threshold levels by an unknown mechanism[6,7].

In contrast, bipolarly flagellated magnetospirilla such as the alphaproteobacterium *Magnetospirillum gryphiswaldense* that seemingly lack C polarity[8] were assumed to employ 'axial magnetotaxis', as cells were observed to swim aligned with magnetic field lines, but to lack a clear swimming polarity[6,9,10]. *M. gryphiswaldense* has been widely used as a model in many recent studies on magnetosome biosynthesis[11]. However, there has been little investigation of its motility and taxis[8,12,13], and it is currently not known whether or how the magnetic behaviour of *M. gryphiswaldense* and other MTB is integrated with other sensory responses at the behavioural and molecular level, or whether it uses a dedicated sensing and signalling machinery.

Here, we studied in detail the motility and behavioural responses of *M. gryphiswaldense* to defined oxygen concentrations. We found that aerotaxis is the dominant sensory system controlling swimming reversals. Unexpectedly, swimming polarity can be selected by serial growth in oxygen gradients with superimposed parallel magnetic fields, and the cells' predominant swimming direction with respect to **B** can be instantaneously reversed by sudden changes in oxygen concentration. Both aerotaxis (that is, control of reversal rate irrespective of (magnetic) directionality) and swimming polarity (that is, control of swimming directionality with respect to the magnetic field) depend on the chemotaxis proteins encoded in just one of the four chemotaxis operons of *M. gryphiswaldense*, suggesting a direct molecular link between both navigational mechanisms.

Results

Aerotaxis is the dominant tactic behaviour. In spatial chemotaxis assays, we observed a strong microaerophilic (that is, both aerophilic and -phobic) response, which obscured any other putative tactic reactions tested (for example, to light or carbon sources, see Methods for details). Cells accumulated as sharp bands within oxygen gradients (Fig. 1a,b). In the absence of oxygen, cells developed distinct tactic bands at millimolar concentrations in gradients of nitrate (an alternative terminal electron acceptor for anaerobic respiration[14], Supplementary Fig. 1a), indicating that the strong aerotaxis behaviour is part of a general energy taxis response similar to that identified in the microaerophilic *A. brasiliense* and other bacteria[15–18]. Swimming speeds of bacteria in the dense cell suspensions under a coverslip (uncontrolled oxic conditions) ranged between 20 and 60 $\mu m\,s^{-1}$ (Fig. 2c) with a mean of $41.6 \pm 3.5\,\mu m\,s^{-1}$ (Supplementary Table 1). Typically, bacteria exhibited long unidirectional runs of over several hundred micrometres (Fig. 2a,b and Supplementary Movie 1), interrupted by short (<150 ms) reversal events (mean frequency $0.031 \pm 0.007\,s^{-1}$). About 50% of cells that tethered

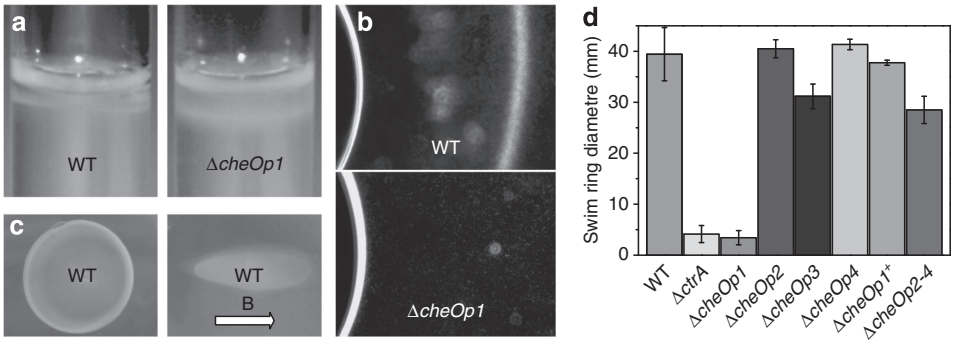

Figure 1 | Aerotactic behaviour of *M. gryphiswaldense*. (**a**) Band formation of WT (left) and Δ*cheOp1* mutant (right) cells in soft agar tubes 2 days after inoculation. Unlike the sharp band observed for the WT, Δ*cheOp1* grew as a diffuse zone more distant to the agar surface. (**b**) Aerotactic band formation in a flat capillary 5 min after filling. (**c**) Swim ring formation of WT in 0.2% motility agar in the absence and presence of magnetic field (**B**). Orientation of **B** is indicated (black arrow). (**d**) Swim ring formation of WT and mutant strains in 0.2% motility agar 2 days after inoculation (mean ± s.d. of three independent replicates). Deletion of *cheOp1* reduced swim ring size to the level of a non-motile Δ*ctrA* mutant, which lacks any flagella filaments similar as described previously[56]. *Cis*-complementation of the Δ*cheOp1* mutant strain (Δ*cheOp1*$^+$) restored WT-like behaviour.

spontaneously to the cover slip by one of their two bipolar flagella rotated unidirectionally either CW or CCW for at least 1 min (Fig. 2d, Supplementary Movie 2), while the others reversed rotation at rates of up to 0.45 s^{-1}, suggesting reversals are caused, as in other bacteria, by reversal of the direction of motor rotation.

We studied the swimming responses of individual bacteria to defined oxygen concentrations at low cell densities within a microscopic gas perfusion chamber (Supplementary Fig. 2) by employing automated video tracking. To separate the effects of magnetic fields from aerotactic behaviour, we first analysed an isogenic non-magnetic (*mag*$^-$) Δ*mamAB* mutant[19], whose swimming speed and reversal frequency were virtually undistinguishable from the magnetic WT (Supplementary Table 1, Supplementary Fig. 3d, Supplementary Movie 3). At a concentration of 1% and 5% oxygen, the mean speed of Δ*mamAB* was 4–7 μm s^{-1} higher than under anoxic conditions (33.3 ± 10.6 μm s^{-1}) (Supplementary Fig. 3a). Conversely, reversal rates were the highest under anoxic conditions (0.126 ± 0.051 s^{-1}) and the lowest at 5% oxygen (0.055 ± 0.010 s^{-1}). Abruptly shifting from micro-oxic (2% O_2) to anoxic conditions resulted in a slow but sustained decrease in swimming speed and in an increase in reversal frequency (approximately from 0.05 to 0.1 s^{-1}) (Supplementary Fig 3b). A reverse shift (that is, challenging anoxic-adapted cells with 2% O_2) had a more pronounced effect and led to a transient threefold increase in reversal frequency (Fig. 3a, Supplementary Movie 4). Within 5 s post-shift, the prestimulus frequency of around 0.1 s^{-1} instantaneously increased to 0.34 s^{-1}. However, 10 s post-shift this drastic response was followed by a drop in reversal frequency to below prestimulus levels, reaching nearly zero after 20 s. In contrast to other bacteria that rapidly adapt and return to prestimulus levels, in the following 80 s, the frequency remained low (average 0.03 ± 0.02 s^{-1}), resulting in long uninterrupted swimming runs.

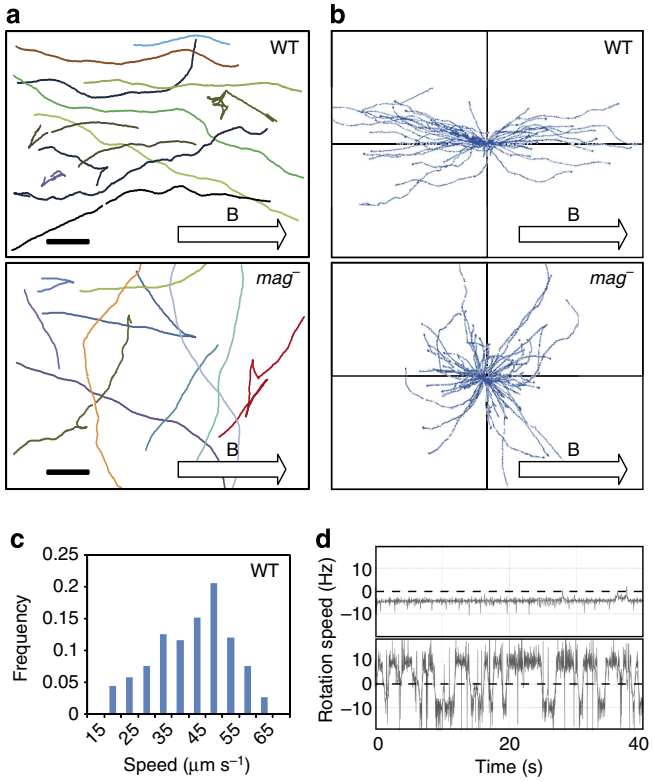

Figure 2 | Run and reversal motility behaviour of *M. gryphiswaldense*. (**a**) Representative tracks of WT and non-magnetic Δ*mamAB* mutant cells under a coverslip exposed to air in a homogenous horizontal magnetic field of 0.26 mT (**B**; orientation indicated by arrow). The bar represents 100 μm. (**b**) Plot of all recorded tracks of WT and non-magnetic Δ*mamAB* mutant cells in a standard wet mount in a homogenous horizontal magnetic field of 0.26 mT (**B**). (**c**) Histogram depicting frequency versus swimming speed of WT cells in a standard wet mount. (**d**) Rotation diagrams of representative tethered WT cells. An extreme case of a cell rotating exclusively CCW (top) and a reversing cell (bottom) is shown. Movies were recorded at 43 fps and analysed using BRAS software[57].

Deletion of *cheOp1* abolishes aerotaxis. Analysis of the *M. gryphiswaldense* genome for genes that might encode proteins involved in aerotaxis revealed at least 56 genes encoding putative chemoreceptors[20], known as methyl-accepting chemotaxis proteins (MCPs) (Supplementary Table 3), and four putative chemotaxis operons designated *cheOp1-4* (Fig. 4). Highly conserved syntenic operons are also present in the related *M. magneticum* and *M. magnetotacticum* (Supplementary Table 2). *cheOp1* homologues belong to the well-conserved F5 class of chemotaxis systems[21], so far almost exclusively found among alphaproteobacteria, whereas *cheOp2* and *cheOp3* homologues belong to the ACF class[21]. All operons encode the canonical set of chemotaxis genes *cheA*, *cheW*, *cheY*, *cheB* and *cheR* (although *cheOp2* only has a hybrid *cheY* homologue) plus additional *che* homologues and putative chemotaxis-related genes encoding MCP, ParA-like[22], EAL or GGDEF[23] domain proteins in *cheOp2-4*. The best hits are to orthologues from other magnetotactic alphaproteobacteria (Supplementary Table 2) followed by *P. molischianum* and different *Rhodospirillum* and *Azospirillum* species. Except for *cheOp3*, representatives from all operons have been shown to be expressed[24,25].

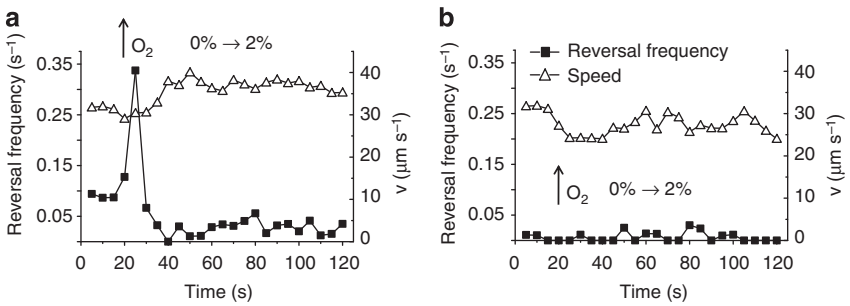

Figure 3 | Addition of oxygen triggers a distinct reversal response. Reversal rates and swimming speeds of Δ*mamAB* (**a**) and Δ*cheOp1* (**b**) cells recorded in the gas perfusion chamber subjected to an abrupt shift from 0 to 2% oxygen after 20 s (↑O_2). Mean values of reversal frequency and speed of three independent experiments calculated for 5-s intervals are shown. On average 61 (**a**) and 17 (**b**) cells were tracked for each graph over the whole duration of the experiment.

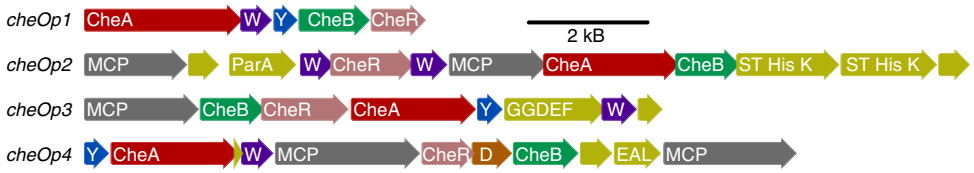

Figure 4 | Molecular organization of chemotaxis operons of *M. gryphiswaldense*. Homologues of the same family are indicated by the same colour. W = *cheW*, Y = *cheY*, D = *cheD*, ST His K = signal transduction histidine kinase, GGDEF + EAL = genes encoding proteins containing the respective domains.

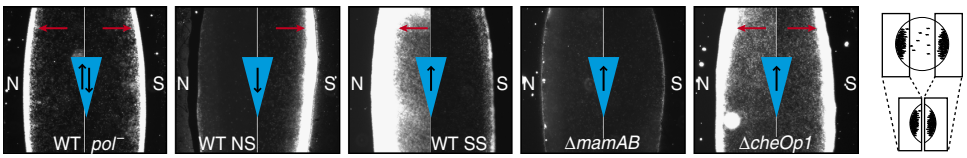

Figure 5 | Selection of magnetic swimming polarity depends on CheOp1. Dark field microsocopy images of WT and mutant cells at ×100 magnification in hanging drop assays exposed to air. Horizontal magnetic fields were applied with a permanent magnet and cells that accumulated at the drop edges corresponding to the north and south magnetic pole (indicated by N and S, respectively) were imaged. Both individual and densely packed cells are visible in dark field microscopy images as white dots or areas (accumulations highlighted by red arrows). For each representative sample, both edges of the same drop are shown (as illustrated in schematic (right)). Except for non-selected WT cells (*pol*$^-$), all cultures were grown under selective conditions for at least two passages to select NS and SS cells. Orientation of the magnetic field (black arrows) with respect to the O_2 gradient (blue triangle) during selective growth is indicated.

We constructed deletion mutants of all operons in the magnetic (*mag*$^+$) WT background. Growth and magnetosome formation of all resulting mutant strains was not affected and motility was very similar to that of the WT, except that the average swimming speed of Δ*cheOp1* was slightly reduced (Fig. 3). Single deletions of *cheOp2*, *cheOp3* and *cheOp4* had no detectable effect on aerotaxis, although Δ*cheOp3* formed slightly smaller halos in swim agar plates (Fig. 1d). Halo size of a triple-deletion mutant, in which *cheOp2-4* were eliminated successively, was the same as for Δ*cheOp3*, indicating that none of these operons is playing a major role in energy taxis. In striking contrast, deletion of *cheOp1* caused a complete loss of the aerotactic response (= *aer*$^-$). Δ*cheOp1* produced no tactic bands in either nitrate gradients (Supplementary Fig. 1) or liquid medium in flat capillaries exposed to air (Fig. 1b), but grew as a diffuse zone close to the surface in soft agar oxygen gradients, unlike the sharp band observed for the WT (Fig. 1a). When Δ*cheOp1* cells were subjected to an oxygen shift from 0 to 2%, they failed to display any behavioural changes, and, unlike the drastic response observed for the WT, reversal frequency remained around zero during the entire experiment (Fig. 3b), resulting in long, uninterrupted runs (Supplementary Movie 5). The sensory pathway encoded by *cheOp1* is therefore the only one controlling aerotaxis.

Magnetic swimming polarity is controlled by aerotaxis. In a magnetic field of 0.26 mT (about 5× the strength of the geomagnetic field) the swimming tracks of WT (*mag*$^+$) cells approximated to more or less straight lines (Fig. 2a,b and Supplementary Movie 1). Distorted swimming halos reflecting the orientation of **B** were formed by the WT inoculated into motility agar exposed to magnetic fields (Fig. 1c). Swimming characteristics of Δ*mamAB* (*mag*$^-$) cells were very similar to those of the WT, except that swimming paths were less straight and not magnetically aligned (Supplementary Table 1, Supplementary Movie 3). In the classical aerobic hanging drop assay (Supplementary Fig. 4), WT cells grown under standard laboratory conditions (that is, in the absence of defined magnetic fields and at permanent agitation) accumulated in approximately equal numbers at both edges of the drop without detectable polarity (*pol*$^-$), whereas Δ*mamAB* did not show any accumulation (Fig. 5 and Supplementary Fig. 5g).

The behaviour observed for non-selected cells was consistent with so-called 'axial' magnetotaxis. However, as previous observations indicated that magnetospirilla freshly isolated from environmental samples displayed strong swimming polarity[26,27], we tested whether polarity could be reinduced in our *M. gryphiswaldense* WT lab strain[28], which has been passaged for many generations in the absence of magnetic selection. We therefore performed serial transfers of cells in oxygen gradients ($Ox_{Low} \rightarrow Ox_{High}$), exposing them to either parallel (north pole → south pole) or antiparallel (south pole ← north pole) magnetic fields of approximately 10× the geomagnetic field strength (0.57 mT) (= selective conditions, Supplementary Fig. 4a). Unexpectedly, after only 2–3 days (equivalent to 2–3 transfers or 7–10 generations) we observed a gradually increasing swimming polarity, with cells predominantly (>80%) accumulating at either the northern- or southernmost edge of the drop (SS or NS), depending on the direction of **B** during selection (Fig. 5). Selected cells (*pol*$^+$) were identical to non-selected cells (*pol*$^-$) with respect to morphology, flagellation and appearance of the magnetosome chains. In contrast to non-selected cells that formed two similar aerotactic bands at each end of a flat capillary oriented parallel to **B**, selected cells formed a very dense band close to the meniscus at one end of the capillary and a fainter band more distant to the meniscus at the opposite end. Intriguingly, Δ*cheOp1* cells lacked any swimming polarity, whether or not they had been grown under selective conditions, and accumulated in equal numbers at both edges of the hanging drop much like non-selected WT cells, suggesting oxygen and/or *cheOp1* has a role in polarizing the magnetotactic response.

To further study the influence of oxygen levels on the observed swimming polarity behaviour, we next analysed non-selected and NS WT cells in magnetic fields under defined conditions in a gas perfusion chamber. To measure the polarity bias at the single-cell level, we manually tracked the movements of individuals under anoxic conditions. As a measure for the relative polarity bias of individuals (PB_{ind}) we calculated the ratio of the relative time periods spent swimming either parallel or anti-parallel to

B within 1-min intervals (Supplementary Fig. 5). Resulting values between 0 and 0.5 reflected an overall directional bias of 50 to 100% towards the magnetic north pole, whereas values between 0 and −0.5 reflected a bias of 50 to 100% towards the magnetic south pole. While PB_{ind} values of non-selected cells were widely scattered with an average of 0.04 ± 0.27, those of NS cells ranged between −0.05 and 0.45 with an average of 0.17 ± 0.17. This means that under anoxic conditions NS cells would gradually swim towards more oxic regions in an environment with the same oxygen gradient configuration as during NS polarity selection (north pole corresponds to high oxygen). To quantitatively estimate the polarity bias of entire populations, we video-tracked numerous swimming cells (in total ≥800) for a short time until they left the microscopic viewing field. From the distances covered by individuals both parallel and antiparallel to **B** we then calculated the mean polarity bias of the population (PB_{pop}). Under anoxic conditions, populations of NS cells displayed a slight but significant bias to swim anti-parallel to the magnetic field lines ($PB_{pop} = 0.07$, which means an idealized cell representing the whole population swam 57% towards the north pole and 43% towards the south pole) (Supplementary Fig. 5b). In contrast, consistent with 'axial' behaviour about equal portions of non-selected WT cells swam parallel or anti-parallel along **B** ($PB_{pop} = 0.00$).

To further investigate the observed link between swimming polarity and aerotaxis, we analysed the response of polarity-selected cells to oxygen up-shifts, which we had found to cause a drastic temporary increase in reversal rates in non-magnetic cells. To this end, we modified the classical oxic hanging drop assay by placing microdroplets (1 µl) of selected WT cells in the gas perfusion chamber. Under anoxic conditions, most cells of a NS culture swam anti-parallel to **B** and accumulated at the northern edge of the drop (Fig. 6a). However, when the chamber was abruptly ventilated with 2% oxygen, within 2 s post-shift virtually all cells displayed multiple reversals that were followed by straight, long and uninterrupted runs parallel to **B** (Supplementary Movie 6). Strikingly, this caused nearly the entire population to move uniformly towards the south pole. The overall directional change was due to swimming reversals parallel to field lines and not to cells performing U-turns, which are observed on reversal of **B**[29]. About 50% of the population had collectively left the northern edge 7 s post-shift, and within 90 s the vast majority of cells (we estimate >80%) had crossed the entire diametre of the drop (1–2 mm) and was accumulated at the opposite southern edge. Manual tracking of individuals before and after oxygen upshifts revealed that non-selected cells showed a very heterogeneous swimming pattern under both conditions (Fig. 6b). Many individuals lacked a clear behavioural response to the shift and did not reverse their swimming bias (as indicated by a change of sign of their PB_{ind}). The average PB_{ind} therefore was close to zero under both conditions, which was corroborated by similar PB_{pop} values obtained through automated mass tracking (Fig. 6c, Supplementary Movie 8). This indicates that the ability to adjust the effective direction of movement after oxygen exposure is compromised in non-selected cells. In contrast, polarity-selected cells displayed a very uniform pattern. After the upshift PB_{ind} values of NS cells on average decreased by 0.49 (compared with a mean absolute change of 0.19 in non-selected cells) and the majority of individuals reversed its swimming bias (Fig. 6b). Again, average PB_{ind} values of selected cells were consistent with PB_{pop} values in population tracking experiments that rapidly decreased from slightly positive to values around −0.3 after the shift and remained on a low level for >60 s (Fig. 6c, Supplementary Movie 7). Analysis of individual cells for extended time periods post-shift further highlighted the described differences between selected and non-selected cells

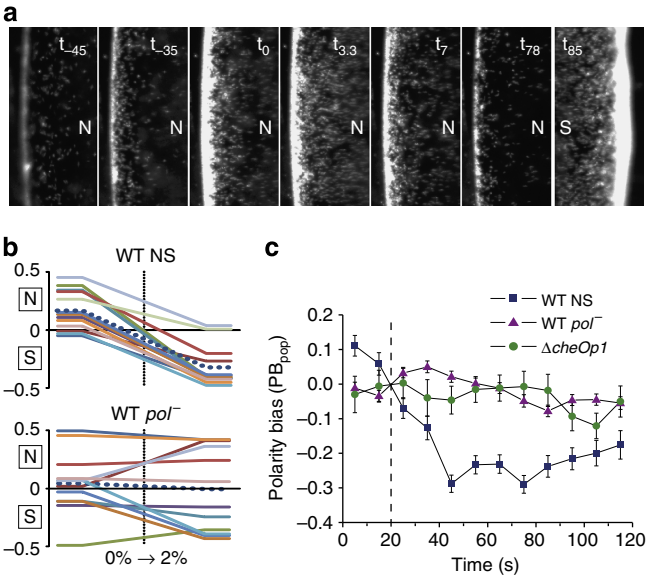

Figure 6 | Magnetic swimming polarity is switched by aerotaxis. (**a**) Dark field video recording (×100 magnification) of a reversing NS WT population in the gas perfusion chamber. Details of individual frames showing the edge of a drop corresponding to the north (N) or south pole (S). A 1-µl sample was equilibrated at 0% O_2 for 3 min before the recording was started. At t_{-40} the sample was exposed to the magnetic field of a bar magnet. Time points of selected images (in s) are given in each image relative to an atmospheric shift from 0 to 2% O_2 (at t_0). (**b**) Polarity bias of individual cells (PB_{ind}) calculated from swimming phase ratios as revealed by manual long-term tracking. Representative PB_{ind} plots of single NS (left, $n = 13$)) and non-selected (*pol*$^-$) WT cells (right, $n = 12$) are shown. PB_{ind} values were calculated from 60-s intervals before and after a shift from 0 to 2% O_2. Corresponding swimming directions relative to the magnetic field are given by N (anti-parallel) and S (parallel). The dotted blue line represents the mean of all analysed cells. (**c**) Polarity bias of populations (PB_{pop}) that were shifted from 0 to 2% O_2 (indicated by dashed line) as revealed by automated mass tracking. The mean ± s.e.m. of all individual cell bias values of selected (NS) WT, non-selected (*pol*$^-$) WT and Δ*cheOp1* mutant cells are shown. For each graph data from 4 to 6 independent experiments were collected.

(Supplementary Fig. 5d,f). Last, equal numbers of cells swimming into either direction were observed for populations of Δ*cheOp1* (Supplementary Movie 5) and corresponding PB_{pop} values were comparable to those of non-selected cells.

Discussion

Magnetosome-based magnetic navigation was discovered in bacteria almost 40 years ago[30] and has been implicated in the magnetoreception of higher organisms[31,32]. Since then various applications of bacterial magnetotaxis have been suggested, such as the transport of drugs or other cargo by magnetically steered bacterial microrobots in microfluidic systems or even blood vessels[33,34]. However, the biological mechanisms governing this behaviour and its integration with other sensory responses have remained unknown.

Here, we demonstrate that polar magnetotaxis could be restored in the hitherto non-polar lab strain of *M. gryphiswaldense,* and this behaviour is tightly coupled with aerotaxis towards low-oxygen levels, the dominant chemotactic response of the bacterium. Chemotactic signal transduction in all bacteria is based on two-component systems involving autophosphorylation of the histidine kinase, CheA, followed by subsequent phospho-transfer to a response regulator, CheY[20]. We found that of the

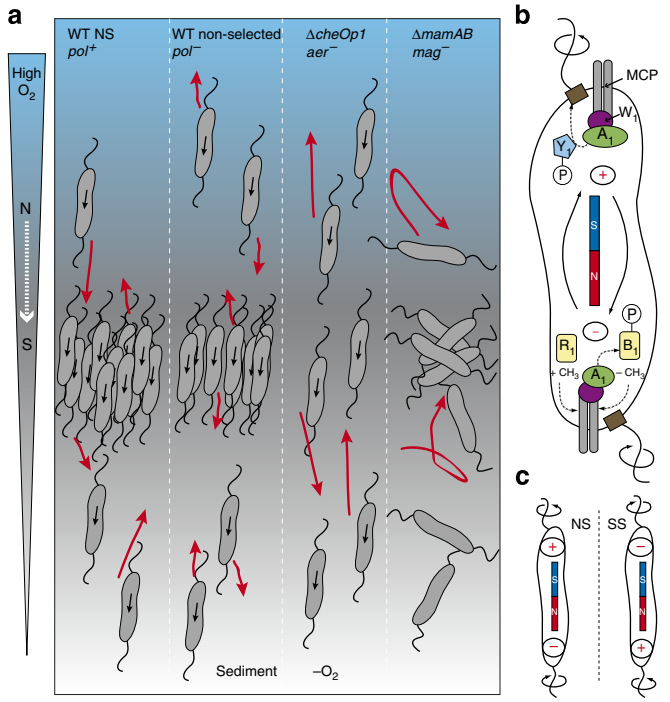

Figure 7 | Behavioural and molecular mechanism of polar magnetotaxis. (**a**) Schematic representation of polar magnetotaxis in magnetospirilla compared with the behaviour of mutants analysed in the study. Representative, idealized swimming tracks of individual cells in a vertical O_2 gradient aligned to the magnetic field (**B**) are shown as red arrows. Polar magnetotactic NS WT cells (*pol*$^+$) form an aerotactic band at the oxic–anoxic transition (OAT). When displaced to hyper- or hypooxic zones, those cells avoid excursions into the 'ecologically wrong' direction and directly swim back to the OAT. In contrast, non-selected WT cells (*pol*$^-$) swim in either direction relative to **B** and therefore their return to the OAT is slowed down. Δ*cheOp1* (*aer*$^-$) mutant cells swim aligned to **B**, but fail to reverse and accumulate at favourable O_2 levels, while Δ*mamAB* (*mag*$^-$) mutant cells behave similar to other non-magnetotactic bacteria and only use temporal gradient sensing to steer towards the OAT. (**b**) Molecular components underlying aerotaxis and swimming polarity in magnetospirilla. CheA, CheW, CheY, CheB and CheR of CheOp1 are shown ($CheY_1$, $CheB_1$ and $CheR_1$ depicted only at one pole to avoid crowding). The histidine kinase $CheA_1$ phosphorylates $CheY_1$, which in its activated form binds to the motor complex causing motor reversals. Direction of flagella rotation is indicated by circular arrows, the bar magnet indicates magnetic (M) polarity. A hypothetical polarity marker (reflecting cellular (C) polarity) gradually influencing motor output is marked with $+/-$ symbols. (**c**) Hypothetical C polarity of NS and SS cells (indicated by $+/-$ axis) resulting in opposite motor output (indicated by arrows).

four identified chemotaxis operons of *M. gryphiswaldense*, only *cheOp1*, comprising the canonical set of chemotaxis genes (*cheAWYBR*), is involved in aerotaxis and swimming polarity (Fig. 7). *cheOp1* encodes a hybrid CheA kinase and no CheZ, suggesting signal termination is through a phosphate sink, as in *S. meliloti*[35]. Owing to the absence of an MCP gene in *cheOp1* and the great number of putative MCP-encoding genes (Supplementary Table 3), an energy/oxygen sensor in *M. gryphiswaldense* has not been identified. In addition, the role of *cheOp2-4* still remains unclear as the triple mutant lacked an obvious phenotype. This finding might suggest that, as in other bacterial species encoding multiple putative chemosensory pathways, these additional pathways may be controlling traits other than swimming behaviour[36], which is supported by the identification of cyclic di-GMP-related motifs in *cheOp2-4*.

Bacterial taxis in chemical gradients is generally accomplished by a combination of straight-line swimming and reversing or reorienting. As has been shown for other polarly flagellated bacteria[37,38], *M. gryphiswaldense* does not tumble between smooth swimming phases, but instead swims in a typical run and reversal pattern, with speeds between 20 and 65 $\mu m\,s^{-1}$, similar to previously reported values[12,13,39]. In equilibrium conditions, cells showed a reversal frequency of 0.126 s^{-1} or less, which is low compared with data reported for non-MTB[40–43]. Consistent with the adaptation of MTB for growth in redox gradients in stratified sediments[27], and also with the dependence of oxygen-sensitive magnetite biomineralization and N_2 fixation on suboxic conditions[44,45], we found a higher proportion of cells swam faster and reversed less frequently under microoxic than under anoxic or fully oxic conditions. The model of energy taxis suggests cells swimming towards lower or higher oxygen concentrations would experience a change in proton motive force or electron transfer rates[15,46], resulting in increased motor reversals. However, on temporal oxygen-upshifts, *M. gryphiswaldense* displayed a very different behavioural response: a short period of highly increased reversal frequency was followed by a rapid and prolonged decrease of reversals, resulting in straight, uninterrupted runs, very different from the prestimulus state. This is in contrast to other bacteria, which typically display a return to prestimulus levels after responding to repellent stimuli[46], mediated through adaptation and resetting of the receptor proteins. The presence of genes encoding conserved adaptation proteins, CheB and CheR, in *cheOp1* suggests that adaptation occurs, but also implies that adaptation resets the CheA signalling state to one tuned to the new environment. This distinct behavioural pattern of *M. gryphiswaldense* resembling a form of 'escape response' would rapidly guide the cells back to suboxic environments after displacement into hyperoxic, harmful zones (Fig. 7) and would prove beneficial in environmental redox gradients, which are prone to strong temporal and spatial changes.

Aerotactic signalling through CheOp1 was essential for magnetic swimming polarity. Contrary to the prevailing model, we show that instead of using the magnetic field only as an axis, *M. gryphiswaldense* is capable of polar magnetotaxis. Swimming polarity appeared to be an inherent property of cells, and the temporary loss of motility bias after non-selective lab cultivation was not caused by genetic loss, but could be restored by appropriate incubation within oxygen gradients superimposed with magnetic fields mimicking the geomagnetic inclination. As all MTB including magnetospirilla sampled from environmental sites generally display swimming polarity[3,26,27], it seems likely that in natural redox gradients in which cells persistently experience polarity selection by the geomagnetic field vector polar rather than 'axial' magnetotaxis is the prevalent mode of magnetic navigation common to all MTB. The previously observed 'axial' behaviour of magnetospirilla therefore might represent an artefact, resulting from the loss of selection during lab cultivation. Selection is probably explained by the cells with the appropriate bias being directed more efficiently towards favourable growth conditions, gradually outcompeting others more regularly exposed to more harmful oxygen concentrations. Selection of swimming polarity was not caused by enrichment of pre-existing unidirectional NS or SS bacteria equally prevalent in non-selected populations, but instead resulted from a gradually increased bias at the single-cell level by which one swimming direction became favoured over time (Fig. 6b and Supplementary Fig. 5). In addition, non-selected cells failed to display a clear switch of swimming bias on oxic shifts, although overall reversal rates were not affected. Thus, the propensity of individual cells to respond towards one particular direction under anoxic conditions

and to reverse the effective direction in the presence of high oxygen was gradually selected.

Increasing run lengths when swimming with one cellular pole ahead is in contrast to other bacteria that exhibit no intrinsic polarity in swimming behaviour. For instance, the sensory system of *E. coli* does not favour one swimming direction over the other[47]. Directional motility requires a fixed orientation of the in-build magnetic moment (M polarity) with respect to the sense of flagellar rotation (reflecting C polarity). It has proved impossible so far to directly visualize the rotation of individual filaments, but for directional motility both motors would turn with opposite senses of rotation, and motor reversals have to be coordinated between the opposing poles (resulting in switching between leading and trailing flagella). This simultaneous motor activity has been observed in other spirilla with bipolar flagellation[37,48] and is also consistent with our observations on tethered cells, which never displayed extended stops as would be expected if the motors rotated and paused alternately. However, the sense of flagellar rotation also depends on the concentration of CheY∼P. It seems improbable that the cell establishes a gradient of CheY∼P between the two cell poles that is instantaneously reversed during swimming reversals. In addition, due to the small size of the bacterial cell the chemotaxis receptors at both poles sense the same stimulus, which probably leads to the same CheY phosphorylation level at both poles. Therefore, the direction of motor rotation might be 'hardwired' into each motor, so that at a low CheY phosphorylation level one motor turns CW while the other turns CCW, and vice versa at higher phosphorylation levels.

At the moment, it is unclear how swimming polarity is determined at the cellular and molecular level. We failed to detect any polarity selection or a reversible swimming bias in cells lacking *cheOp1*. This highlights that magnetic swimming polarity depends on signalling via CheOp1 and is not autonomously controlled by a dedicated sensory pathway exclusively serving magnetotaxis. However, the observed behaviour cannot be fully explained by a simple temporal sensing mechanism, as in this case cells would be expected to exhibit equally timed average swim phases with each pole ahead. As already noted by Frankel *et al.*[6], polar magnetotaxis might involve a means to measure absolute oxygen concentrations. Unlike magnetic cocci, which have inherent C polarity owing to their asymmetric monopolar flagellation (Supplementary Fig. 5h), bipolarly flagellated spirilla exhibit apparently symmetric morphology. So far, we can also only speculate about what determines the C polarity axis in magnetospirilla, but it is clear that the relative output of the motors of NS and SS cells has to be opposite, and, therefore, swimming polarity must be based on some sort of symmetry breaking at subcellular level (C polarity symbolized by '+' and '−' in Fig. 7) parallel to the M polarity axis. As $CheW_1$-GFP fusions show a bipolar localization pattern in both polarity-selected and non-selected cells similar as observed in other magnetospirilla[49], asymmetric chemoreceptor localization, however, appears to be an improbable mechanism. For instance, a spatial bias might be established by a modification of motor components, an uneven distribution of signal transduction components or of a dedicated marker molecule. There are precedents for C polarity-determining factors and plasticity of polar identity in other bacteria[50], even though the molecular processes controlling polarity axis redefinition are largely unknown. It had been proposed by Lumsden that after cell division swimming polarity might be inherited non-genetically by daughter cells via the M polarity of the inherited magnetosome chain[51]. However, swimming polarity was selected in *M. gryphiswaldense* within fewer than 10 generations, suggesting that selection is independent of the rarely occurring loss through missegregation and *de novo* formation of the magnetosome chain. Our data also argue against a rapid, merely physical effect of re-magnetization (reversal of M polarity) caused by exposure to artificial magnetic fields, but point to a mechanism that gradually defines, modifies and passes on the relative orientation of the magnetotactic C polarity axis of magnetospirilla.

In conclusion, we demonstrate that polar magnetotaxis can be selected even in magnetospirilla thus far believed to be non-polar, and this magnetic swimming polarity is controlled by aerotactic signal transduction through CheOp1. Contrary to previous assumptions that magnetotaxis is passive and independent of sensory pathways, we provide first evidence for a genetic link between aero- and magnetotaxis and magnetotactic polarity.

Methods

Bacterial strains, plasmids and culture conditions. Bacterial strains and plasmids used in this study are listed in Supplementary Tables 4 and 5. For genetic experiments *M. gryphiswaldense* strains were grown microaerobically in modified flask standard medium (FSM) at 30 °C under moderate agitation (120 r.p.m.)[45]. To grow *E. coli* BW29427, 1 mM DL-α, ε-diaminopimelic acid (DAP) was added to LB medium. For strains carrying recombinant plasmids, media were supplemented with 25 g ml^{-1} kanamycin, 12 g ml^{-1} tetracycline and 15 g ml^{-1} gentamicin for *E. coli* strains, and 5 g ml^{-1} kanamycin, 5 g ml^{-1} tetracycline and 20 g ml^{-1} gentamycin for *M. gryphiswaldense* strains, respectively.

Molecular and genetic techniques. The draft genome sequence of *M. gryphiswaldense* (GenBank accession number CU459003) was used for primer design. Oligonucleotides were purchased from Sigma-Aldrich (Steinheim, Germany). All constructs were sequenced on an ABI 3700 capillary sequencer (Applied Biosystems, Darmstadt, Germany), utilizing BigDye Terminator v3.1. Sequence data were analysed with Geneious Software (Biomatters).

Using both *E. coli* CheA and *R. sphaeroides* CheA2 sequences as a query in BlastP searches, we identified four predicted proteins with strong similarity (E-value below E − 40) that were encoded on several contigs of the draft genome sequence of *M. gryphiswaldense*. Genes neighbouring the four *cheA* sequences were identified by alignment with the known sequences of *M. magneticum* AMB-1, *M. magnetotacticum* MS-1 and *M. marinus* MC-1 on nine different contigs in the *M. gryphiswaldense* genomic assembly. Gaps between contigs were closed by bridging PCR reactions (Supplementary Table 5) resulting in four contiguous operon sequences (Supplementary Table 2).

Plasmids were constructed by standard recombinant techniques. For deletion mutagenesis upstream and downstream fragments of all operons were amplified by PCR with primers including suitable restriction sites (Supplementary Table 5) and ligated into pAL01_MCS1 and pAL02/2_MCS2, respectively, resulting in pFP01 and pFP04 to pFP10. Deletion mutant strains were obtained by a two-step conjugation method involving cre-lox recombination as described before[24]. Resulting mutant strains (Supplementary Table 4) were verified by PCR reactions with primers binding to genomic sequences outside of the homologous regions used for plasmid integration (Supplementary Table 5). Successful deletions were checked by sequencing the obtained PCR products.

For the complementation of strain FP20 (MSR Δ*cheOp1*), the *cheOp1* sequence was amplified from genetic DNA with primers fp13 and fp71 and subcloned into pJet1.2. After digestion the fragment was ligated into pOR093 to obtain pFP11. This plasmid was used to obtain strain FP56 through a two-step homologous recombination method using *galK*-based counterselection[52].

Culture conditions for motility experiments. After testing of different cultivation parameters (inoculum size, cultivation temperature, oxygen concentration, medium composition and incubation time) we found that, using a small inoculum (OD 0.005), preculturing the cells under denitrifying conditions, as well as harvesting young, early logarithmic phase cells (OD 0.05), yielded maximum motility. Therefore, cells were grown under these conditions and diluted in FSM medium where needed in all subsequent chemotaxis experiments.

For selection of polarity, cells were cultured in Hungate tubes that had been sparged with 98% N_2/2% O_2 mixtures before autoclaving. Hungate tubes were placed in a Helmholtz coil cage (Supplementary Fig. 4a) and subjected to vertical magnetic fields of 0.57 mT (∼10 × the geomagnetic field strength) during growth for at least two serial transfers. Magnetic fields were applied either parallel (north pole → south pole) or antiparallel (south pole ← north pole) to oxygen gradients in the tubes ($Ox_{Low} \rightarrow Ox_{High}$). For release of magnetic selection Hungate tubes were agitated on a tube rotator at 60 r.p.m.

Chemotaxis experiments. To test for tactic reactions, we performed a set of classical chemotaxis experiments (swarm plates[8], plug-in-pond assays[53], mini-plug slides[54], commercial microscope slide chemotaxis chambers (μ-slide chemotaxis, Ibidi GmbH[16]) with different carbon sources as putative attractants (lactate,

pyruvate, acetate). Swarming occurred in soft agar with all chemicals tested, but no positive responses were detected in any other assay performed. Also light of different wavelengths did not have a detectable effect. In mini-plug assays band formation was observed even in the absence of any chemical in the plug. This pointed towards a strong aerotaxis response that possibly overrides other tactic reactions.

For the preparation of gradient soft agar tubes the FSM medium was modified by supplementing 0.3% agar, adding only 1.5 mM lactate (10% of normal concentration) and omitting peptone and nitrate. A 10 ml of sterile soft agar was poured into test tubes, and 100 µl of a microoxically grown overnight culture was dispersed into the agar. Tubes were incubated at 30 °C under oxic conditions for 2 days.

To test taxis towards nitrate, a vertical nitrate gradient was preformed in anoxic soft agar tubes by an agar plug at the bottom of test tubes containing variable nitrate concentrations (0, 10 and 100 mM). A 50 ml of an overnight batch culture was washed once in nitrate-free 10 mM HEPES buffer pH 7, resuspended in 500 µl buffer, mixed with 0.3% nitrate-free soft agar and directly poured onto previously prepared agar plugs. Tubes were directly transferred to an anaerobic glove box and incubated for 4 h. Nitrate concentration at the position where the band had formed was analysed by taking agar samples with a Pasteur pipette and using a commercial Szechrome reagent nitrate quantification kit (Polysciences).

For the preparation of swim plates only 0.2% agar was used, the concentration of carbon source (lactate) was lowered to 1.5 mM and peptone was omitted from FSM medium. Five microlitres of overnight culture was pipetted into the swim agar and plates were incubated under microxic conditions for 2 days (protocol modified from ref. 8).

Video microscopy and analysis of swimming parameters. Swimming behaviour of cells was analysed and recorded using dark-field microscopy on an upright Zeiss Axioplan microscope (Zeiss, Jena, Germany) at × 100 magnification. Cells tethered spontaneously to the coverslip by one of their flagella were recorded at × 400 magnification and 43 fps. For routine observation of swimming populations, 5 µl of an OD 0.1 cell suspension was placed under a coverslip and sealed with nail varnish. For aerobic hanging drop assays, 3 µl of cell suspension was pipetted onto a coverslip that was placed upside-down on an O-ring (Supplementary Fig. 4b). All other motility experiments were performed within a microscopic gas perfusion chamber (Ludin Chamber, Life Imaging Services) that was equilibrated with variable moisturized and precisely adjusted O_2-N_2 gas mixtures containing between 0 and 21% oxygen (Supplementary Fig. 2).

As the quantititative analysis of freely swimming WT cells was hampered by their tendency to align magnetically and distribute inhomogenously within the sample droplets, basic swimming characteristics in equilibrium conditions were analysed in the non-magnetic Δ*mamAB* strain. Homogeneous conditions within sample droplets were maintained by using strongly diluted cell suspensions (OD 0.005) and placing 0.25 µl droplets of cell suspension under a constant gas flow of 50 ml min^{-1}.

Videos were recorded with a UK1158–M camera (EHD, Damme, Germany) at a frame rate of 15 fps and a standard resolution of 1360 × 1024 pixels using VirtualDub software. Dark-field video records were analysed by a custom-made automated tracking software ('WimTaxis—Bacteria Tracking', Wimasis GmbH, München, Germany) specifically adapted to determine basic swimming characteristics. The software automatically detected swimming reversals and provided the *x*-*y* coordinates of every tracked cell for each frame.

The minimum track length was set to be 50 frames. Within the usual tracking times (depending on the time bacteria stayed in the viewing field, usually below 10 s) reversals generally were too infrequent to simply average reversal rates of single cells. Therefore, the reversal frequency analysis for each experiment was performed at the population level, and all detected reversals were divided by the total respective tracking time (sum of the temporal length of all tracks) to obtain the population average.

For the analysis of switching behaviour at different equilibrium oxygen levels, reversal frequencies were determined for each video, and the mean and s.d. of five to nine such independent experiments were determined. To illustrate the biological variability of swimming speed, the curvilinear speed values (track length divided by tracking time) corresponding to individual tracks from all independent experiments were pooled to calculate the average speed of all tracked cells.

To analyse the cell reaction to oxygen shifts, the gas stream was manually switched between oxic and anoxic. For this purpose we equipped our set-up with a three-way valve and a flow meter to adjust the flow of N_2 gas to 50 ml min^{-1} (Supplementary Fig. 2a). To determine the average reversal frequency over time, the number of detected reversals within 5-s intervals was added up from three independent video recordings and normalized to the total corresponding tracking time. To calculate mean speeds within the same 5-s intervals the instantaneous speeds (derived from the increment in *x* and *y* per frame per cell) of all tracks extending into the same window were averaged.

Analysis of swimming polarity. To analyse swimming polarity we used a modified version of the magnetodrome[55] to create homogenous tunable magnetic fields parallel to the focal plane of our microscope (Supplementary Fig. 2a). Magnetodrome software was used to control two pairs of coils in Helmholtz configuration, and a field strength of 0.26 mT (parallel to the *y*-axis of the viewing field) was used in all polarity experiments. The behaviour of polarity-selected populations was assayed by placing 0.25 µl sample droplets onto the lower coverslip of the gas perfusion chamber. After equilibration with N_2 gas for 3 min the magnetic field was switched on. After 40 s the atmosphere was shifted to 2% O_2 and the behaviour of the population was recorded.

To determine the polarity bias of individual cells, the number of focal planes within the liquid phase had to be minimized. For this purpose 1 µl of sample was sandwiched between the coverslip of the perfusion chamber and a thin agar slice. The movements of individual cells were followed manually and video-recorded. From the cumulated time periods swimming either parallel (t_{south}) or anti-parallel to **B** (t_{north}) within 1-min intervals, the population bias of individual cells (PB_{ind}) was calculated:

$$PB_{ind} = 0.5*(t_{north} - t_{south})/(t_{north} + t_{south}).$$

When cells were tracked for extended time periods (Supplementary Fig. 5d,f), PB_{ind} was calculated from all available data.

To quantitatively estimate the polarity bias of populations, we recorded 3–6 videos (40 s each for equilibrium conditions, 120 s each for shift experiments), and all swimming cells within the viewing field were tracked automatically. From the cumulated swimming distances of single cells within 10-s intervals, either anti-parallel to B (d_{north}) or parallel to B (d_{south}), the polarity bias of individuals ($PB_{distance}$) was calculated. The mean polarity bias of the population (PB_{pop}) over time was obtained by averaging the bias values of all individually tracked cells within the same intervals.

$$PB_{distance} = 0.5*(d_{north} - d_{south})/(d_{north} + d_{south})$$

$$PB_{pop} = \text{mean of } PB_{distance}$$

References

1. Bazylinski, D. A. & Frankel, R. B. Magnetosome formation in prokaryotes. *Nat. Rev. Microbiol.* **2,** 217–230 (2004).
2. Blakemore, R. P., Frankel, R. B. & Kalmijn, A. J. South-seeking magnetotactic bacteria in the Southern Hemisphere. *Nature* **286,** 384–385 (1980).
3. Simmons, S. L., Bazylinski, D. A. & Edwards, K. J. South-seeking magnetotactic bacteria in the Northern Hemisphere. *Science* **311,** 371–374 (2006).
4. De Araujo, F. F. T., Germano, F. A., Gonçalves, L. L., Pires, M. A. & Frankel, R. B. Magnetic polarity fractions in magnetotactic bacterial populations near the geomagnetic equator. *Biophys. J.* **58,** 549–555 (1990).
5. Blakemore, R. P. Magnetotactic bacteria. *Annu. Rev. Microbiol.* **36,** 217–238 (1982).
6. Frankel, R. B., Bazylinski, D. A., Johnson, M. S. & Taylor, B. L. Magneto-aerotaxis in marine coccoid bacteria. *Biophys. J.* **73,** 994–1000 (1997).
7. Zhang, W.-J., Chen, C., Li, Y., Song, T. & Wu, L.-F. Configuration of redox gradient determines magnetotactic polarity of the marine bacteria MO-1. *Environ. Microbiol. Rep.* **2,** 646–650 (2010).
8. Schultheiss, D., Kube, M. & Schüler, D. Inactivation of the flagellin gene flaA in Magnetospirillum gryphiswaldense results in nonmagnetotactic mutants lacking flagellar filaments. *Appl. Environ. Microbiol.* **70,** 3624 (2004).
9. Spormann, A. M. & Wolfe, R. S. Chemotactic, magnetotactic and tactile behaviour in a magnetic spirillum. *FEMS Microbiol. Lett.* **22,** 171–177 (1984).
10. Lefèvre, C. T., Song, T., Yonnet, J.-P. & Wu, L.-F. Characterization of bacterial magnetotactic behaviors by using a magnetospectrophotometry assay. *Appl. Environ. Microbiol.* **75,** 3835–3841 (2009).
11. Jogler, C. & Schüler, D. Genomics, genetics, and cell biology of magnetosome formation. *Annu. Rev. Microbiol.* **63,** 501–521 (2009).
12. Erglis, K. *et al.* Dynamics of magnetotactic bacteria in a rotating magnetic field. *Biophys. J.* **93,** 1402–1412 (2007).
13. Reufer, M. *et al.* Switching of Swimming Modes in Magnetospirillium gryphiswaldense. *Biophys. J.* **106,** 37–46 (2014).
14. Li, Y., Katzmann, E., Borg, S. & Schüler, D. The periplasmic nitrate reductase nap is required for anaerobic growth and involved in redox control of magnetite biomineralization in *Magnetospirillum gryphiswaldense*. *J. Bacteriol.* **194,** 4847–4856 (2012).
15. Alexandre, G., Greer, S. E. & Zhulin, I. B. Energy taxis is the dominant behavior in *Azospirillum brasilense*. *J. Bacteriol.* **182,** 6042–6048 (2000).
16. Baraquet, C., Théraulaz, L., Iobbi-Nivol, C., Méjean, V. & Jourlin-Castelli, C. Unexpected chemoreceptors mediate energy taxis towards electron acceptors in Shewanella oneidensis. *Mol. Microbiol.* **73,** 278–290 (2009).
17. Hendrixson, D. R., Akerley, B. J. & DiRita, V. J. Transposon mutagenesis of *Campylobacter jejuni* identifies a bipartite energy taxis system required for motility. *Mol. Microbiol.* **40,** 214–224 (2001).
18. Rebbapragada, A. *et al.* The Aer protein and the serine chemoreceptor Tsr independently sense intracellular energy levels and transduce oxygen, redox, and energy signals for *Escherichia coli* behavior. *Proc. Natl Acad. Sci. USA* **94,** 10541–10546 (1997).

19. Ullrich, S. & Schüler, D. Cre-lox-based method for generation of large deletions within the genomic magnetosome island of Magnetospirillum gryphiswaldense. *Appl. Environ. Microbiol.* **76,** 2439–2444 (2010).
20. Porter, S. L., Wadhams, G. H. & Armitage, J. P. Signal processing in complex chemotaxis pathways. *Nat. Rev. Microbiol.* **9,** 153–165 (2011).
21. Wuichet, K. & Zhulin, I. B. Origins and diversification of a complex signal transduction system in prokaryotes. *Sci. Signal* **3,** ra50 (2010).
22. Szardenings, F., Guymer, D. & Gerdes, K. ParA ATPases can move and position DNA and subcellular structures. *Curr. Opin. Microbiol.* **14,** 712–718 (2011).
23. Hengge, R. Principles of c-di-GMP signalling in bacteria. *Nat. Rev. Microbiol.* **7,** 263–273 (2009).
24. Lohße, A. *et al.* Functional analysis of the magnetosome island in *Magnetospirillum gryphiswaldense*: The mamAB operon is sufficient for magnetite biomineralization. *PLoS ONE* **6,** e25561 (2011).
25. Uebe, R. *et al.* Deletion of a fur-like gene affects iron homeostasis and magnetosome formation in Magnetospirillum gryphiswaldense. *J. Bacteriol.* **192,** 4192–4204 (2010).
26. Schüler, D., Spring, S. & Bazylinski, D. A. Improved technique for the isolation of magnetotactic spirilla from a freshwater sediment and their phylogenetic characterization. *Syst. Appl. Microbiol.* **22,** 466–471 (1999).
27. Flies, C. B. *et al.* Diversity and vertical distribution of magnetotactic bacteria along chemical gradients in freshwater microcosms. *FEMS Microbiol. Ecol.* **52,** 185–195 (2005).
28. Schleifer, K. H. *et al.* The Genus Magnetospirillum gen. nov. Description of Magnetospirillum gryphiswaldense sp. nov. and Transfer of Aquaspirillum magnetotacticum to Magnetospirillum magnetotacticum comb. nov. *Syst. Appl. Microbiol.* **14,** 379–385 (1991).
29. Esquivel, D. M. & Lins De Barros, H. G. P. Motion of magnetotactic microorganisms. *J. Exp. Biol.* **163,** 153–163 (1986).
30. Blakemore, R. Magnetotactic bacteria. *Science* **190,** 377–379 (1975).
31. Kirschvink, J. L. Magnetoreception: Homing in on vertebrates. *Nature* **390,** 339–340 (1997).
32. Kirschvink, J. L., Walker, M. M. & Diebel, C. E. Magnetite-based magnetoreception. *Curr. Opin. Neurobiol.* **11,** 462–467 (2001).
33. Ma, Q., Chen, C. C., Wei, S., Wu, L.-F. & Song, T. Construction and operation of a microrobot based on magnetotactic bacteria in a microfluidic chip. *Biomicrofluidics* **6,** 24107–2410712 (2012).
34. Taherkhani, S., Mohammadi, M., Daoud, J., Martel, S. & Tabrizian, M. Covalent binding of nanoliposomes to the surface of magnetotactic bacteria for the synthesis of self propelled therapeutic agents. *ACS Nano* **8,** 5049–5060 (2014).
35. Dogra, G. *et al.* Sinorhizobium meliloti CheA complexed with CheS exhibits enhanced binding to CheY1, resulting in accelerated CheY1 dephosphorylation. *J. Bacteriol.* **194,** 1075–1087 (2012).
36. Kirby, J. R. Chemotaxis-like regulatory systems: unique roles in diverse bacteria. *Annu. Rev. Microbiol.* **63,** 45–59 (2009).
37. Thar, R. & Fenchel, T. Survey of motile microaerophilic bacterial morphotypes in the oxygen gradient above a marine sulfidic sediment. *Appl. Environ. Microbiol.* **71,** 3682–3691 (2005).
38. Mitchell, J. G. & Kogure, K. Bacterial motility: links to the environment and a driving force for microbial physics. *FEMS Microbiol. Ecol.* **55,** 3–16 (2006).
39. Martel, S., Tremblay, C. C., Ngakeng, S. & Langlois, G. Controlled manipulation and actuation of micro-objects with magnetotactic bacteria. *Appl. Phys. Lett.* **89,** 233904 (2006).
40. Berg, H. C. & Brown, D. A. Chemotaxis in *Escherichia coli* analysed by three-dimensional tracking. *Nature* **239,** 500–504 (1972).
41. Zhulin, I. B. & Armitage, J. P. Motility, chemokinesis, and methylation-independent chemotaxis in Azospirillum brasilense. *J. Bacteriol.* **175,** 952–958 (1993).
42. Armitage, J. P., Pitta, T. P., Vigeant, M. A., Packer, H. L. & Ford, R. M. Transformations in flagellar structure of Rhodobacter sphaeroides and possible relationship to changes in swimming speed. *J. Bacteriol.* **181,** 4825–4833 (1999).
43. Yamaichi, Y. *et al.* A multidomain hub anchors the chromosome segregation and chemotactic machinery to the bacterial pole. *Genes Dev.* **26,** 2348–2360 (2012).
44. Bazylinski, D. A., Dean, A. J., Schüler, D., Phillips, E. J. & Lovley, D. R. N2-dependent growth and nitrogenase activity in the metal-metabolizing bacteria, Geobacter and Magnetospirillum species. *Environ. Microbiol.* **2,** 266–273 (2000).
45. Heyen, U. & Schüler, D. Growth and magnetosome formation by microaerophilic Magnetospirillum strains in an oxygen-controlled fermentor. *Appl. Microbiol. Biotechnol.* **61,** 536–544 (2003).
46. Zhulin, I. B., Bespalov, V. A., Johnson, M. S. & Taylor, B. L. Oxygen taxis and proton motive force in *Azospirillum brasilense*. *J. Bacteriol.* **178,** 5199–5204 (1996).
47. Berg, H. C. & Turner, L. Cells of *Escherichia coli* swim either end forward. *Proc. Natl Acad. Sci. USA* **92,** 477–479 (1995).
48. Krieg, N. R., Tomelty, J. P. & Wells, J. S. Inhibition of flagellar coordination in Spirillum volutans. *J. Bacteriol.* **94,** 1431–1436 (1967).
49. Philippe, N. & Wu, L.-F. An MCP-like protein interacts with the MamK cytoskeleton and is involved in magnetotaxis in Magnetospirillum magneticum AMB-1. *J. Mol. Biol.* **400,** 309–322 (2010).
50. Davis, B. M. & Waldor, M. K. Establishing polar identity in gram-negative rods. *Curr. Opin. Microbiol.* **16,** 752–759 (2013).
51. Lumsden, C. J. Dual inheritance in haploid organisms: a model of magnetotactic bacteria. *J. Theor. Biol.* **111,** 1–16 (1984).
52. Raschdorf, O., Plitzko, J. M., Schüler, D. & Müller, F. D. A tailored galK counterselection system for efficient markerless gene deletion and chromosomal tagging in *Magnetospirillum gryphiswaldense*. *Appl. Environ. Microbiol.* **80,** 4323–4330 (2014).
53. Tso, W. & Adler, J. Negative chemotaxis in *Escherichia coli*. *J. Bacteriol.* **118,** 560–576 (1974).
54. Parales, R. E., Ditty, J. L. & Harwood, C. S. Toluene-degrading bacteria are chemotactic towards the environmental pollutants benzene, toluene, and trichloroethylene. *Appl. Environ. Microbiol.* **66,** 4098–4104 (2000).
55. Steinberger, B., Petersen, N., Petermann, H. & Weiss, D. G. Movement of magnetic bacteria in time-varying magnetic fields. *J. Fluid Mech.* **273,** 189 (2006).
56. Greene, S. E., Brilli, M., Biondi, E. G. & Komeili, A. Analysis of the CtrA pathway in Magnetospirillum reveals an ancestral role in motility in alphaproteobacteria. *J. Bacteriol.* **194,** 2973–2986 (2012).
57. Kojadinovic, M., Sirinelli, A., Wadhams, G. H. & Armitage, J. P. New motion analysis system for characterization of the chemosensory response kinetics of Rhodobacter sphaeroides under different growth conditions. *Appl. Environ. Microbiol.* **77,** 4082–4088 (2011).

Acknowledgements

We thank. Richard B. Frankel for helpful discussions at different stages of the project, Nikolai Petersen for help with the magnetodrome set-up and Denis Bartolo for advice on the microdroplet assays. We thank Julia Hofmann and Isabelle Mai for construction of deletion strains. The project was funded by a grant of the Deutsche Forschungsgemeinschaft (Schu 1080/16-1). F.P. has been supported by a BayEFG scholarship. J.P.A. is funded by UK BBSRC.

Author contributions

F.P., J.P.A. and D.S. designed research; F.P. performed research; F.P., D.S. and J.P.A. analysed data; F.P., D.S., and J.P.A. wrote the paper.

Additional information

Supplementary Information accompanies this paper at http://www.nature.com/naturecommunications

Competing financial interests: The authors declare no competing financial interests.

Reprints and permission information is available online at http://npg.nature.com/reprintsandpermissions/

How to cite this article: Popp, F. *et al.* Polarity of bacterial magnetotaxis is controlled by aerotaxis through a common sensory pathway. *Nat. Commun.* 5:5398 doi: 10.1038/ncomms6398 (2014).

Supplement Publication 1

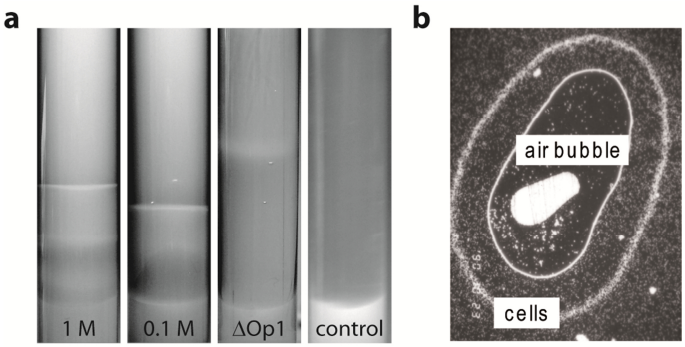

Supplementary Fig. 1. **Energy taxis of *M. gryphiswaldense*.** (a) Nitrate taxis in gradient tubes. Concentrated cells were washed and mixed with nitrate-free 0.3% soft-agar that was layered over 2% agar plugs containing 0.1 M, 1 M or no nitrate. Tubes were incubated for 4-8 h in an oxygen-free atmosphere at room temperature. The position of band formation was correlated with nitrate concentration in the plug. (b) WT cells forming an aerotactic band around an air bubble entrapped under a cover slip.

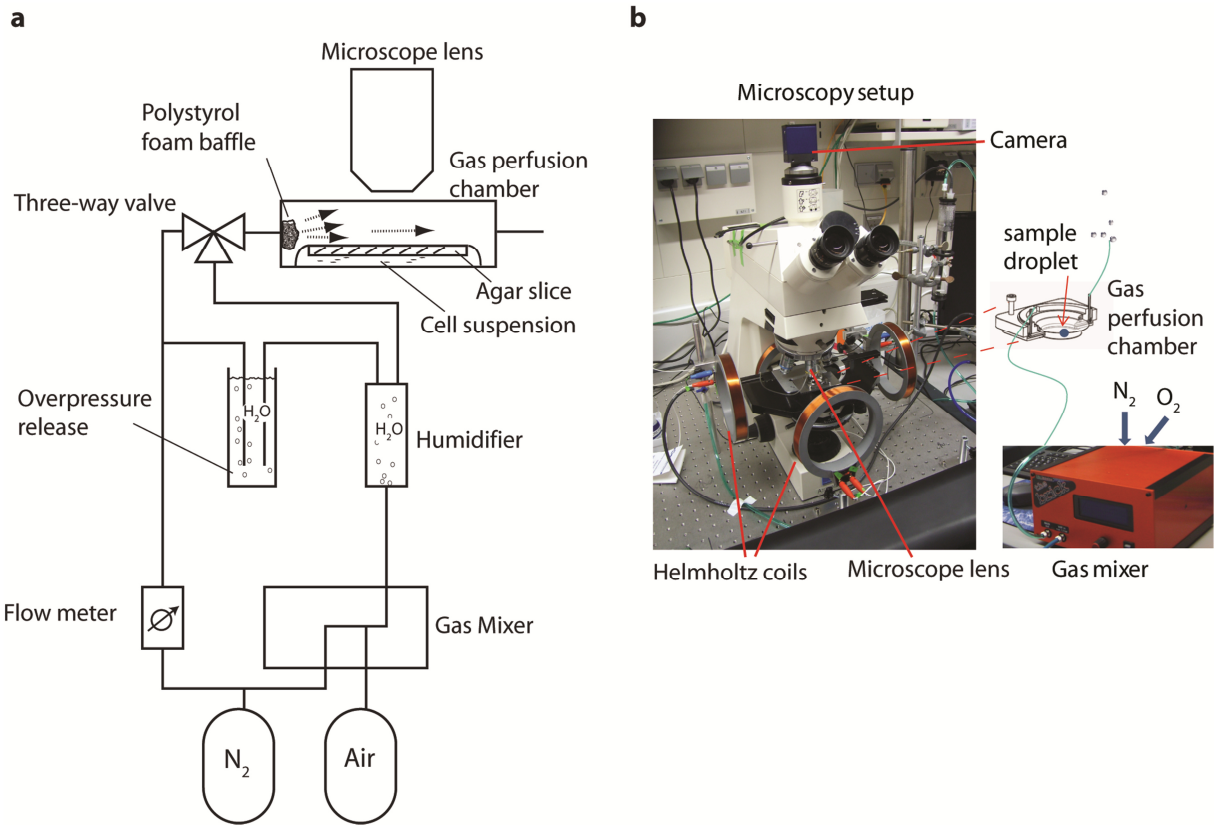

Supplementary Fig. 2. **Microscopy setup used for analysis of swimming behavior under defined atmospheric conditions.** Gas flow diagram (a) and overview picture (b) of microscopy setup. Nitrogen and air were mixed with a gas mixer (The Brick, Life Imaging Services) to obtain precisely adjusted gas mixtures. Samples were pipetted onto the lower coverslip of a gas perfusion chamber and cells were observed with a Zeiss Axioplan microscope at 100x magnification using dark-field microscopy. Cells were exposed to homogenous magnetic fields parallel to the focal plane by using a modified version of the magnetodrome (Steinberger et al. 2006).

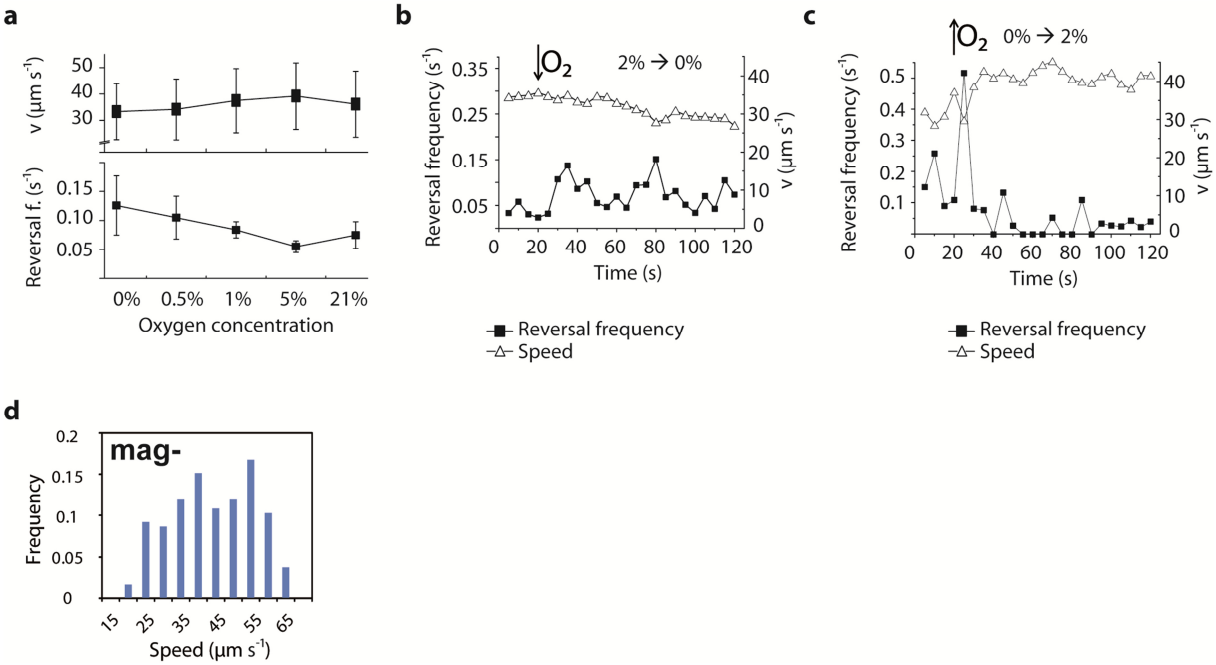

Supplementary Fig. 3. **Swimming speed and reversal frequency under equilibrium and temporal shift conditions.** (a) Swimming speeds and reversal rates of non-magnetic Δ*mamAB* mutant cells under equilibrium conditions. Mean and standard deviation of at least five videos are shown. (b) Reversal rates and swimming speeds of Δ*mamAB* cells recorded in the gas perfusion chamber. Cells were subjected to an abrupt shift from 2% to 0% oxygen after 20 s (↓O_2). Mean values of reversal frequency and speed of three independent experiments calculated for 5-s intervals are shown. Cells were equilibrated at 2% oxygen for 3 min before the shift. (c) Speed and reversal frequency of complemented Δ*cheOp1*$^+$ cells upon upshift from 0% to 2% oxygen after 20 s (↑O_2). (d) Histogram depicting frequency versus swimming speed of Δ*mamAB* cells in a standard wet mount.

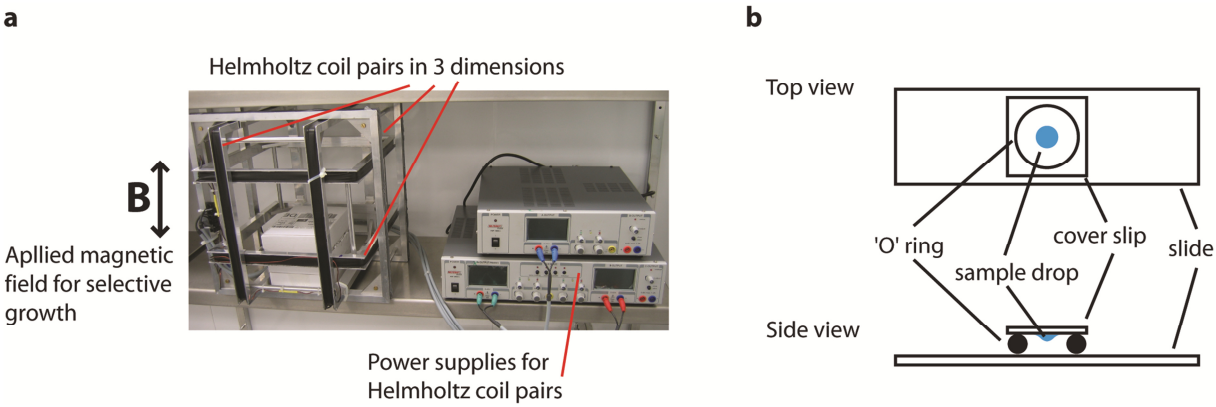

Supplementary Fig. 4. **Selective cultivation and standard assay for analysis of magnetic swimming polarity.** (a) Helmholtz coil cage consisting of three mutually perpendicular pairs of Helmholtz coils used for selective cultivation in defined magnetic fields. Cells were exposed to magnetic fields mimicking the inclination of the geomagnetic field on the northern and southern hemisphere. (b) Schematic top and side view of the classical aerobic hanging drop assay.

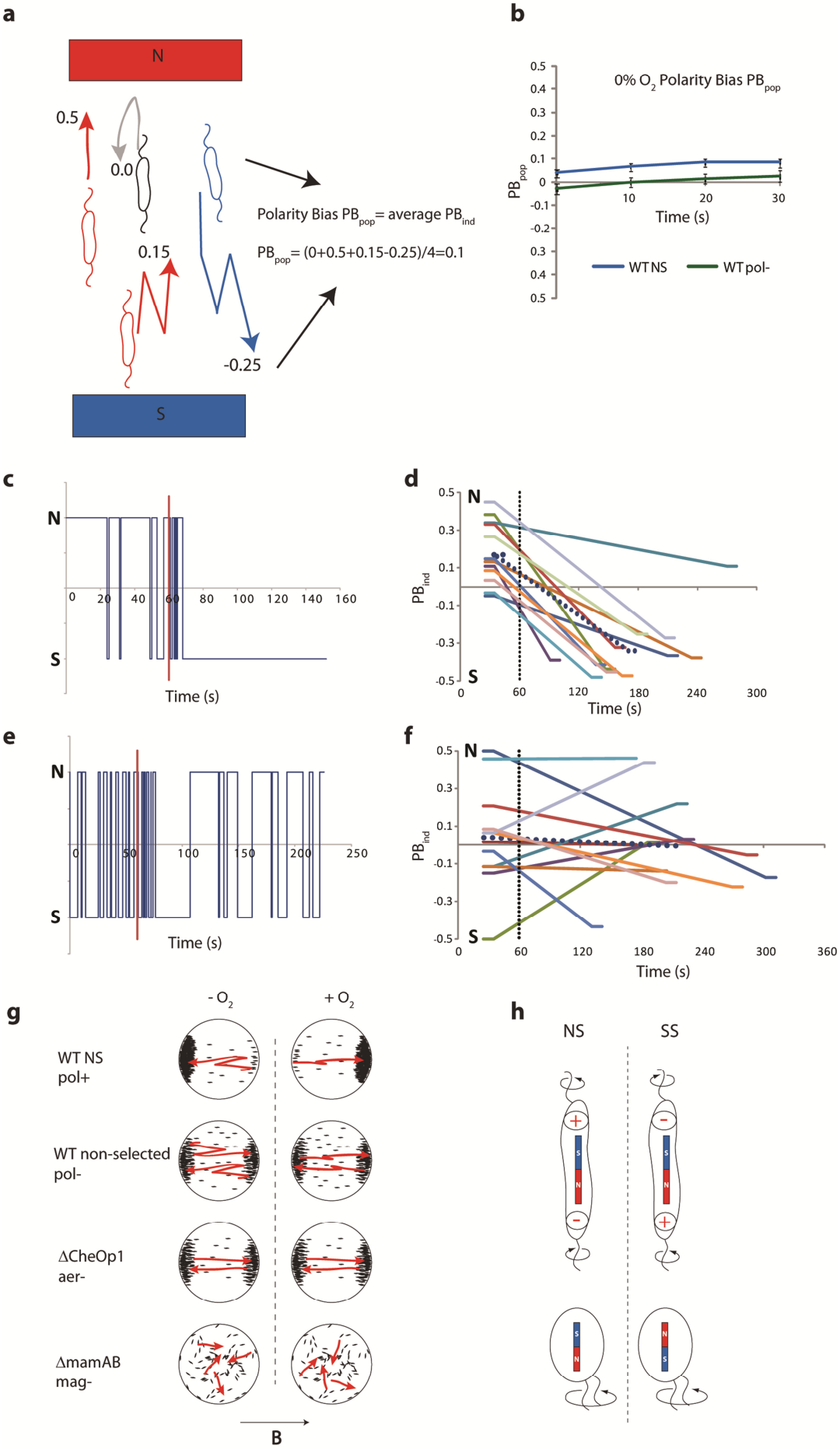
a
N
S
0.5
0.0
0.15
-0.25
Polarity Bias PB$_{pop}$= average PB$_{ind}$
PB$_{pop}$= (0+0.5+0.15-0.25)/4=0.1
b
0% O$_2$ Polarity Bias PB$_{pop}$
PB$_{pop}$
Time (s)
WT NS
WT pol-
c
N
S
Time (s)
d
PB$_{ind}$
Time (s)
e
Time (s)
f
PB$_{ind}$
Time (s)
g
- O$_2$
+ O$_2$
WT NS pol+
WT non-selected pol-
ΔCheOp1 aer-
ΔmamAB mag-
B
h
NS
SS

Supplementary Fig. 5. **Analysis of swimming polarity.** (a) Determination of single cell and population polarity bias. Sketch of idealized swimming tracks (arrows) of an exemplary population. Cells predominantly swimming towards the north pole or south pole (of a bar magnet) are marked in red and blue, respectively. Polarity bias values of individuals (PB_{ind}) ranging between -0.5 and 0.5 are indicated at the end of the respective tracks. Polarity bias of the population (PB_{pop}) is calculated by averaging over all PB_{ind} values. (b) Population polarity bias (PB_{pop}) of WT *pol*- and WT NS cells under anoxic equilibrium conditions calculated for 10s-intervals. (c and e**)** Single cell plots of a representative WT NS and WT *pol*- cell, respectively, illustrating swimming periods towards north and south derived from analysis of video recordings of manually tracked single cells. Cells were subjected to an atmospheric shift from 0% to 2% oxygen after 60 s (red line), causing numerous swimming reversals. (d and f) Extended version of Fig. 6b showing PB_{ind} values of WT NS and WT *pol*- cells, respectively, before and after the shift from 0% to 2% oxygen. PB_{ind} values were obtained by manual long-term tracking of single cells. Cells were observed as long as feasible after the shift. Lines representing single cells end at the respective time points when the tracking was stopped. (g) Idealized reaction of bulk populations in microdroplets exposed to a horizontal magnetic field to anoxic (left side) and oxic conditions (right side). Behavior of selected and non-selected WT cells, and of non-aerotactic and non-magnetic mutant cells is shown. Representative, idealized swimming tracks of individual cells are depicted as red arrows. (h) Hypothetical model for determination of swimming polarity in spirilla and cocci. In spirilla reversal of swimming polarity might involve reshaping the cellular polarity axis (+/-symbols), resulting in inversed motor behavior. Conversely, in magnetococci reversal of swimming polarity might depend on the rare reversal of the magnetic dipole of the inherited magnetosome chain, as indicated by the inability of magnetococci to grow in fields of the "wrong" inclination (Zhang et al. 2010).

Supplementary Table 1. **Swimming parameters of *M. gryphiswaldense* WT and Δ*mamAB* in a standard wet mount exposed to a homogenous magnetic field of 0.26 mT.**

	Reversal frequency [s^{-1}]	Speed [μm^{-1}]	Directionality*	Theoretical track length [μm]†	Mean reversal angle‡
WT	0.031 ± 0.007	41.6 ± 3.5	0.887 ± 0.021	1322	13.3° ± 11.4°
Δ*mamAB*	0.032 ± 0.014	41.6 ± 1.0	0.833 ± 0.003	1288	14.3° ± 9.0°

Mean and standard deviation of the population averages of three independent replicates. *Ratio of cell displacement and track length. †Average speed divided by reversal frequency. ‡Mean reversal angle was calculated by comparing the tracking positions 10 frames (0.67 s) before and after the reversal relative to the coordinates of the reversal event.

Supplementary Table 2. **Sequence characteristics of components of *M. gryphiswaldense* chemotaxis operons.**

Operon	Gene (locus tag*)	gene product (important domains)	expressed[†]	number of aa	size [kDa]	Best BLAST hit[‡]	E value	Conserved in MTB[§]
CheOp1								
	cheA1 (*mgr3029, mgr1821*)	CheA histidine kinase + Rec domain	+	885	96.0	CheA signal transduction histidine kinase [*Rhodospirillum rubrum*]	0.0	AMB-1, MS-1, MC-1
	cheW1 (*mgr1820*)	CheW adaptor protein		161	17.8	Chemotaxis protein cheW [*Phaeospirillum molischianum*]	4E-89	AMB-1, MS-1, MC-1
	cheY1 (*mgr1819*)	CheY-like receiver		121	13.6	Two component response regulator cheY [*Phaeospirillum molischianum*]	4E-76	AMB-1, MS-1, MC-1
	cheB1 (*mgr1818*)	CheB MCP-methylesterase		385	40.4	CheB-glutamate methylesterase [*Phaeospirillum molischianum*]	0.0	AMB-1, MS-1, MC-1
	cheR1 (*mgr1817*)	CheR MCP-methylase	+	293	32.9	Chemotaxis protein methyltransferase [*Phaeospirillum molischianum*]	5E-168	AMB-1, MS-1, MC-1
CheOp2								
	mcp2-1 (*mgr0265*)	Methyl-accepting chemotaxis protein	+	566	58.8	putative methyl-accepting chemotaxis protein [*Azospirillum lipoferum*]	2E-103	AMB-1, MS-1
	mgr0266	conserved hyp. protein (Cache_2 domain)		152	16.7	hypothetical protein TH3_13629 [*Thalassospira xiamenensis*]	7E-42	AMB-1, MS-1
	parA2 (*mgr0267*)	parA-like ATPase	+	362	39.5	ATPase involved in chromosome partitioning [*Phaeospirillum molischianum*]	0.0	AMB-1, MS-1
	cheW2-1 (*mgr0268*)	CheW adaptor protein		171	18.3	chemotaxis signal transduction protein [*Microvirga* sp. WSM3557]	1E-17	AMB-1, MS-1
	cheR2 (*mgr0139*)	CheR MCP-methylase+ TPR domain		461	51.8	Methylase of chemotaxis methyl-accepting protein [*Verrucomicrobium spinosum* DSM 4136]	0.0	AMB-1, MS-1, MC-1
	cheW2-2 (*mgr0140*)	CheW adaptor protein		188	20.8	chemotaxis signal transduction protein [*Desulfomonile tiedjei*]	2E-16	AMB-1, MS-1, MC-1
	mcp2-2 (*mgr0141*)	Methyl-accepting	+	539	58.6	methyl-accepting chemotaxis protein	3E-138	AMB-1, MS-1,

		chemotaxis protein				[*Rhodospirillum centenum*]		MC-1
	cheA2 (*mgr0142*)	CheA histidine kinase + Rec domain	+	758	82.7	Histidine Sensor Kinase CheA3 [*Rhodospirillum centenum*]	5E-175	MS-1, MC-1
	cheB2 (*mgr0143*)	CheB MCP-methylesterase		348	36.6	protein-glutamate methylesterase CheB [*Rhodospirillum centenum*]	2E-119	AMB-1, MS-1, MC-1
	mgr0144	Signal transduction histidine kinase	+	565	62.7	Signal transduction histidine kinase [*Azospirillum amazonense*]	3E-175	AMB-1, MS-1
	mgr0145	Signal transduction histidine kinase containing PAS domain		530	58.0	histidine kinase [*Azospirillum amazonense* Y2]	3E-89	AMB-1, MS-1
	mgr0146	conserved hyp. protein, DUF2478 P-loop NTPase superfamily		160	17.3	conserved protein of unknown function [*Azospirillum brasilense*]	9E-36	-
CheOp3								
	mcp3 (*mgr0209*)	Methyl-accepting chemotaxis protein		637	67.6	Methyl-accepting chemotaxis protein [*Rhodospirillum photometricum*]	0.0	AMB-1, MS-1, MC-1
	cheB3	CheB MCP-methylesterase		351	36.2	Chemotaxis response regulator protein-glutamate methylesterase 5 [*Rhodospirillum photometricum*]	5E-146	AMB-1, MS-1, MC-1
	cheR3	CheR MCP-methylase+ TPR domain		477	52.4	Methylase of chemotaxis methyl-accepting protein [*Rhodospirillum photometricum*]	6E-133	AMB-1, MS-1, MC-1
	cheA3 (*mgr0059*)	CheA histidine kinase + Rec domain		695	75.6	CheA signal transduction histidine kinase [*Thiorhodospira sibirica*]	0.0	AMB-1, MS-1, MC-1
	cheY3 (*mgr0058*)	CheY-like receiver		120	12.9	response regulator receiver protein [*Thiorhodospira sibirica*]	2E-37	AMB-1, MS-1, MC-1
	mgr0057	signal transduction protein containing GGDEF domain		556	61.1	response regulator containing a CheY-like receiver domain and a GGDEF domain [*Rhodospirillum photometricum*]	0.0	AMB-1, MS-1, MC-1
	cheW3 (*mgr0056*)	CheW adaptor protein		179	19.6	CheW protein [Thiorhodospira sibirica]	2E-53	AMB-1, MS-1, MC-1
	mgr0055	conserved hyp. protein		113	12.3	hypothetical protein ThisiDRAFT_0830 [Thiorhodospira	1E-07	AMB-1, MS-1, MC-1

						sibirica]		
CheOp4								
	cheY4 (*mgr0962*)	CheY-like receiver	+	121	13.0	Chemotaxis two-component response regulatory protein cheY [*Phaeospirillum molischianum*]	2E-74	MC-1, RS-1
	cheA4 (*mgr0963*, *mgr0535*)	CheA histidine kinase	+	711	75.6	Two-component sensor histidine kinase chemotaxis protein cheA [*Phaeospirillum molischianum*]	0.0	MC-1, RS-1
	mgr0536	hypothetical protein		33	3.6	-	-	-
	cheW4 (*mgr0537*)	CheW adaptor protein		163	17.5	Chemotaxis protein cheW [*Phaeospirillum molischianum*]	1E-65	-
	mcp4.1 (*mgr0538*)	Methyl-accepting chemotaxis protein	+	806	86.3	Putative Methyl-accepting chemotaxis protein [*Phaeospirillum molischianum*]	0.0	MS-1, MC-1
	cheR4 (*mgr0539*)	CheR MCP-methylase		287	33.4	Chemotaxis protein methyltransferase [*Phaeospirillum molischianum*]	3E-138	MC-1, RS-1
	cheD4 (*mgr0540*)	CheD MCP glutamine deamidase CheD		213	23.7	Chemotaxis protein cheD [*Phaeospirillum molischianum*]	8E-118	-
	cheB4 (*mgr0541*)	CheB MCP-methylesterase		353	37.4	CheB-glutamate methylesterase [*Phaeospirillum molischianum*]	0.0	MC-1, RS-1
	mgr0542	conserved hyp. protein		162	18.1	conserved hypothetical protein [*Phaeospirillum molischianum*]	2E-43	-
	mgr0543	diguanylate phosphodiesterase		247	27.6	diguanylate phosphodiesterase [*Rhodospirillum rubrum*]	7E-100	AMB-1, MS-1
	mcp4.2 (*mgr0544*)	Methyl-accepting chemotaxis protein		739	79.1	methyl-accepting chemotaxis protein [*Bradyrhizobium* sp. S23321]	6E-110	AMB-1, MS-1

*underlined: respective ORF contains only part of the described gene [†]found expressed in available proteomic data (Uebe et al. 2010; Lohße et al. 2011) [‡]the best hit is shown, MTB hits were omitted [§]sharing at least 25% identity and conserved in operons with similar organisation containing homologous genes

Supplementary Table 3. **Methyl-accepting chemotaxis proteins of *M. gryphiswaldense***

Uniprot Accession	Submitted name	ORF name	Length [aa]	HAMP + MA domain	found in proteomic data set
A4TVY3	Histidine kinase, HAMP region:Bacterial chemotaxis sensory transducer	MGR_0019	535	x	
A4TUV0	Methyl-accepting chemotaxis protein	MGR_0141	539	x	x
A4TUV7	Methyl-accepting chemotaxis protein	MGR_0148	413	x	x
A4U3M2	Histidine kinase, HAMP region:Bacterial chemotaxis sensory transducer	MGR_0183	566	x	
A4TUL7	Histidine kinase, HAMP region:Bacterial chemotaxis sensory transducer	MGR_0209	618	x	
A4TU91	Methyl-accepting chemotaxis protein	MGR_0265	210		x
A4U0G0	PAS	MGR_0403	975		x
A4TYK4	Histidine kinase, HAMP region:Bacterial chemotaxis sensory transducer	MGR_0485	567	x	
A4TYA4	Histidine kinase, HAMP region:Bacterial chemotaxis sensory transducer	MGR_0520	564	x	
A4TXX5	Methyl-accepting chemotaxis protein	MGR_0538	806	x	x
A4TXY1	Histidine kinase, HAMP region:Bacterial chemotaxis sensory transducer	MGR_0544	739	x	
A4TXZ3	Methyl-accepting chemotaxis protein	MGR_0556	626	x	x
A4TXB0	Chemotaxis sensory transducer	MGR_0592	461		
A4U265	Methyl-accepting chemotaxis protein	MGR_0691	666	x	
A4TWM5	Methyl-accepting chemotaxis sensory transducer	MGR_0748	645	x	x
A4U2R4	Methyl-accepting chemotaxis protein	MGR_0816	441		x
A4TVU3	Methyl-accepting chemotaxis protein	MGR_0838	462		
A4U2K5	Methyl-accepting chemotaxis protein	MGR_0874	474	x	x
A4TV14	Histidine kinase, HAMP region:Bacterial chemotaxis sensory transducer	MGR_0983	773	x	x
A4TUR6	Methyl-accepting chemotaxis protein	MGR_1006	770	x	x
A4U1U8	Methyl-accepting chemotaxis protein	MGR_1102	560	x	
A4U0Z3	Methyl-accepting chemotaxis protein	MGR_1222	567	x	x
A4TZG9	Methyl-accepting chemotaxis protein	MGR_1492	696	x	
A4TZI1	Methyl-accepting chemotaxis protein	MGR_1504	539	x	x
A4TYD6	Methyl-accepting chemotaxis protein	MGR_1567	231		x
A4TXG0	Methyl-accepting chemotaxis protein	MGR_1637	560	x	x
A4U2B3	Methyl-accepting chemotaxis sensory transducer	MGR_1707	434		x
A4U2K6	Histidine kinase, HAMP region:Bacterial chemotaxis sensory transducer	MGR_1824	189		
A4U2L0	Methyl-accepting chemotaxis protein	MGR_1828	552	x	
A4U2Q0	Chemotaxis sensory transducer	MGR_1868	295		x
A4U446	Methyl-accepting chemotaxis protein	MGR_1945	652	x	x
A4TUD0	Methyl-accepting chemotaxis protein	MGR_2040	165		

A4TU86	Methyl-accepting chemotaxis protein	MGR_2047	260		
A4U0B5	Methyl-accepting chemotaxis protein	MGR_2126	444		
A4U015	Methyl-accepting chemotaxis protein	MGR_2167	356		
A4TZ92	Methyl-accepting chemotaxis sensory transducer	MGR_2253	690	x	
A4TY59	Methyl-accepting chemotaxis protein	MGR_2382	565	x	x
A4TY60	Histidine kinase, HAMP region:Bacterial chemotaxis sensory transducer	MGR_2383	565	x	x
A4TX79	Methyl-accepting chemotaxis sensory transducer	MGR_2563	562	x	
A4TUY6	Methyl-accepting chemotaxis protein	MGR_2852	565	x	x
A4TUU6	Methyl-accepting chemotaxis protein	MGR_2868	831	x	x
A4TU99	Methyl-accepting chemotaxis protein	MGR_2966	254		x
A4U0S6	ABC-type branched-chain amino acid transport systems, periplasmic component	MGR_3210	733	x	
A4TZA6	Methyl-accepting chemotaxis protein	MGR_3291	692	x	x
A4TYH4	PAS	MGR_3404	560	x	
A4U3V6	Methyl-accepting chemotaxis protein	MGR_3507	642	x	
A4U2D4	Methyl-accepting chemotaxis protein	MGR_3544	642		
A4U2E9	Histidine kinase, HAMP region:Bacterial chemotaxis sensory transducer	MGR_3559	653	x	
A4U2F5	Histidine kinase, HAMP region:Bacterial chemotaxis sensory transducer	MGR_3565	565	x	x
A4TW49	Chemotaxis sensory transducer	MGR_3782	342		x
A4U4U5	Methyl-accepting chemotaxis receptor/sensory transducer	MGR_3970	676		
A4U4W9	Predicted Methyl-accepting chemotaxis protein	MGR_3994	479		x
A4U4X2	Pmethyl-accepting chemotaxis receptor/sensory transducer	MGR_3997	562	x	x
A4U5H6	Methyl-accepting chemotaxis receptor/sensory transducer	MGR_4201	598	x	x
A4U5I5	Predicted methyl-accepting chemotaxis protein	MGR_4210	859	x	
A4U5I6	Methyl-aceppting chemotaxis transducer	MGR_4211	479	x	x

Supplementary Table 4. **Strains and Plasmids used in this study**

Name	Description	Reference/Source
Plasmids		
pJet1.2	Ap^r, *eco47IR*, *rep* (pMB-1)	Fermentas
pK19mobGII	Km^r, pMB-1 replicon, *gusA*, *lacZα*	(Katzen et al. 1999)
pAL01_MCS1	pK19mobGII, lox71, MCS from pBBR-MCS5	(Lohße et al. 2011)
pAL02/2_MCS2	pT18*mob*2, lox66, MCS from pBBR-MCS5	(Lohße et al. 2011)
pCM157	Tet^r, Cre expression vector	(Marx & Lidstrom 2002)
pOR093	*galK* counterselection	(Raschdorf et al. 2013)
pFP01	pK19mobGII with *cheOp2* upstr fragment	this study
pFP04	pAL02/2 with *cheOp2* dstr fragment	this study
pFP05	pAL01 with *cheOp1* upstr fragment	this study
pFP06	pAL01 with *cheOp4* upstr fragment	this study
pFP07	pAL02/2 with *cheOp1* dstr fragment	this study
pFP08	pAL02/2 with *cheOp4* dstr fragment	this study
pFP09	pAL01 with *cheOp3* upstr fragment	this study
pFP10	pAL02/2 with *cheOp3* dstr fragment	this study
pFP11	pOR093 with *cheOp1* fragment	this study
Strains		
E. coli BW29427	*thrB1004 pro thi rpsL hsdSlacZ* ΔM15 *RP4-1360 Δ(araBAD)567 ΔdapA1341::[erm pir]tra*	Datsenko and Wanner (unpublishe
E. coli DH5a	*fhuA2 Δ(argF-lacZ)U169 phoA glnV44* ϕ80 *Δ(lacZ)*M15 *gyrA96 recA1 relA1 endA1 thi-1 hsdR17*	Invitrogen
MSR-1 WT	*M. gryphiswaldense* MSR-1 R3/S1,Rif^r Sm^r, spontaneous mutant	(Schultheiss & Schüler 2003)
ΔmamAB#K7	MSR Δ*mamAB*	(Ullrich & Schüler 2010)
ΔctrA	MSR Δ*ctrA*, non-motile mutant	I. Mai (unpublished)
FP13	MSR Δ*cheOp2*	this study
FP14	MSR Δ*cheOp4*	this study
FP20	MSR Δ*cheOp1*	this study
FP24	MSR Δ*cheOp3*	this study
FP56	MSR Δ*cheOp1* complemented	this study
FP57	MSR Δ*cheOp2+4*	this study
FP63	MSR Δ*cheOp234*	this study

Supplementary Table 5. **Primers used in this study**

	Name	Sequence
Primer sequences used to connect chemotaxis operon sequences		
fp01	mgr3029-1821_for	ACGGAAACCTCGGAGAGTC
fp02	mgr3029-1821_rev	AGCACCAGCTCGGAAACC
fp03	mgr0371-0265_for	GCTTTGTTCATCGGCATTTCC
fp04	mgr0371-0265_rev	CTGGGTCAGGCTTTTCAC
fp05	mgr0268-0139_for	CACCGACATCAACCAGAAATTCC
fp06	mgr0268-0139_rev	TTCAGGGCATCACCAATCAACG
fp07	mgr0209-0059_for	CACCGCCTTCAGCCATACC
fp08	mgr0209-0059_rev	CACCACCTCGCCCATCAG
fp09	mgr0963-0535_for	CACGAACCGCTGCTGATGC
fp10	mgr0963-0535_rev	CGCCTTGGAAAACAACGCCTTG
fp11	mgr0209-0059_for2	TCTTGGTGGTGTCGTCGGTG
fp12	mgr0209-0059_rev2	TCCTCCATCAGCAATTCCTGG
fp13	mgr3029-1821_for2	CGTGCCTGCGATAAGTGGAC
fp14	mgr3029-1821_rev2	TCGGTGGTGATGTGGCTCAAG
fp39	mgr3028_for3	TGCTCAACCTGATGCTGTTGG
fp40	mgr1821_rev3	GGTCAGTTCCACCTTCAGGC
Primer sequences used for construction of deletion vectors		
fp32	Op3downstr_rev	GAGCTCGGTGGTGAAATCCAGTTGACC
fp33	Op4upstr_for	ATGATTACGAATTCGAGCTCGGTACCCGGGCCAGCGGAAGAAGGCATACG
fp37	Op2upstr_for	CCCGGGAAGCCAAAGCCAATGGAGCC
fp38	Op2upstr_rev	ATAACTTCGTATAATGTATGCTATACGAACGGTACCATTTTCTTAGCGGCAACCG
fp43	Op2dstr_for	TAGGATCCAGGTAAAGCCCGAGACTTCC
fp44	Op2dstr_rev	GGAAGCTTACATCGACGCCCTGAAAGAGG
fp50	Op1_Ins_rev	ATGCGGCCGCTTATCCTCGTCGCTACCTTCGG
fp51	Op1_Ins_for	GTCGCTGGAAGCACGCCTG
fp52	Op4_Ins_rev	ATGCGGCCGCTTAGGTGATGCCGTCCATTTCC
fp54	Op1_dIns_for	ATGGATCCTTCCATGACATCGACCGCTGC
fp55	Op1_dIns_rev	CAGGGCATCGGGATAGTCG
fp56	Op4_dIns_for	ATGGATCCTTGATGTCGCCTAATCCTCGC
fp57	Op4_dIns_rev	GGAACAATTCGCCGTCATCG
fp71	Op1dstr_scr	CCTTGCTGGGAGTGGAGCC
fp74	Op3_upIns_for	ATGGATCCGATGTTGCTGATGATGGCACC
fp75	Op3_upIns_rev	ATGCGGCCGCTTGCCCGTCCCCAAATCATC
fp77	Op3_dIns_for	ATGGATCCGGTCCGATAAAGCAACAGCC
Primer sequences used to verify operon deletions		
fp45	Op2up_int	CCAAGGACTATCCCGATCTG
fp49	Op2dstr_Scr	TGCCGTTGCTGACCACCTTG

fp72	Op4upstr_scr	CAACTGAACCAACTGACCACC
fp73	Op4dstr_scr	CTGGGGCTGGTGCTTTACG
fp78	Op1_upIns_scr	GACGATCTGTGCGTGAAAACC
fp79	Op1_dIns_scr2	TGGCGGCGTTCCATGCGTG
fp84	Op3del_upscr	GGTTTTCAGCGGCACTCAACGG
fp85	Op3del_dscr	TGAAGGCGGCGCTGAAATCC
fp115	Op4dIns_scr	ACCATGCTTTCCGACTGCCG

Supplementary References

1. Steinberger, B., Petersen, N., Petermann, H. & Weiss, D. G. Movement of magnetic bacteria in time-varying magnetic fields. *J. Fluid Mech*. **273**, 189 (2006).

2. Zhang, W.-J., Chen, C., Li, Y., Song, T. & Wu, L.-F. Configuration of redox gradient determines magnetotactic polarity of the marine bacteria MO-1. *Environ. Microbiol. Rep*. **2**, 646–650 (2010).

3. Uebe, R. et al. Deletion of a fur-like gene affects iron homeostasis and magnetosome formation in Magnetospirillum gryphiswaldense. *J. Bacteriol*. **192**, 4192–204 (2010).

4. Lohße, A. et al. Functional Analysis of the Magnetosome Island in Magnetospirillum gryphiswaldense: The mamAB Operon Is Sufficient for Magnetite Biomineralization. *PLoS One* **6**, e25561 (2011).

5. Katzen, F., Becker, A., Ielmini, M. V, Oddo, C. G. & Ielpi, L. New mobilizable vectors suitable for gene replacement in gram-negative bacteria and their use in mapping of the 3' end of the Xanthomonas campestris pv. campestris gum operon. *Appl. Environ. Microbiol*. **65**, 278–82 (1999).

6. Marx, C. J. & Lidstrom, M. E. Broad-host-range cre-lox system for antibiotic marker recycling in gram-negative bacteria. *Biotechniques* **33**, 1062–7 (2002).

7. Raschdorf, O., Müller, F. D., Pósfai, M., Plitzko, J. M. & Schüler, D. The magnetosome proteins MamX, MamZ and MamH are involved in redox control of magnetite biomineralization in Magnetospirillum gryphiswaldense. *Mol. Microbiol.* **89**, 872–86 (2013).

8. Schultheiss, D. & Schüler, D. Development of a genetic system for Magnetospirillum gryphiswaldense. *Arch. Microbiol*. **179**, 89–94 (2003).

9. Ullrich, S. & Schüler, D. Cre-lox-based method for generation of large deletions within the genomic magnetosome island of Magnetospirillum gryphiswaldense. *Appl. Environ. Microbiol*. **76**, 2439–44 (2010).

Movie S1. **Magnetically aligned, uninterrupted run episodes displayed by *M. gryphiswaldense.*** Dark-field microscopy video recording of *M. gryphiswaldense* WT cells in a standard wet mount at 100x magnification. Cells were exposed to a homogenous vertical magnetic field of 0.26 mT. After 10 s the tracking result of the same sequence is shown.

http://www.nature.com/ncomms/2014/141114/ncomms6398/extref/ncomms6398-s2.avi

Movie S2. **Swimming reversals are caused by motor reversals.** Dark-field video of a spontaneously tethered cell reversing rotation frequently imaged at 43 fps.

http://www.nature.com/ncomms/2014/141114/ncomms6398/extref/ncomms6398-s3.avi

Movie S3. **Swimming behavior of non-magnetic cells.** Tracking video of non-magnetic cells of strain Δ*mamAB* at 100x magnification in standard a wet mount preparation. Cells were exposed to a homogenous vertical magnetic field of 0.26 mT.

http://www.nature.com/ncomms/2014/141114/ncomms6398/extref/ncomms6398-s4.avi

Movie S4. **Exposure to oxygen triggers cumulated reversals followed by exceptionally long runs.** Atmospheric shift from 0% to 2% oxygen after 20 s. Tracking video at 100x magnification of non-magnetic cells of strain Δ*mamAB* freely swimming in equilibrated mini-droplets in the gas perfusion chamber. Reversals are shown as dots on individual tracking paths.

http://www.nature.com/ncomms/2014/141114/ncomms6398/extref/ncomms6398-s5.avi

Movie S5. **Δ*cheOp1* mutant cells do not respond to atmospheric shifts**. Tracking video at 100x magnification of Δ*cheOp1* mutant cells grown under selective conditions before and after atmospheric shift from 0% to 2% oxygen (after 20 s).

http://www.nature.com/ncomms/2014/141114/ncomms6398/extref/ncomms6398-s6.avi

Movie S6. **Oxygen reverses the prevalent swimming direction of entire populations.** Sw polarity-selected NS WT cells recorded in a sitting drop in the gas perfusion chamber that are shifted from anoxic conditions to 2% oxygen after 5 s. A homogeneous magnetic field of 0.26 mT was applied (the north pole being at the top of the image).

http://www.nature.com/ncomms/2014/141114/ncomms6398/extref/ncomms6398-s7.avi

Movie S7. **Quantitative analysis of swimming polarity in selected cells.** Population tracking experiment of Sw polarity-selected NS WT cells in the gas perfusion chamber with an applied magnetic field of 0.26 mT (the north pole being at the top of the image). After 20 s shift from anoxic conditions to 2% oxygen.

http://www.nature.com/ncomms/2014/141114/ncomms6398/extref/ncomms6398-s8.avi

2.1 Publication 2:

An intracellular nanotrap

redirects proteins and organelles in live bacteria.

Borg S.*, Popp F. *, Hofmann J., Rothbauer U., Leonhardt H., and Schüler D.

mBio 6(1):e02117-14. doi:10.1128/mBio.02117-14 (2015).

* These authors contributed equally to this study.

RESEARCH ARTICLE

An Intracellular Nanotrap Redirects Proteins and Organelles in Live Bacteria

Sarah Borg,[a] Felix Popp,[a] Julia Hofmann,[a]* Heinrich Leonhardt,[a] Ulrich Rothbauer,[c] Dirk Schüler[a,b]

Department of Biology, Ludwig Maximillians University Munich, LMU Biozentrum, Martinsried, Germany[a]; Department of Microbiology, University of Bayreuth, Bayreuth, Germany[b]; Department of Natural Science and Medicine, University of Tübingen, Reutlingen, Germany[c]

* Present address: Julia Hofmann, Sequiserve GmbH, Vaterstetten, Germany.

S. Borg and F. Popp contributed equally to this work.

ABSTRACT **Owing to their small size and enhanced stability, nanobodies derived from camelids have previously been used for the construction of intracellular "nanotraps," which enable redirection and manipulation of green fluorescent protein (GFP)-tagged targets within living plant and animal cells. By taking advantage of intracellular compartmentalization in the magnetic bacterium *Magnetospirillum gryphiswaldense*, we demonstrate that proteins and even entire organelles can be retargeted also within prokaryotic cells by versatile nanotrap technology. Expression of multivalent GFP-binding nanobodies on magnetosomes ectopically recruited the chemotaxis protein $CheW_1$-GFP from polar chemoreceptor clusters to the midcell, resulting in a gradual knockdown of aerotaxis. Conversely, entire magnetosome chains could be redirected from the midcell and tethered to one of the cell poles. Similar approaches could potentially be used for building synthetic cellular structures and targeted protein knockdowns in other bacteria.**

IMPORTANCE **Intrabodies are commonly used in eukaryotic systems for intracellular analysis and manipulation of proteins within distinct subcellular compartments. In particular, so-called nanobodies have great potential for synthetic biology approaches because they can be expressed easily in heterologous hosts and actively interact with intracellular targets, for instance, by the construction of intracellular "nanotraps" in living animal and plant cells. Although prokaryotic cells also exhibit a considerable degree of intracellular organization, there are few tools available equivalent to the well-established methods used in eukaryotes. Here, we demonstrate the ectopic retargeting and depletion of polar membrane proteins and entire organelles to distinct compartments in a magnetotactic bacterium, resulting in a gradual knockdown of magneto-aerotaxis. This intracellular nanotrap approach has the potential to be applied in other bacteria for building synthetic cellular structures, manipulating protein function, and creating gradual targeted knockdowns. Our findings provide a proof of principle for the universal use of fluorescently tagged proteins as targets for nanotraps to fulfill these tasks.**

Received 14 November 2014 **Accepted** 1 December 2014 **Published** 13 January 2015

Citation Borg S, Popp F, Hofmann J, Leonhardt H, Rothbauer U, Schüler D. 2015. An intracellular nanotrap redirects proteins and organelles in live bacteria. mBio 6(1):e02117-14. doi:10.1128/mBio.02117-14.

Editor Sang Yup Lee, Korea Advanced Institute of Science and Technology

Address correspondence to Dirk Schüler, Dirk.Schueler@uni-bayreuth.de.

Intrabodies are functional fragments derived from full-length antibodies that can be expressed in heterologous hosts and which specifically recognize their antigen within cells. In various eukaryotic systems, they have been demonstrated to be powerful tools that enable the intracellular analysis and manipulation of protein functions (1–5). Among the various types of intrabodies, so-called nanobodies have proven to be particularly useful due to their small size, solubility, enhanced stability, and the relative ease of screening, cloning, and expression procedures (6–9). Nanobodies are routinely derived from camelid heavy-chain antibodies, which lack the light chains present in conventional IgG antibodies and recognize their target by interaction with single VHH (variable domain of heavy chain antibodies) domains (10). After the genetic repertoire of B cells is extracted from an immunized camelid, antigen-binding VHHs can be selected and expressed as highly robust single-domain antibodies. Because of their special topology, nanobodies preferentially bind to concave surfaces of antigens which are often inaccessible to conventional antibodies (11). Examples for nanobody-based applications in living plant and animal cells include the inhibition of enzyme activity through specific binding to the active site (7, 12), modulation of spectral properties of fluorescent proteins (13), and the construction of nanobody-mediated synthetic regulatory circuits (14). Furthermore, different strategies for nanobody-based protein knockdowns have been reported, either by targeting nanobody-bound proteins to degradation pathways (15) or by artificially retargeting interaction partners to specific intracellular localizations (16–18). Artificial relocalization of targeted proteins was either caused by trapping of nanobody-bound proteins in the cytoplasm due to interference with protein translocation to cellular compartments (18) or by specifically anchoring the nanobody to distinct structures and compartments of the eukaryotic cell, such as distinct

DNA regions, plasma membranes, or the centrioles of animal cells, resulting in ectopic recruitment of green fluorescent protein (GFP)-tagged targets (16, 17, 19). The application of anchored nanobodies against GFP (GFP-binding protein [GBP]) as an intracellular nanotrap is a particularly versatile tool because of the widespread use of derivatives of this fluorescent tag.

It has been realized only rather recently that prokaryotic cells also contain highly organized subcellular structures (20). Bacteria possess, for example, structural homologs to eukaryotic cytoskeletal elements that define cell shape, structure, and function (21, 22). In addition, they form large supramolecular protein complexes, contain microcompartments, and even biosynthesize canonical membrane-enveloped organelles that show distinct subcellular localization patterns (22–24).

The ability to target proteins intracellularly and possibly even redirect macromolecular complexes to defined subcellular locations in bacteria has great potential for synthetic intracellular scaffolding and targeting of proteins or protein complexes (25, 26). For instance, such techniques could be used for protein knockdowns through spatial separation of interaction partners. Other possible applications are specific targeting of proteins to bacterial subcellular compartments (27–29), the setup of synthetic intracellular gradients (30), or even artificially compartmentalizing and distributing different cellular processes and organelles to distinct subcellular localizations. However, so far there are few tools available that are equivalent to the well-established methods used in eukaryotic cells and that would efficiently fulfill these tasks in bacteria.

One of the most intricate examples of natural compartmentalization in prokaryotic cells is magnetosomes, which are nanosized ferromagnetic crystals synthesized within intracellular membrane vesicles by magnetotactic bacteria such as *Magnetospirillum gryphiswaldense*. These organelles are attached to a cytoskeletal filament formed by the actin-like protein MamK and arranged in a chain that is positioned at the midcell (31, 32). The resulting magnetic dipole moment rotates the bacterial cell into alignment with the geomagnetic field, thereby enhancing the movement of the bacteria toward growth-favoring oxygen levels (33). Recently, our lab demonstrated the display of nanobodies on magnetosomes that were functional in recognizing their antigen not only *in vitro* but also *in vivo*. Expression of MamC–red fluorescent protein (RFP)-binding protein (RBP) fusions resulted in the recruitment of cytoplasmic RFP to the magnetosomes (34), showing that intracellular localization of soluble heterologous proteins can be manipulated in bacteria. This motivated us to further investigate whether magnetosome anchors can also be used to trap proteins with distinct functions from other cellular compartments. For this purpose, we chose the chemotaxis protein CheW, which is part of the chemoreceptor clusters that are universally found in chemotactic bacteria and typically display a distinct polar localization (35). We demonstrate that $CheW_1$ fused to enhanced GFP (EGFP) can be depleted from cell poles by expression of multivalent GBP nanobodies fused to the magnetosome protein MamC on endogenous levels, resulting in ectopic recruitment of $CheW_1$ to the magnetosome chain of *M. gryphiswaldense*. Depletion of $CheW_1$ from polar clusters resulted in a gradual impairment of aerotaxis. Intriguingly, the interaction between the magnetosome anchor and polar $CheW_1$-EGFP also led to artificial repositioning of the entire magnetosome chain from its midcell position toward one of the cell poles, indicating that entire organelles can be redirected by nanobodies and tethered to ectopic positions. Our study establishes the application of nanotrap technology for artificial targeting of proteins and even entire organelles to bacterial cells. Similar approaches could be used for building tailored subcellular structures in synthetic biology and for gradual protein knockdowns in other prokaryotic systems.

RESULTS

Recruitment of CheW1-EGFP to magnetosomes with a GBP nanotrap. In *M. gryphiswaldense*, $CheW_1$ is encoded within the *cheOp1* chemotaxis operon, which was recently demonstrated to control magneto-aerotactic swimming polarity (36). It is well established in various bacteria that CheW acts as a linker and interacts both with the chemoreceptor and the histidine kinase CheA proteins, thereby enhancing the polar chemoreceptor clustering and function (37). First, we replaced the native $cheW_1$ gene with $cheW_1$-*egfp* via chromosomal insertion. Similarly as observed in other bacteria (38–40), spot-like fluorescent signals originating from EGFP-tagged $CheW_1$ were exclusively found at both cell poles in the wild-type background in fluorescence micrographs (Fig. 1ai and f). This is consistent with previous results of cryo-electron microscopy of *M. gryphiswaldense* cells, where chemoreceptor complexes were identified near the poles (31). Only in elongated cells close to completion of cell division, two new clusters were formed at the midcell (see Fig. S1 in the supplemental material). In mutant backgrounds either forming magnetosome clusters instead of chains (Δ*mamJ* mutant) (32) or entirely lacking any magnetite particles (Δ*mamM* mutant) (41), the same $CheW_1$-EGFP fluorescence localization pattern as in the wild-type background was observed (Fig. 1di; see also Fig. S2b), indicating that polar chemoreceptor localization was independent of the presence and configuration of magnetosome chains, as expected.

Next, we asked whether the localization of $CheW_1$-EGFP was affected by coexpression of a GBP nanobody that had been identified by Rothbauer and colleagues before (42). To trap $CheW_1$-EGFP, GBP was expressed either alone in the cytoplasm ($MagGBP_{cyt}$) or fused to the abundant magnetosome membrane protein MamC (43), which has routinely been used as a magnetosome anchor for immobilization of various functional moieties, such as EGFP, enzymes, or an RBP (34, 43–46). In addition to the native *gbp* gene, we used a synthetic allele that was specifically optimized for the expression in *M. gryphiswaldense* (*Magnetospirillum*-optimized green-binding protein [*maggbp*]). MamC was fused to either one single copy of GBP connected to mCherry (mCherry-GBP, also referred to as "chromobody") (42), and the resulting MamC-mCherry-GBP fusion is referred to as MamC-1×GBP here, or to a tandem copy of *maggbp-gbp* (resulting in MamC-MagGBP-GBP, referred to as MamC-2×GBP here). All different *gbp* constructs were inserted into chromosomes of parent strains coexpressing $CheW_1$-EGFP. Western blot analysis of cell extracts of all strains carrying the generated fusions revealed reacting protein bands with expected sizes, indicating that the mono- and bivalent GBP nanobodies were stably expressed on magnetosomes (see Fig. S3 in the supplemental material).

Cytoplasmic expression of unfused $MagGBP_{cyt}$ alone had no effect on the localization of $CheW_1$-EGFP fluorescence in the wild-type background (see Fig. S2d). However, upon coexpression of MamC-1×GBP and $CheW_1$-EGFP, we detected weaker, secondary fluorescent foci at approximately the midcell position in addition to the two polar $CheW_1$-EGFP signals (Fig. 1bi). We

scored the number of fluorescent foci in four equidistant sectors along lengths of a representative set of cells and calculated the relative abundance of fluorescence intensity in each of the sectors (see Materials and Methods for details). In contrast to the wild-type background, which displayed only polar foci, about 30% of fluorescence intensity was detected within the cytoplasm upon coexpression of MamC-1×GBP (a representative cell is shown in Fig. 1bi and f). Recruitment of $CheW_1$-EGFP was likely due to interaction with GBP expressed on magnetosomes, as green ($CheW_1$-EGFP) and red (mCherry-tagged magnetosomes) fluorescence signals coincided in all analyzed cells, indicating that direct GBP-EGFP interaction caused the observed redirection of $CheW_1$ (see Fig. S2e and f). In cells coexpressing two GBP copies in tandem (MamC-2×GBP), a single large, nonpolar fluorescence signal was detected in the vast majority of cells. Ninety percent of the $CheW_1$-EGFP fluorescence intensity was shifted toward the midcell (Fig. 1ci and 4), while only 10% of the fluorescence signal remained at the cell pole (Fig. 1f). Instead of the spot-like, exclusively polar foci of the parent strain, a linear fluorescence signal was present near the midcell in most MamC-2×GBP-expressing cells, demonstrating efficient redirection of membrane complex-associated GFP-tagged proteins (Fig. 1ci; see also Fig. S4).

Next, we investigated whether the absence of magnetic nanoparticles would affect the recruitment of $CheW_1$-EGFP through MamC-GBP fusions by analyzing nonmagnetic cells. Due to loss of the magnetosomal iron transporter MamM, Δ*mamM* cells lack any magnetite crystals but still produce empty magnetosome membrane vesicles (41). $CheW_1$-EGFP fluorescence was shifted toward the midcell in the Δ*mamM* strain coexpressing MamC-2×GBP to the same extent as in the magnetite-containing strains (see Fig. S2c). To analyze whether the configuration of magnetosome chains had an effect on $CheW_1$-EGFP recruitment, we also expressed MamC-1×GBP in the Δ*mamJ* background, in which the physical interaction of magnetosome chains with the actin-like MamK filaments is abolished (32), resulting in agglomerated clusters rather than linear, well-ordered chains of magnetosomes (Fig. 1dii and eii). In the vast majority of analyzed Δ*mamJ* MamC-1×GBP cells, the major proportion of $CheW_1$-EGFP fluorescence (>85% of all foci) was located at only 1 cell pole (Fig. 1f) and appeared to be slightly distorted longitudinally (Fig. 1ei).

Effect of $CheW_1$-EGFP recruitment on magnetosome localization. We noticed that all strains which showed strong $CheW_1$ mislocalization were increasingly affected in their magnetic alignment, as indicated by reduced magnetic response (C_{mag}) values (e.g., MamC-2×GBP, 0.60 ± 0.07; wild type, 1.24 ± 0.20). The C_{mag} value provides an optical measure of the relative alignment of cells in a cuvette by applying a strong magnetic field either parallel or perpendicular to the light beam of a photometer. Transmission electron microscopy (TEM) analysis revealed that wild-type cells expressing $CheW_1$-EGFP alone displayed the same magnetosome localization pattern as that of their parent strain (Fig. 1aii). Both automated image analysis by the Chain Analysis Program (CHAP) (47) and manual scoring of magnetosome position (see Materials and Methods for details; Fig. 1g) indicated that the linear chains of magnetosomes were consistently positioned at the midcell and displayed the same configuration as typically observed for the *M. gryphiswaldense* parent strain (48, 49), with approximately 35 particles per cell that had an average crystal size of 35 to 47 nm (49). Additional cytoplasmic expression of $MagGBP_{cyt}$ in the same background did not affect magnetosome chain configuration (see Fig. S5b). Coexpression of MamC-1×GBP and $CheW_1$-EGFP did not affect the midcell position of magnetosome chains either, but chains were less compact, i.e., particles were more widely spaced, as indicated by the fuzzier, slightly stretched appearance of magnetosome chains in CHAP analysis heat maps (Fig. 1biii). TEM analysis of Δ*mamJ* cells expressing $CheW_1$-EGFP alone revealed the same magnetosome localization pattern as that of their parent strain (Fig. 1dii). Consistent with the observed shift of the $CheW_1$-EGFP fluorescence toward one pole in the Δ*mamJ* MamC-1×GBP strain, 90% of magnetosome clusters detected in TEM micrographs were localized at a single cell pole only, while clusters were no longer observed at the midcell or along the cell length, as commonly found in the Δ*mamJ* parent strain (32, 50) (Fig. 1g). Moreover, the loose magnetosome assemblies observed at the poles were slightly elongated compared to the compact, rounded magnetosome clusters of the parent strain (Fig. 1diii and eiii). This indicated that targeted recruitment and partial rearrangement of magnetosomes were facilitated in cells in which magnetosome particles were no longer bound to the MamK filament by their molecular connector MamJ (33). As observed for mislocalization of $CheW_1$-EGFP fluorescence, in wild-type cells coexpressing divalent tandem fusions of GBP (MamC-2×GBP), magnetosome chains were predominantly drawn to one of the cell poles (Fig. 1cii; see also Fig. S6). Magnetosome chains were even less compact than in the presence of the monovalent nanobody, as reflected by the rather scattered pattern of poorly aligned magnetosome chains (Fig. 1ciii). Consistent with the overall shift of the chain, the mean fraction of magnetosome particles located at one of the cell poles increased from 7 to 36% (Fig. 1g).

Effect of $CheW_1$-EGFP recruitment on chemotaxis of *M. gryphiswaldense*. The observed mislocalization of chains also affected the magnetic alignment of swimming cells. While wild-type cells expressing only $CheW_1$-EGFP predominantly swam aligned to the ambient magnetic field, as did the parent strain, a large fraction of cells coexpressing MamC-2×GBP displayed trajectories that were oriented at random angles to the ambient magnetic field (Fig. 2a). As indicated by video microscopy, motility and mean swimming speed were not affected in any of the analyzed strains. Compared to the Δ*cheW*$_1$ and Δ*cheOp1* control strains, in which aerotaxis was entirely abolished, as indicated by the formation of small aerotactic halos in swim plate assays (see Fig. S7) (36), coexpression of cytoplasmic $MagGBP_{cyt}$ and $CheW_1$-EGFP in the wild-type background did not affect the size of swim halos that were virtually identical to those of the parent strain (Fig. 2b and c).

While the Δ*cheW*$_1$ strain did not show any response when shifted from anaerobic conditions to 2% oxygen in a microscopic gas perfusion chamber (Fig. 2d) and displayed a straight-swimming phenotype comparable to that of the Δ*cheOp1* deletion strain, wild-type cells expressing $CheW_1$-EGFP showed a reaction very similar to that observed in the parent strain (36). The reversal frequency instantaneously rose from less than 0.1 s^{-1} to more than 0.2 s^{-1} after microoxic upshift. This was followed by a rapid drop in reversal frequency below prestimulus levels within 15 s (Fig. 2d). However, coexpression of MamC-1×GBP and $CheW_1$-EGFP led to slightly reduced halo sizes in swim plates and a lower number of reversals in response to the oxygen shift. The maximum reversal frequency remained below 0.15 s^{-1} and peaked at approximately 60% of the wild-type rate. Interestingly, coexpres-

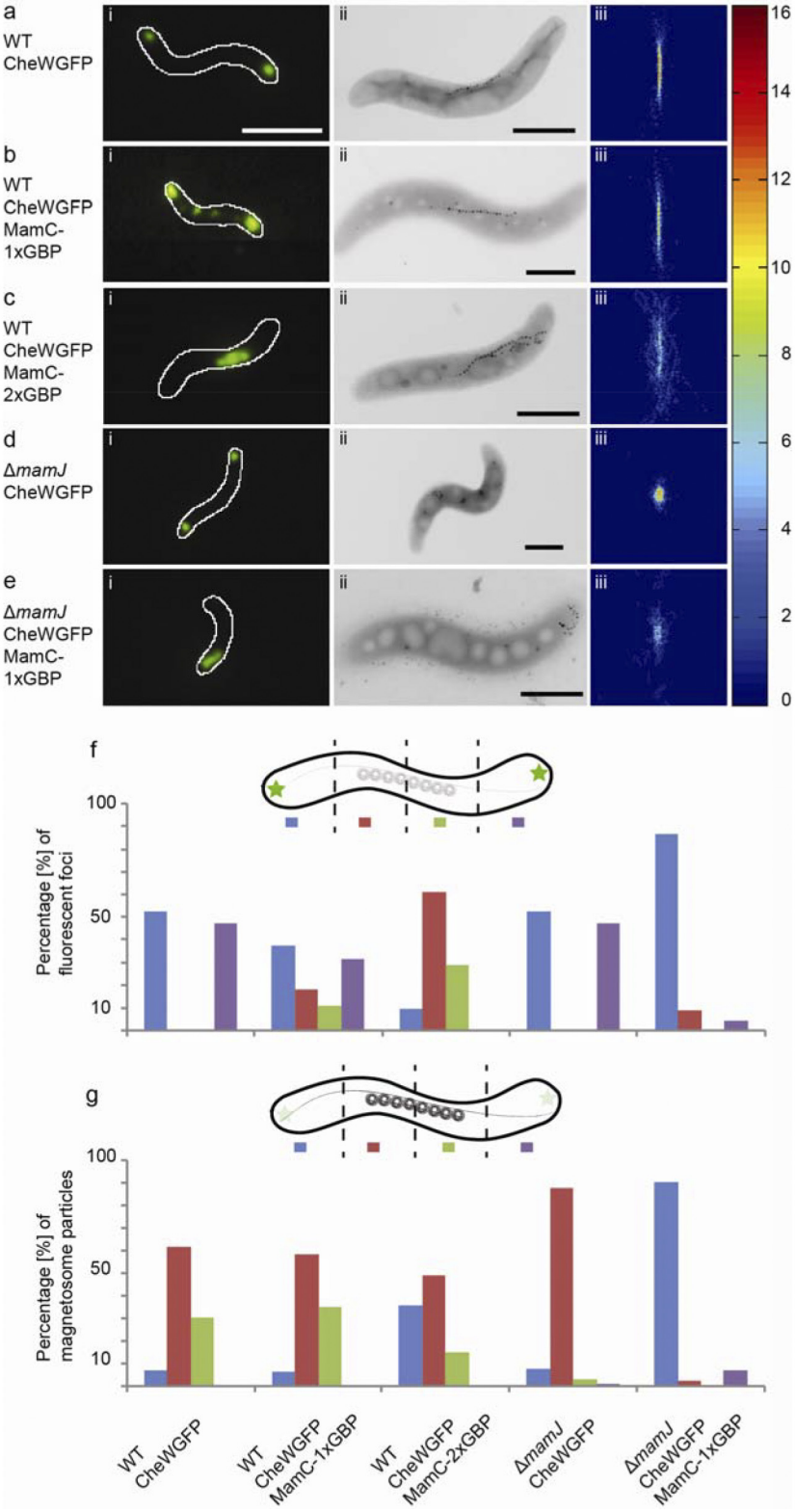

FIG 1 Analysis of subcellular $CheW_1$-EGFP and magnetosome localization. Fluorescence (i) and TEM (ii) micrographs of representative *M. gryphiswaldense* $CheW_1$-EGFP (a), $CheW_1$-EGFP MamC-1×GBP (b), $CheW_1$-EGFP MamC-2×GBP (c), Δ*mamJ* $CheW_1$-EGFP (d), and Δ*mamJ* $CheW_1$-EGFP MamC-1×GBP (e) cells. Cells were analyzed by CHAP (iii) and scored for the distribution of fluorescence signal, represented by the percentage of fluorescent foci detected within 4 equidistant compartments (f), and magnetosomes, represented by the percentage of magnetosomes detected within 4 equidistant compartments (g). White scale bar, 2 μm; black scale bar, 1 μm. Twenty cells were aligned by CHAP for each strain, and heat maps display the numbers of magnetosomes. Single cells were segmented into four compartments, and for each strain 20 cells were scored to obtain fluorescence and magnetosome distributions.

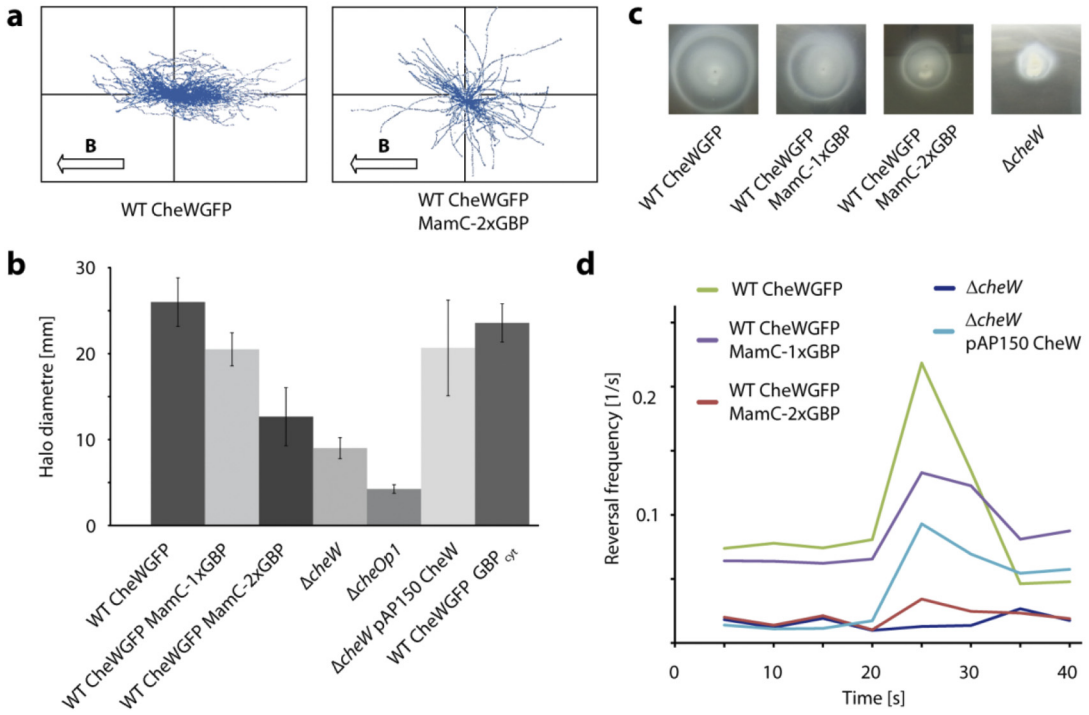

FIG 2 Magneto-aerotactic swimming behavior of *M. gryphiswaldense* strains expressing $CheW_1$-EGFP and MamC-GBP fusions. (a) Magnetic alignment of swimming cells expressing $CheW_1$-EGFP alone or in combination with MamC-2×GBP. A plot of all tracks from a representative video record is shown for each strain. Cells swimming in the gas perfusion chamber were exposed to a homogenous vertical magnetic field of 0.26 mT (B). (b) Average halo diameter of strains expressing MamC-GBP fusions in swim plates (means ± standard deviations [SD] from at least 3 independent replicates). The Δ*cheW*$_1$ and Δ*cheOp1* chemotaxis gene deletion mutants were used as controls. Transcomplementation of the Δ*cheW*$_1$ mutant strain by constitutive expression of $CheW_1$-EGFP from a plasmid restored chemotactic efficiency to 80% of the wild-type cells expressing $CheW_1$-EGFP at wild-type levels. (c) Halo formation of wild-type $CheW_1$-EGFP, $CheW_1$-EGFP MamC-1×GBP, $CheW_1$-EGFP MamC-2×GBP, and Δ*cheW* cells in 0.2 % motility agar 3 days after inoculation. (d) Aerotactic reversal response upon abrupt shift from 0% to 2% oxygen in a microscopic gas perfusion chamber. Video records were analyzed by automated tracking software (WimTaxis; Wimasis) to obtain swim tracks and reversal events of individual cells (72), and reversal rates were calculated for 5-s intervals by averaging single-cell data from at least 3 independent recordings.

sion of MamC-1×GBP also caused delayed adaptation after the shift, as the reversal frequency remained above prestimulus levels within 20 s postshift.

Coexpression of MamC-2×GBP and $CheW_1$-EGFP, which completely depleted $CheW_1$-EGFP from the cell poles as suggested by fluorescence microscopy (Fig. 1ci), also had a dramatic effect on the cells' switching behavior under anoxic equilibrium conditions and the response elicited by oxygen exposure. The prestimulus reversal frequency was comparable to that of the Δ*cheW*$_1$ strain and rose only minimally after oxygen upshift to 2% O_2, remaining on a very low level (maximum frequency below 0.05 s^{-1}). In conclusion, an increase in the copy number of GBP led to gradually stronger impairment of aerotaxis, eventually reducing the number of reversals in a strain coexpressing $CheW_1$-EGFP and the divalent MamC-2×GBP fusion to the level of a Δ*cheW*$_1$ null mutant.

DISCUSSION

We investigated the interaction between components of the universal bacterial chemotaxis signaling pathway and nanobodies expressed on the magnetosome organelles of *M. gryphiswaldense*, which enabled us to easily follow the structural and behavioral effects of artificial recruitment by TEM and fluorescence microscopy (FM) imaging and video microscopy at the single cell level. We observed that by anchoring GBP to the magnetosome membrane, the localization of $CheW_1$-GFP was shifted from the poles to the midcell, i.e., to the typical position of the magnetosome chain. There are two possible explanations for the observed redirection of $CheW_1$ from the polar clusters to the magnetosomes: (i) unbound $CheW_1$, in equilibrium with the receptor-bound form, could be recruited from a cytoplasmic pool, whereas (ii) membrane-bound $CheW_1$ could be directly withdrawn from preexisting polar clusters. CheW is a soluble protein that lacks transmembrane domains but *in vitro* forms ultrastable ternary complexes together with CheA and chemoreceptors (51). However, in living cells, signaling complexes are weakly dynamic and display slow turnover (of approximately 12 min), as indicated by fluorescence recovery after photobleaching (FRAP) experiments on CheA and CheW constructs (52). Consistent with these observations, it has been suggested that small amounts of CheA might be permanently present in an unbound state in the cytoplasm (53). However, the relative copy numbers of all cluster components are tightly regulated, and since overexpression of CheW leads to impaired chemotactic signaling (due to competitive inhibition of CheA binding to the chemoreceptors) (51), the pool of free CheW in the cytoplasm must be rather small. Thus, it seems most probable that soluble CheW present at low concentrations in the cytoplasm is sequestered by magnetosome-anchored GBP, and over time also those molecules initially bound to the chemoreceptor

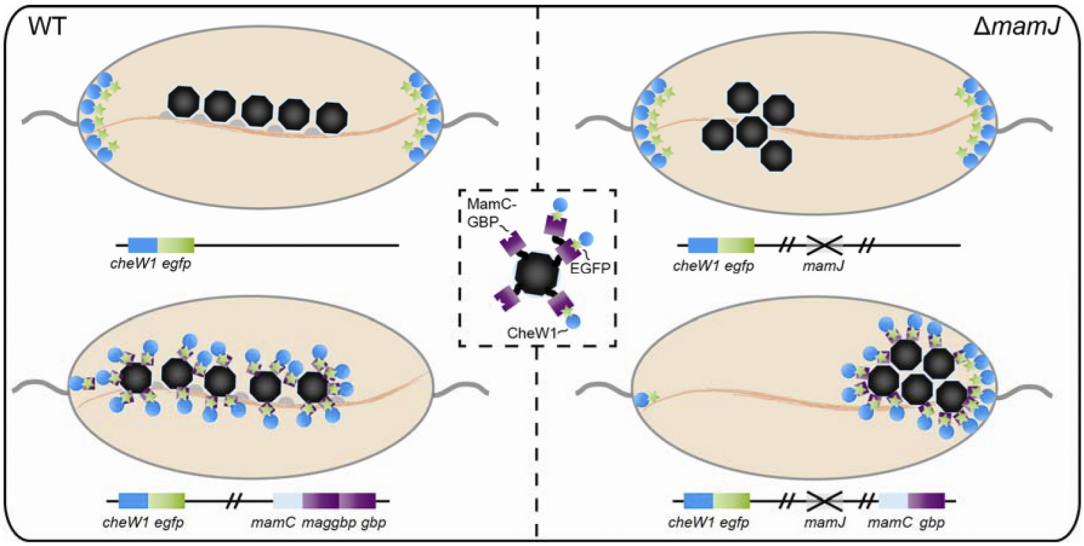

FIG 3 Model of MamC-GBP and $CheW_1$-EGFP interaction. $CheW_1$-EGFP localizes distinctly at the cell poles if expressed chromosomally in the wild-type and Δ*mamJ* backgrounds (top right and left). If MamC-GBP is coexpressed in the wild type (bottom left), $CheW_1$-EGFP is depleted completely from the poles. Expression of MamC-GBP in the Δ*mamJ* $CheW_1$-EGFP background leads to recruitment of whole magnetosomes to the cell poles (bottom right). Expression of monovalent and divalent nanobodies on a magnetosomes and interaction with $CheW_1$-EGFP is illustrated in the inset. Expressed proteins are illustrated in same colors as genes.

clusters might gradually be released and trapped at ectopic positions by a strong interaction with the nanobody.

The localization of $CheW_1$-GFP was unaffected by coexpression of cytoplasmic (unfused) GBP in the wild-type background but shifted toward the midcell upon MamC-2×GBP expression in the nonmagnetic Δ*mamM* strain, which lacks any electron-dense magnetic crystals but still forms empty vesicles of the magnetosome membrane (41). This demonstrates that GBP immobilized on magnetite-free membrane vesicles is sufficiently effective to specifically redirect localized proteins. Furthermore, this suggests that recruitment and retargeting could be achieved in other bacteria lacking magnetosomes by using different spatial determinants as intracellular traps.

Although the presence of magnetic particles was no absolute prerequisite for efficient recruitment, redistribution of CheW was strongly affected by magnetosome chain configuration. Magnetosome clusters were drawn to only one pole in the Δ*mamJ* background upon expression of MamC-1×GBP and acted as efficient nanotraps for $CheW_1$-GFP. In contrast to the undefined midcell fluorescence caused by partial depletion from polar clusters observed upon expression of MamC-1×GBP in the wild-type background, virtually no $CheW_1$-GFP signal was detected at the midcell or the opposite pole in the Δ*mamJ* mutant strain. This either might be due to increased avidity of nanobodies concentrated in the tightly clustered magnetosome assemblies or might reflect a stochastic shift of CheW diffusion equilibrium due to the concentration of two sinks (i.e., the native chemoreceptor cluster and the artificial magnetosomal nanobody cluster) at a single pole (Fig. 3, bottom right).

Interaction of MamC-GBP and $CheW_1$-GFP reciprocally affected configuration and positioning of the magnetosome chain. Binding of $CheW_1$-GFP to magnetosome particles disturbed their proper alignment into regular, densely spaced chains. Increasing the expression of GBP (MamC-1×GBP and -2×GBP) also gradually increased the interparticle spacing, possibly by additional protein bound to the magnetosome surface which might weaken the magnetostatic interactions between particles. Overexpression of MamC-2×GBP in the wild-type background caused a nearly complete shift of the magnetosome chains toward the poles, with the majority of magnetosome chains originating at polar or subpolar positions (see Fig. S6), which was probably caused by redirecting and tethering the chains to a fraction of membrane-bound $CheW_1$-GFP remaining at the cell pole (Fig. 3, bottom left). Although the magnetosome chain of wild-type cells generally occupies the midcell position, it becomes mobilized during cell division, when the chain is split and repositioned by MamK dynamics to the midcell of daughter cells (50). We found that magnetosome chain localization was most severely impaired in cells lacking the acidic MamJ protein, which is assumed to connect magnetosome particles to the cytoskeletal magnetosome filament formed by the actin-like MamK protein (32). In the Δ*mamJ* background, overexpression of the monovalent nanobody was already sufficient to rearrange (Fig. 1eiii) and recruit (Fig. 1eii) the magnetosome cluster to 1 cell pole (Fig. 3, bottom right). The increased intracellular mobility of Δ*mamJ* magnetosome clusters might be explained by a lack of the presumed MamK-mediated interactions with divisome constituents (50). In wild-type cells, these interactions need to be overcome by interaction with polar CheW, whereas in Δ*mamJ* cells, magnetosome redirection is facilitated because MamK-magnetosome interactions are abolished.

The level of $CheW_1$-GFP recruitment clearly depended on gene dosage. While redirection of $CheW_1$-GFP was only partial in cells expressing MamC-1×GBP, overexpression of MamC-2×GBP caused a complete shift of $CheW_1$-GFP localization toward the midcell. There is precedence for significantly increased avidity (500×) of a nanobody consisting of a fusion of two identical domains compared to the monovalent nanobody (54). Similarly, in our experiments, the binding of $CheW_1$-GFP to the monovalent

GBP was apparently comparable to the *in vivo* turnover of the chemoreceptor-CheW complexes, since polar- and midcell-localized $CheW_1$-GFP could be detected. In contrast, the avidity of the bivalent nanobody was much stronger, more endogenous $CheW_1$-GFP was bound, and the equilibrium was shifted toward the GBP-bound state.

In addition to demonstrating efficient redirection of entire organelles to distinct locations, we observed that ectopic redirection of $CheW_1$-GFP also gradually modulated chemotactic efficiency of *M. gryphiswaldense* cells. While chemoreceptors readily form complexes in the absence of CheA and CheW, the latter is essential for stabilizing native CheA-receptor interactions and lattice formation (37, 53). Partial depletion of $CheW_1$ gradually reduced chemotactic efficiency, while expression of the bivalent nanobody essentially phenocopied the deletion of *cheW*$_1$ (Fig. 2c). As GBP expressed in the cytoplasm had no effect on aerotaxis, this was not due to inactivation of $CheW_1$-GFP but caused by redirection and depletion from its native polar environment. Although bacteria do not display the same level of compartmentalization as eukaryotic cells, the functionality of many bacterial proteins similarly depends on their localization. Our results show that testing protein function by manipulating its subcellular localization as applied to eukaryotic systems (2, 18) can be extended to much smaller bacterial cells and be used to efficiently modulate protein function by subcellular retargeting.

Compared to other approaches for silencing or manipulating the expression of selected genes at the DNA or RNA (55, 56) level, the biggest advantage of regulating gene expression at the protein level is that there is no change of mRNA transcript or native protein expression level (57). Especially for bacterial genes encoded in operons, gradual knockdown of individual proteins might be difficult to achieve at the transcriptional level, if polar effects on transcription of downstream genes are to be avoided. Additionally, it would be desirable to develop inducible systems, e.g., to gradually control *in vivo* the stoichiometry of proteins in larger clusters. This might facilitate the study of complex regulatory pathways, such as cell division or cell differentiation processes in other bacteria.

Intrabodies are well established as powerful tools in eukaryotic cells for trapping soluble proteins at defined subcellular locations (16–18) or for inhibition of protein function (12). Although recombinant nanobodies can be produced easily in bacteria such as *Escherichia coli* (10), to date the use of intrabodies in bacterial cells has been restricted to only very few studies. Two early publications reported the intracellular expression of single-chain Fv antibody fragments (e.g., to block transcriptional activation) (58, 59), and more recently nanobodies have been applied in bacteria to inhibit enzyme activity (60). However, in these approaches, intrabodies were not anchored to defined positions, and inhibition of enzymes was achieved by neutralization rather than redirection to completely different compartments of the cell. Although for proof of principle we took advantage of the specific compartmentalization in *M. gryphiswaldense*, in which the magnetosomes provide a natural anchor for setting up an intracellular nanotrap, this approach could also be extended and adapted for application in other bacteria. By using universal tags like GFP for recruitment, many proteins can be targeted with the same nanobody by applying the same strategy, obviating the need of camelid immunization and screening of whole libraries. Multiple other applications are possible, because GFP fusion proteins can be combined with any cellular anchor point, such as subcellular locations (e.g., poles, midcell), specific protein complexes, compartments, organelles, or other spatial determinants. For instance, potential applications of our approach in bacteria could be building synthetic cellular structures (e.g., artificial tethering of heterologously expressed bacterial microcompartments) or compartmentalization of biosynthetic pathways, which can dramatically increase production by restricting reactions spatially to subcellular compartments (61, 62).

MATERIALS AND METHODS

Bacterial strains, plasmids, and culture conditions. Bacterial strains and plasmids used in this study are listed in Table S1 and S2 in the supplemental material. *M. gryphiswaldense* strains were grown microaerobically with 1% oxygen in modified flask standard medium (FSM) at 30°C (63) and moderate shaking (120 rpm). *E. coli* strains were cultivated as previously described (64). For growth of *E. coli* WM3064 (W. Metcalf, unpublished data) or BW29427 (K. Datsenko and B. L. Wanner, unpublished data), 1 mM DL-α,ε-diaminopimelic acid (DAP) was added to lysogeny broth medium (LB). Strains were routinely cultured on plates solidified with 1.5% (wt/vol) agar. For strains carrying recombinant plasmids, media were supplemented with 25 $\mu g \cdot ml^{-1}$ kanamycin and 50 $\mu g \cdot ml^{-1}$ ampicillin (Amp) for *E. coli* strains and 5 $\mu g \cdot ml^{-1}$ kanamycin (km) for *M. gryphiswaldense* strains.

For the preparation of swim plates, only 0.2% agar was used, the concentration of carbon source (lactate) was lowered to 1.5 mM, and peptone was omitted from FSM. Five microliters of overnight culture was pipetted into the swim agar, and plates were incubated under microoxic conditions for 2 days (protocol modified from that of Schultheiss et al. [65]).

Molecular and genetic techniques. Oligonucleotides were purchased from Sigma-Aldrich (Steinheim, Germany), and sequences can be supplied on request. Plasmids were constructed by standard recombinant techniques as described in detail below. All constructs were sequenced on an ABI 3730 capillary sequencer (Applied Biosystems, Darmstadt, Germany), utilizing BigDye Terminator v3.1. Sequence data were analyzed with Software Vector NTI Advance 11.5 (Invitrogen, Darmstadt, Germany). The GBP nanobody (42) was provided by ChromoTek GmbH (Planegg-Martinsried), and a synthetic GBP was specifically optimized for the expression in *M. gryphiswaldense* with respect to its codon usage and purchased from ATG:biosynthetics (Merzhausen, Germany).

Construction of plasmids for chromosomal gene insertion, deletion, and fusion. For chromosomal exchange of *cheW*$_1$ against *cheW*$_1$-*egfp*, the fluorescence marker was fused via overlap extension PCR (66) to *cheW*$_1$ and to a 1,000-bp downstream fragment of the gene. The fused product was inserted into pORFM, and the native *cheW*$_1$ copy was exchanged chromosomally against *cheW*$_1$-*egfp* by homologous recombination facilitated by GalK counterselection (67). Deletion of *cheW*$_1$ was achieved following a similar strategy by fusion of approximately 1,000-bp fragments upstream and downstream of *cheW*$_1$ connected by 12 nonsense bp replacing the native *cheW*$_1$. For complementation of *cheW*$_1$ deletion, *cheW*$_1$ was amplified from the genome and inserted into pAP150 (46).

All *mamC-gbp* fusions were chromosomally introduced by transposition; therefore, all gene fusions created by overlap PCR were inserted into transposable pSB6 and pSB7 plasmids (46).

Analytical methods. Magnetic reaction of cells was validated by light microscopy applying a bar magnet. Optical density (OD) and magnetic response (C_{mag}) of exponentially growing cells were measured photometrically at 565 nm as previously reported (68). For C_{mag} measurement, a magnetic field of approximately 70 mT was used.

Biochemical methods. Polyacrylamide gels were prepared according to the method of Laemmli (69). Strains were grown overnight and spun down via centrifugation, OD_{565} was set to 10, and 20 μl was loaded onto 12% (wt/vol) SDS gels and analyzed via immunoblotting. Proteins were electroblotted onto polyvinylidene difluoride (PVDF) membranes (Roth, Germany). Membranes were blocked for 1 h at room temperature with

blocking solution (2.5% [wt/vol] milk powder in Tris-buffered saline [TBS] [50 mM Tris-HCl, pH 7.6, and 150 mM NaCl]) and incubated for another hour with primary rabbit anti-MamC IgG antibody (1:500 dilution; Santa Cruz, CA). Membranes were washed 4 times with TBS for 5 min and incubated with a secondary alkaline phosphatase-labeled goat anti-rabbit IgG antibody (1:2,000 dilution; Promega, United States) for 45 min. Membranes were washed 4 times with TBS for 5 min, and immunoreactive proteins were visualized with nitroblue tetrazolium (NBT)/5-bromo-4-chloro-3-indolylphosphate (BCIP) (Roche kit).

Phase contrast and fluorescence microscopy. Strains with genomic $CheW_1$-EGFP fusions and additional MamC-GBP fusions were grown in 1 ml FSM in 24-well plates for 16 h at 30°C and 1% O_2 without agitation. For microscopy, cells were immobilized on agarose pads (phosphate-buffered saline [PBS] buffer supplemented with 1% agarose) and imaged with an Olympus BX81 microscope equipped with a 100 UPLSAPO100XO objective (numerical aperture of 1.40) and a Hamamatsu Orca AG camera. The Olympus xcellence pro software was used to capture and analyze images.

To analyze relative positions of fluorescent foci, we manually segmented each cell along its long axis into four equal sectors and scored the fluorescent foci within each sector. The strongest fluorescence signal(s) was scored as "++," and weaker signals were scored as "+." Since the orientation of imaged cells was random and in many cases the distribution of fluorescent foci was not perfectly symmetric, we rotated the cells where necessary so that the sectors with the highest cumulated score were sectors 1 and 2. We then calculated relative frequencies of fluorescent focus positions based on the ratio of cumulated scoring points of all analyzed cells per sector divided by the total number of scoring points in all cells.

Transmission electron microscopy. Magnetosome chain localization was examined by transmission electron microscopy (TEM), for which cells were concentrated via centrifugation and adsorbed onto carbon-coated copper grids. Cells were imaged with an FEI Morgagni 268 (FEI, Eindhoven, Netherlands) electron microscope at an accelerating voltage of 80 kV. For analysis of magnetosome alignment and chain compactness, we used the CHAP script implemented in Matlab and ran the program for 20 cells for each strain (48). For analysis of magnetosome position, we manually segmented each cell along its long axis into four equal sectors and scored the number of magnetosomes within each sector. Since the orientation of imaged cells was random and in many cases the distributions of magnetosomes were not perfectly symmetric, we rotated the cells where necessary so that the sector with the most magnetosomes scored was either sector 1 or 2. We then calculated relative frequencies of magnetosome positions based on the ratio of cumulated magnetosomes of all analyzed cells per sector divided by the total number of magnetosomes in all cells.

Video microscopy and analysis of swimming parameters. The swimming behavior of cells was analyzed and recorded using dark-field microscopy on an upright Zeiss Axioplan microscope (Zeiss, Jena, Germany) at ×100 magnification. All microscopic motility experiments were performed within a microscopic gas perfusion chamber (Ludin Chamber, Life Imaging Services) that was equilibrated with variably moisturized and precisely adjusted O_2-N_2 gas mixtures containing between 0 and 2% oxygen (70).

Homogeneous conditions were maintained by using strongly diluted cell suspensions (OD of 0.005) and exposing cell suspensions to a constant gas flow of 50 ml · min^{-1}, protected against turbulence by placing a gas-permeable agar sheet on top.

Videos were recorded with a UK1158-M camera (EHD, Damme, Germany) at a frame rate of 15 frames per second and a standard resolution of 1,360 by 1,024 pixels using VirtualDub software. Dark-field video records were analyzed by a custom-made automated tracking software (WimTaxis—Bacteria Tracking; Wimasis GmbH, Munich, Germany) specifically adapted to determine the basic swimming characteristics. The software automatically detected swimming reversals and provided the *x-y* coordinates of every tracked cell for each frame.

The minimum track length was set to be 50 frames. Within the usual tracking times (depending on the time bacteria stayed in the viewing field [usually fewer than 10 s]), reversals generally were too infrequent to simply average the reversal rates for single cells. Therefore, the reversal frequency analysis for each experiment was performed at the population level, and all detected reversals were divided by the total respective tracking time (sum of the temporal length of all tracks) to obtain the population average.

To analyze the cells' reaction to oxygen shifts, the gas stream was manually switched between oxic and anoxic. For this purpose, we equipped our setup with a three-way valve and a flowmeter to adjust the flow of N_2 gas to 50 ml · min^{-1} (70). Cells were first equilibrated for 3 min under anoxic conditions before the video recording was started. After 20 s, the gas flow was shifted to 2% O_2, and cells were recorded for an additional 20 s. To determine the average reversal frequency over time, the numbers of detected reversals within 5-s intervals were added from three independent video recordings and normalized to the total corresponding tracking time.

SUPPLEMENTAL MATERIAL

Supplemental material for this article may be found at http://mbio.asm.org/lookup/suppl/doi:10.1128/mBio.02117-14/-/DCSupplemental.

Figure S1, PDF file, 0.1 MB.
Figure S2, PDF file, 0.1 MB.
Figure S3, PDF file, 0.1 MB.
Figure S4, PDF file, 0.01 MB.
Figure S5, PDF file, 0.02 MB.
Figure S6, PDF file, 0.02 MB.
Figure S7, PDF file, 0.2 MB.
Table S1, PDF file, 0.01 MB.
Table S2, PDF file, 0.03 MB.

ACKNOWLEDGMENTS

We thank ChromoTek GmbH for providing the GBP nanobody. We also thank M. Eibauer and A. Heins for help with CHAP implementation.

This work was funded by DFG grants Schu1080/9-1, 15-1, and 16-1 to D.S.

S.B., F.P., and D.S. designed the research; S.B., F.P., and J.H. performed the research; S.B., F.P., and D.S. analyzed the data; S.B., F.P., and D.S. wrote the paper.

REFERENCES

1. **Carlson JR, Weissman IL.** 1988. Molecular tools for inactivating a yeast enzyme *in vivo*. Mol Cell Biol **8:**2647–2650.
2. **Kaiser PD, Maier J, Traenkle B, Emele F, Rothbauer U.** 2014. Recent progress in generating intracellular functional antibody fragments to target and trace cellular components in living cells. Biochim Biophys Acta **1844:**1933–1942. http://dx.doi.org/10.1016/j.bbapap.2014.04.019.
3. **Marasco WA, Haseltine WA, Chen SY.** 1993. Design, intracellular expression, and activity of a human anti-human immunodeficiency virus type 1 Gp120 single-chain antibody. Proc Natl Acad Sci U S A **90:**7889–7893. http://dx.doi.org/10.1073/pnas.90.16.7889.
4. **Tavladoraki P, Benvenuto E, Trinca S, De Martinis D, Cattaneo A, Galeffi P.** 1993. Transgenic plants expressing a functional single-chain Fv antibody are specifically protected from virus attack. Nature **366:**469–472. http://dx.doi.org/10.1038/366469a0.
5. **Wesolowski J, Alzogaray V, Reyelt J, Unger M, Juarez K, Urrutia M, Cauerhff A, Danquah W, Rissiek B, Scheuplein F, Schwarz N, Adriouch S, Boyer O, Seman M, Licea A, Serreze DV, Goldbaum FA, Haag F, Koch-Nolte F.** 2009. Single domain antibodies: promising experimental and therapeutic tools in infection and immunity. Med Microbiol Immunol **198:**157–174. http://dx.doi.org/10.1007/s00430-009-0116-7.
6. **Bodelón G, Palomino C, Fernández LÁ.** 2013. Immunoglobulin domains in *Escherichia coli* and other enterobacteria: from pathogenesis to applications in antibody technologies. FEMS Microbiol Rev **37:**204–250. http://dx.doi.org/10.1111/j.1574-6976.2012.00347.x.
7. **Lauwereys M, Arbabi Ghahroudi M, Desmyter A, Kinne J, Hölzer W, De Genst E, Wyns L, Muyldermans S.** 1998. Potent enzyme inhibitors

derived from dromedary heavy-chain antibodies. EMBO J **17:**3512–3520. http://dx.doi.org/10.1093/emboj/17.13.3512.

8. **Pellis M, Pardon E, Zolghadr K, Rothbauer U, Vincke C, Kinne J, Dierynck I, Hertogs K, Leonhardt H, Messens J, Muyldermans S, Conrath K.** 2012. A bacterial-two-hybrid selection system for one-step isolation of intracellularly functional nanobodies. Arch Biochem Biophys **526:**114–123. http://dx.doi.org/10.1016/j.abb.2012.04.023.
9. **De Meyer T, Muyldermans S, Depicker A.** 2014. Nanobody-based products as research and diagnostic tools. Trends Biotechnol **32:**263–270. http://dx.doi.org/10.1016/j.tibtech.2014.03.001.
10. **Muyldermans S.** 2013. Nanobodies: natural single-domain antibodies. Annu Rev Biochem **82:**775–797. http://dx.doi.org/10.1146/annurev-biochem-063011-092449.
11. **De Genst E, Silence K, Decanniere K, Conrath K, Loris R, Kinne J, Muyldermans S, Wyns L.** 2006. Molecular basis for the preferential cleft recognition by dromedary heavy-chain antibodies. Proc Natl Acad Sci U S A **103:**4586–4591. http://dx.doi.org/10.1073/pnas.0505379103.
12. **Jobling SA, Jarman C, Teh MM, Holmberg N, Blake C, Verhoeyen ME.** 2003. Immunomodulation of enzyme function in plants by single-domain antibody fragments. Nat Biotechnol **21:**77–80. http://dx.doi.org/10.1038/nbt772.
13. **Kirchhofer A, Helma J, Schmidthals K, Frauer C, Cui S, Karcher A, Pellis M, Muyldermans S, Casas-Delucchi CS, Cardoso MC, Leonhardt H, Hopfner KP, Rothbauer U.** 2010. Modulation of protein properties in living cells using nanobodies. Nat Struct Mol Biol **17:**133–138. http://dx.doi.org/10.1038/nsmb.1727.
14. **Tang JC, Szikra T, Kozorovitskiy Y, Teixiera M, Sabatini BL, Roska B, Cepko CL.** 2013. A nanobody-based system using fluorescent proteins as scaffolds for cell-specific gene manipulation. Cell **154:**928–939. http://dx.doi.org/10.1016/j.cell.2013.07.021.
15. **Caussinus E, Kanca O, Affolter M.** 2012. Fluorescent fusion protein knockout mediated by anti-GFP nanobody. Nat Struct Mol Biol **19:**117–121. http://dx.doi.org/10.1038/nsmb.2180.
16. **Herce HD, Deng W, Helma J, Leonhardt H, Cardoso MC.** 2013. Visualization and targeted disruption of protein interactions in living cells. Nat Commun **4:**2660. http://dx.doi.org/10.1038/ncomms3660.
17. **Rothbauer U, Zolghadr K, Muyldermans S, Schepers A, Cardoso MC, Leonhardt H.** 2008. A versatile nanotrap for biochemical and functional studies with fluorescent fusion proteins. Mol Cell Proteomics **7:**282–289. http://dx.doi.org/10.1074/mcp.M700342-MCP200.
18. **Schornack S, Fuchs R, Huitema E, Rothbauer U, Lipka V, Kamoun S.** 2009. Protein mislocalization in plant cells using a GFP-binding chromobody. Plant J **60:**744–754. http://dx.doi.org/10.1111/j.1365-313X.2009.03982.x.
19. **Spira F, Mueller NS, Beck G, von Olshausen P, Beig J, Wedlich-Söldner R.** 2012. Patchwork organization of the yeast plasma membrane into numerous coexisting domains. Nat Cell Biol **14:**640–648. http://dx.doi.org/10.1038/ncb2487.
20. **Gitai Z.** 2005. The new bacterial cell biology: moving parts and subcellular architecture. Cell **120:**577–586. http://dx.doi.org/10.1016/j.cell.2005.02.026.
21. **Margolin W.** 2009. Sculpting the bacterial cell. Curr Biol **19:**R812–R822. http://dx.doi.org/10.1016/j.cub.2009.06.033.
22. **Shapiro L, McAdams HH, Losick R.** 2009. Why and how bacteria localize proteins. Science **326:**1225–1228. http://dx.doi.org/10.1126/science.1175685.
23. **Cornejo E, Abreu N, Komeili A.** 2014. Compartmentalization and organelle formation in bacteria. Curr Opin Cell Biol **26:**132–138. http://dx.doi.org/10.1016/j.ceb.2013.12.007.
24. **Murat D, Byrne M, Komeili A.** 2010. Cell biology of prokaryotic organelles. Cold Spring Harbor Perspect Biol **2:**a000422. http://dx.doi.org/10.1101/cshperspect.a000422.
25. **Chen AH, Silver PA.** 2012. Designing biological compartmentalization. Trends Cell Biol **22:**662–670. http://dx.doi.org/10.1016/j.tcb.2012.07.002.
26. **Bashor CJ, Horwitz AA, Peisajovich SG, Lim WA.** 2010. Rewiring cells: synthetic biology as a tool to interrogate the organizational principles of living systems. Annu Rev Biophys **39:**515–537. http://dx.doi.org/10.1146/annurev.biophys.050708.133652.
27. **Choudhary S, Quin MB, Sanders MA, Johnson ET, Schmidt-Dannert C.** 2012. Engineered protein nano-compartments for targeted enzyme localization. PLoS One **7:**e33342. http://dx.doi.org/10.1371/journal.pone.0033342.
28. **Frank S, Lawrence AD, Prentice MB, Warren MJ.** 2013. Bacterial microcompartments moving into a synthetic biological world. J Biotechnol **163:**273–279. http://dx.doi.org/10.1016/j.jbiotec.2012.09.002.
29. **Kerfeld CA, Heinhorst S, Cannon GC.** 2010. Bacterial microcompartments. Annu Rev Microbiol **64:**391–408. http://dx.doi.org/10.1146/annurev.micro.112408.134211.
30. **Chau AH, Walter JM, Gerardin J, Tang C, Lim WA.** 2012. Designing synthetic regulatory networks capable of self-organizing cell polarization. Cell **151:**320–332. http://dx.doi.org/10.1016/j.cell.2012.08.040.
31. **Katzmann E, Scheffel A, Gruska M, Plitzko JM, Schüler D.** 2010. Loss of the actin-like protein MamK has pleiotropic effects on magnetosome formation and chain assembly in *Magnetospirillum gryphiswaldense*. Mol Microbiol **77:**208–224. http://dx.doi.org/10.1111/j.1365-2958.2010.07202.x.
32. **Scheffel A, Gruska M, Faivre D, Linaroudis A, Graumann PL, Plitzko JM, Schüler D.** 2006. Corrigendum: an acidic protein aligns magnetosomes along a filamentous structure in magnetotactic bacteria. Nature **441:**248. http://dx.doi.org/10.1038/nature04777.
33. **Faivre D, Schüler D.** 2008. Magnetotactic bacteria and magnetosomes. Chem Rev **108:**4875–4898. http://dx.doi.org/10.1021/cr078258w.
34. **Pollithy A, Romer T, Lang C, Müller FD, Helma J, Leonhardt H, Rothbauer U, Schüler D.** 2011. Magnetosome expression of functional camelid antibody fragments (nanobodies) in *Magnetospirillum gryphiswaldense*. Appl Environ Microbiol **77:**6165–6171. http://dx.doi.org/10.1128/AEM.05282-11.
35. **Briegel A, Ortega DR, Tocheva EI, Wuichet K, Li Z, Chen S, Müller A, Iancu CV, Murphy GE, Dobro MJ, Zhulin IB, Jensen GJ.** 2009. Universal architecture of bacterial chemoreceptor arrays. Proc Natl Acad Sci U S A **106:**17181–17186. http://dx.doi.org/10.1073/pnas.0905181106.
36. **Popp F, Armitage JP, Schüler D.** 2014. Polarity of bacterial magnetotaxis is controlled by aerotaxis through a common sensory pathway. Nat Commun **5:**5398. http://dx.doi.org/10.1038/ncomms6398.
37. **Kentner D, Thiem S, Hildenbeutel M, Sourjik V.** 2006. Determinants of chemoreceptor cluster formation in *Escherichia coli*. Mol Microbiol **61:**407–417. http://dx.doi.org/10.1111/j.1365-2958.2006.05250.x.
38. **Maddock JR, Shapiro L.** 1993. Polar location of the chemoreceptor complex in the *Escherichia coli* cell. Science **259:**1717–1723. http://dx.doi.org/10.1126/science.8456299.
39. **Wadhams GH, Warren AV, Martin AC, Armitage JP.** 2003. Targeting of two signal transduction pathways to different regions of the bacterial cell. Mol Microbiol **50:**763–770. http://dx.doi.org/10.1046/j.1365-2958.2003.03716.x.
40. **Ringgaard S, Schirner K, Davis BM, Waldor MK.** 2011. A family of ParA-like ATPases promotes cell pole maturation by facilitating polar localization of chemotaxis proteins. Genes Dev **25:**1544–1555. http://dx.doi.org/10.1101/gad.2061811.
41. **Uebe R, Junge K, Henn V, Poxleitner G, Katzmann E, Plitzko JM, Zarivach R, Kasama T, Wanner G, Pósfai M, Böttger L, Matzanke B, Schüler D.** 2011. The cation diffusion facilitator proteins MamB and MamM of *Magnetospirillum gryphiswaldense* have distinct and complex functions, and are involved in magnetite biomineralization and magnetosome membrane assembly. Mol Microbiol **82:**818–835. http://dx.doi.org/10.1111/j.1365-2958.2011.07863.x.
42. **Rothbauer U, Zolghadr K, Tillib S, Nowak D, Schermelleh L, Gahl A, Backmann N, Conrath K, Muyldermans S, Cardoso MC, Leonhardt H.** 2006. Targeting and tracing antigens in live cells with fluorescent nanobodies. Nat Methods **3:**887–889. http://dx.doi.org/10.1038/nmeth953.
43. **Lang C, Schüler D.** 2008. Expression of green fluorescent protein fused to magnetosome proteins in microaerophilic magnetotactic bacteria. Appl Environ Microbiol **74:**4944–4953. http://dx.doi.org/10.1128/AEM.00231-08.
44. **Grünberg K, Müller EC, Otto A, Reszka R, Linder D, Kube M, Reinhardt R, Schüler D.** 2004. Biochemical and proteomic analysis of the magnetosome membrane in *Magnetospirillum gryphiswaldense*. Appl Environ Microbiol **70:**1040–1050. http://dx.doi.org/10.1128/AEM.70.2.1040-1050.2004.
45. **Ohuchi S, Schüler D.** 2009. *In vivo* display of a multisubunit enzyme complex on biogenic magnetic nanoparticles. Appl Environ Microbiol **75:**7734–7738. http://dx.doi.org/10.1128/AEM.01640-09.
46. **Borg S, Hofmann J, Pollithy A, Lang C, Schüler D.** 2014. New vectors for chromosomal integration enable high-level constitutive or inducible magnetosome expression of fusion proteins in *Magnetospirillum gryphiswaldense*. Appl Environ Microbiol **80:**2609–2616. http://dx.doi.org/10.1128/AEM.00192-14.
47. **Katzmann E, Eibauer M, Lin W, Pan Y, Plitzko JM, Schüler D.** 2013.

Analysis of magnetosome chains in magnetotactic bacteria by magnetic measurements and automated image analysis of electron micrographs. Appl Environ Microbiol **79:**7755–7762. http://dx.doi.org/10.1128/AEM.02143-13.

48. **Jogler C, Schüler D.** 2009. Genomics, genetics, and cell biology of magnetosome formation. Annu Rev Microbiol **63:**501–521. http://dx.doi.org/10.1146/annurev.micro.62.081307.162908.
49. **Lohsse A, Ullrich S, Katzmann E, Borg S, Wanner G, Richter M, Voigt B, Schweder T, Schüler D.** 2011. Functional analysis of the magnetosome island in *Magnetospirillum gryphiswaldense*: the *mamAB* operon is sufficient for magnetite biomineralization. PLoS One **6:**e25561. http://dx.doi.org/10.1371/journal.pone.0025561.
50. **Katzmann E, Müller FD, Lang C, Messerer M, Winklhofer M, Plitzko JM, Schüler D.** 2011. Magnetosome chains are recruited to cellular division sites and split by asymmetric septation. Mol Microbiol **82:**1316–1329. http://dx.doi.org/10.1111/j.1365-2958.2011.07874.x.
51. **Erbse AH, Falke JJ.** 2009. The core signaling proteins of bacterial chemotaxis assemble to form an ultrastable complex. Biochemistry **48:**6975–6987. http://dx.doi.org/10.1021/bi900641c.
52. **Schulmeister S, Ruttorf M, Thiem S, Kentner D, Lebiedz D, Sourjik V.** 2008. Protein exchange dynamics at chemoreceptor clusters in *Escherichia coli*. Proc Natl Acad Sci U S A **105:**6403–6408. http://dx.doi.org/10.1073/pnas.0710611105.
53. **Briegel A, Wong ML, Hodges HL, Oikonomou CM, Piasta KN, Harris MJ, Fowler DJ, Thompson LK, Falke JJ, Kiessling LL, Jensen GJ.** 2014. New insights into bacterial chemoreceptor array structure and assembly from electron cryotomography. Biochemistry **53:**1575–1585. http://dx.doi.org/10.1021/bi5000614.
54. **Coppieters K, Dreier T, Silence K, de Haard H, Lauwereys M, Casteels P, Beirnaert E, Jonckheere H, Van de Wiele C, Staelens L, Hostens J, Revets H, Remaut E, Elewaut D, Rottiers P.** 2006. Formatted anti-tumor necrosis factor α VHH proteins derived from camelids show superior potency and targeting to inflamed joints in a murine model of collagen-induced arthritis. Arthritis Rheum **54:**1856–1866. http://dx.doi.org/10.1002/art.21827.
55. **Man S, Cheng R, Miao C, Gong Q, Gu Y, Lu X, Han F, Yu W.** 2011. Artificial trans-encoded small non-coding RNAs specifically silence the selected gene expression in bacteria. Nucleic Acids Res **39:**e50. http://dx.doi.org/10.1093/nar/gkr034.
56. **Na D, Yoo SM, Chung H, Park H, Park JH, Lee SY.** 2013. Metabolic engineering of *Escherichia coli* using synthetic small regulatory RNAs. Nat Biotechnol **31:**170–174. http://dx.doi.org/10.1038/nbt.2461.
57. **Melchionna T, Cattaneo A.** 2007. A protein silencing switch by ligand-induced proteasome-targeting intrabodies. J Mol Biol **374:**641–654. http://dx.doi.org/10.1016/j.jmb.2007.09.053.
58. **Garcillán-Barcia MP, Jurado P, González-Pérez B, Moncalián G, Fernández LA, de la Cruz F.** 2007. Conjugative transfer can be inhibited by blocking relaxase activity within recipient cells with intrabodies. Mol Microbiol **63:**404–416. http://dx.doi.org/10.1111/j.1365-2958.2006.05523.x.
59. **Jurado P, Fernández LA, De Lorenzo V.** 2006. *In vivo* drafting of single-chain antibodies for regulatory duty on the sigma54-promoter Pu of the TOL plasmid. Mol Microbiol **60:**1218–1227. http://dx.doi.org/10.1111/j.1365-2958.2006.05183.x.
60. **Zafra O, Fraile S, Gutiérrez C, Haro A, Páez-Espino AD, Jiménez JI, de Lorenzo V.** 2011. Monitoring biodegradative enzymes with nanobodies raised in *Camelus dromedarius* with mixtures of catabolic proteins. Environ Microbiol **13:**960–974. http://dx.doi.org/10.1111/j.1462-2920.2010.02401.x.
61. **Avalos JL, Fink GR, Stephanopoulos G.** 2013. Compartmentalization of metabolic pathways in yeast mitochondria improves the production of branched-chain alcohols. Nat Biotechnol **31:**335–341. http://dx.doi.org/10.1038/nbt.2509.
62. **DeLoache WC, Dueber JE.** 2013. Compartmentalizing metabolic pathways in organelles. Nat Biotechnol **31:**320–321. http://dx.doi.org/10.1038/nbt.2549.
63. **Heyen U, Schüler D.** 2003. Growth and magnetosome formation by microaerophilic *Magnetospirillum* strains in an oxygen-controlled fermenter. Appl Microbiol Biotechnol **61:**536–544. http://dx.doi.org/10.1007/s00253-002-1219-x.
64. **Sambrook J, Russell D.** 2001. Molecular cloning: a laboratory manual. Cold Spring Harbor Laboratory Press, New York, NY.
65. **Schultheiss D, Kube M, Schüler D.** 2004. Inactivation of the flagellin gene *flaA* in *Magnetospirillum gryphiswaldense* results in nonmagnetotactic mutants lacking flagellar filaments. Appl Environ Microbiol **70:**3624–3631. http://dx.doi.org/10.1128/AEM.70.6.3624-3631.2004.
66. **Heckman KL, Pease LR.** 2007. Gene splicing and mutagenesis by PCR-driven overlap extension. Nat Protoc **2:**924–932. http://dx.doi.org/10.1038/nprot.2007.132.
67. **Raschdorf O, Plitzko JM, Schüler D, Müller FD.** 2014. A tailored *galK* counterselection system for efficient markerless gene deletion and chromosomal tagging in *Magnetospirillum gryphiswaldense*. Appl Environ Microbiol **80:**4323–4330. http://dx.doi.org/10.1128/AEM.00588-14.
68. **Schüler D, Rainer U, Bäuerlein E.** 1995. A simple light scattering method to assay magnetism in *Magnetospirillum gryphiswaldense*. FEMS Microbiol Lett **132:**139–145. http://dx.doi.org/10.1111/j.1574-6968.1995.tb07823.x.
69. **Laemmli UK.** 1970. Cleavage of structural proteins during assembly of head of bacteriophage-T4. Nature **227:**680–685. http://dx.doi.org/10.1038/227680a0.
70. **Popp F, Armitage JP, Schüler D.** 2014. Polarity of bacterial magnetotaxis is controlled by aerotaxis through a common sensory pathway. Nat Commun **5:**5398.

Supplement Publication 2

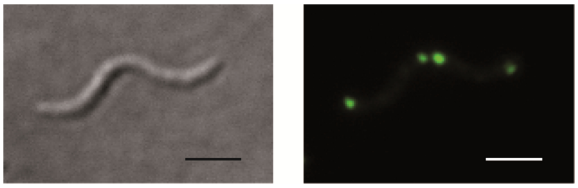

Supplementary Fig. S1: $CheW_1$-EGFP localization in a dividing cell. Representative DIC and fluorescence micrograph of a cell chromosomally expressing $CheW_1$-EGFP close to cell division. $CheW_1$-EGFP localizes distinctly at the cell poles and forms two new foci at mid-cell at the expected position of septum formation. Scale bar 2 µm.

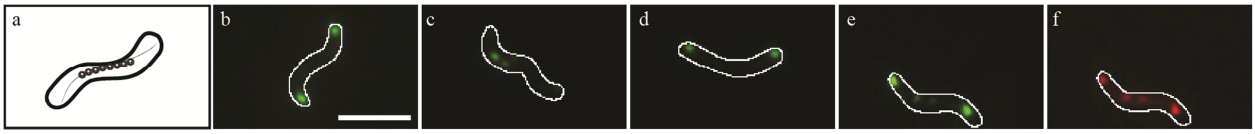

Supplementary Fig. S2: Schematics (a) and fluorescence micrograph of *M. gryphiswaldense* Δ*mamM* mutant cells expressing $CheW_1$-EGFP alone (b) or in combination with MamC-2xGBP (c) and wild type cells expressing chromosomal $CheW_1$-EGFP and cytoplasmic GBP (d), or $CheW_1$-EGFP and MamC-mCherry-GBP (e,f). Scale bar 2 µm.

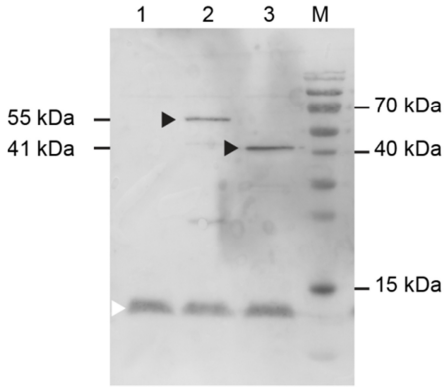

Supplementary Fig. S3: Western blot of *M. gryphiswaldense* cells expressing $CheW_1$-EGFP (1), $CheW_1$-EGFP MamC-mCherry-GBP (55.43 kDa) (2) and $CheW_1$-EGFP MamC-2xGBP (41.07 kDa), protein bands are indicated by black arrow heads (3). The native MamC (12.35 kDa) is present in all strains, indicated by white arrow head. Additional bands are visible for all strains expressing MamC fusions proving stable expression. MamC was detected using rabbit αMamC IgG as primary, and goat anti-rabbit IgG alkaline phosphatase antibodies as secondary antibody. PageRuler™ Prestained Protein Ladder from fermentas was used as a standard.

Supplementary Fig. S4: Fluorescence distribution in fluorescence micrographs of *M. gryphiswaldense* cells expressing chromosomal $CheW_1$-EGFP MamC-2xGBP. Scale bar 2 µm.

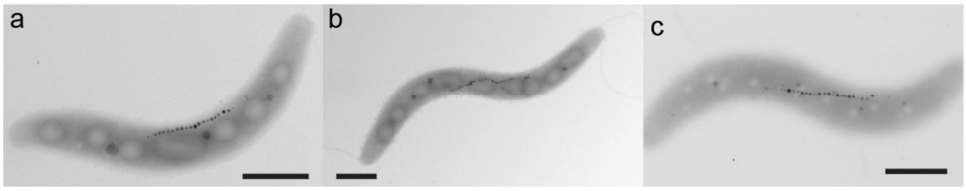

Supplementary Fig. S5: TEM micrographs of *M. gryphiswaldense* Δ*cheW*$_1$ (a) and cells expressing CheW$_1$-EGFP and cytoplasmic MagGBP (b) or CheW$_1$-EGFP and MamC-mCherry-GBP (c). Scale bar 1 µm.

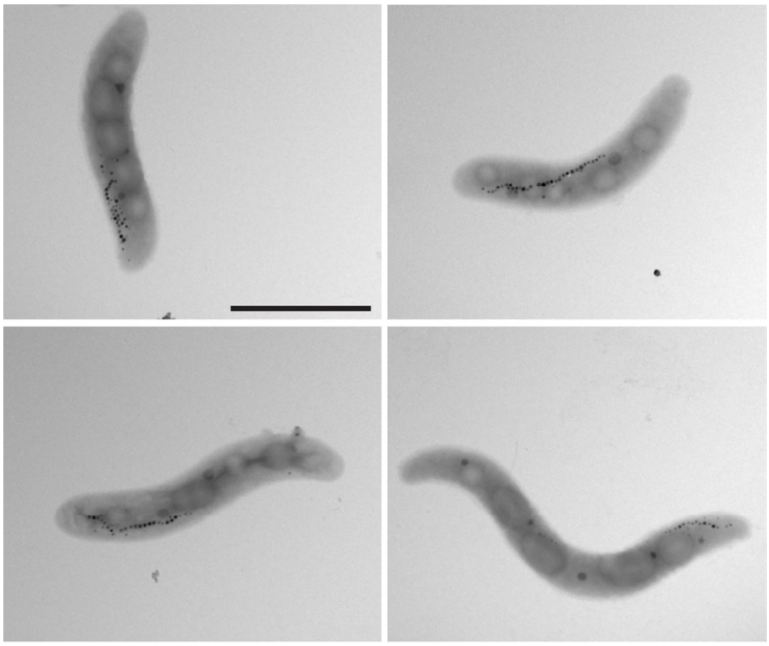

Supplementary Fig. S6: TEM micrographs of *M. gryphiswaldense* cells expressing CheW$_1$-EGFP and MamC-2xGBP. Scale bar 2 µm.

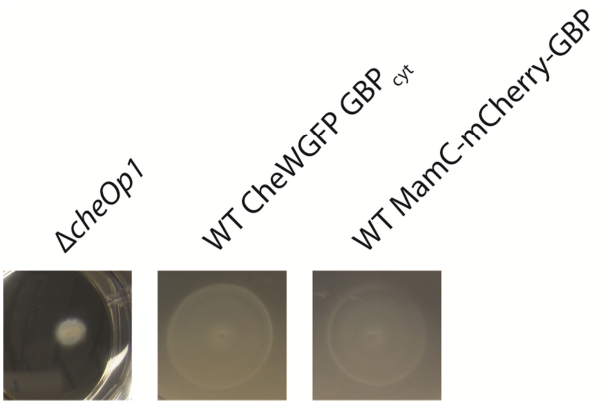

Supplementary Fig. S7: Swim halos of *M. gryphiswaldense* Δ*cheOp1* cells, wild type cells co-expressing either $CheW_1$-EGFP and MagGBPcyt or $CheW_1$-EGFP and MamC-mCherry-GBP.

Supplementary Table S1: Plasmids used in this study

Plasmid name	Description	Source or reference
pJET1.2/blunt	Cloning vector; Amp^R	Fermentas, Schwerte
pBBR-MCS2	Mobilizable broad-host-range vector; Km^R	M. E. Kovach, *et al*,. 1995
pBAM1	Km^R , Amp^R, oriR6K, *tnpA*	E. Martinez-Garcia, *et al.*, 2011
pORFM	pK19mobGII, universal in-frame deletion/in-frame fusion vector with GalK-based counterselection and MCS	O. Raschdorf and F. Müller, 2014
pMA-T GBPopt	Amp^R,ColE1 ori, *maggbp*	GeneArt® (Invitrogen), life technologies, Darmstadt
pGH-Trpl GBP	Amp^R, *maggbp-gbp-maggbp*	ATG:biosynthetics, Merzhausen
pSB6	pBAM1 with $P_{mamDC45}$, *magegfp*, Km^R, Amp^R	S. Borg, *et al.*, 2014
pSB7	pBAM1 with P_{tet}, *magegfp*, P_{Neo}-TetR, Km^R, Amp^R	S. Borg, *et al.*, 2014
pFP66	fusion of *cheW1-egfp-cheW1* downstream fragment inserted into pORFM	this study
pJH01	pAP150 with $P_{mamDC45}$, *cheW1-egfp*, Km^R	this study
pJH16	pBAM1 with $P_{mamDC45}$, *mamC-maggbp*, Km^R, Amp^R	this study
pJH17	pBAM1 with P_{tet}, *mamC-maggbp*, P_{Neo}-TetR, Km^R, Amp^R	this study
pJH39	pBAM1 with $P_{mamDC45}$, *mamC-maggbp-gbp*, Km^R, Amp^R	this study
pJH40	pBAM1 with P_{tet}, *mamC-maggbp-gbp*, P_{Neo}-TetR, Km^R, Amp^R	this study
pJH60	pBAM1 with $P_{mamDC45}$, *mamC-mCherry-maggbp*, Km^R, Amp^R	this study
pJH61	pBAM1 with P_{tet}, *mamC-mCherry-maggbp*, P_{Neo}-TetR, Km^R, Amp^R	this study
pJH97	pBAM1 with $P_{mamDC45}$, *mamC-maggbp-gbp-maggbp*, Km^R, Amp^R	this study
pJH100	pORFM with fused up- and downstream region of *cheW1* for deletion of *cheW1*	this study
pJH104	pBAM1 with $P_{mamDC45}$, *maggbp*, Km^R, Amp^R	this study

Supplementary Table S2: Strains used in this study

Strain	Description	Source or reference
Escherichia coli		
DH5α	F⁻ *sup*E44 Δ*lac*U169 (Φ 80 *lacZ*DM15) *hsd*R17 *recA*1 *end*A1 *gyr*A96 *thi*-1 *rel*A1	Invitrogen, life technologies, Darmstadt
WM3064	*thrB1004 pro thi rpsL hsdS lacZΔM15 RP4-1360 Δ(araBAD)567 ΔdapA1341::[erm pir]*	W. Metcalf, unpublished
BW29427	DAP auxotroph derivative of *E. coli* strain B2155	K. Datsenko and B. L. Wanner, unpublished
Magnetospirillum gryphiswaldense		
M. gryphiswaldense MSR-1 R3/S1	Rif^R, Sm^R spontaneous mutant, lab strain	D. Schultheiss, *et al.*, 2003
M. gryphiswaldense Δ*mamJ*	*ΔmamJ*	A. Scheffel, *et al.*, 2006
M. gryphiswaldense Δ*mamM*	*ΔmamM*	R. Uebe, *et al.*, 2011
M. gryphiswaldense Δ$cheW_1$	Δ$cheW_1$	this study
M. gryphiswaldense MSR-1 FP66	in frame fusion of *egfp* to $cheW_1$	this study
M. gryphiswaldense Δ$cheW_1$ (pJH01)	Δ$cheW_1$ complemented with p JH01	this study
M. gryphiswaldense MSR-1 JH5	FP66 transposon mutant with inserted *maggbp* from $P_{mamDC45}$, Km^R	this study
M. gryphiswaldense MSR-1 JH6	FP66 transposon mutant with inserted *mamC-maggbp* from $P_{mamDC45}$, Km^R	this study
M. gryphiswaldense MSR-1 JH7	FP66 transposon mutant with inserted *mamC-maggbp-gbp* from $P_{mamDC45}$, Km^R	this study
M. gryphiswaldense MSR-1 JH8	FP66 transposon mutant with inserted *mamC-mCherry-maggbp* from P_{tet}, Km^R	this study
M. gryphiswaldense MSR-1 JH9	FP66 transposon mutant with inserted *mamC-maggbp-gbp* from P_{tet}, Km^R	this study

M. gryphiswaldense MSR-1 JH10	FP66 transposon mutant with inserted *mamC-maggbp-gbp-maggbp* from P_{tet}, Km^R	this study
M. gryphiswaldense MSR-1 JH11	*ΔmamJ* with inframe fusion of *egfp* to *cheW1*	this study
M. gryphiswaldense MSR-1 JH12	JH11 transposon mutant with inserted *mamC-maggbp* from $P_{mamDC45}$, Km^R	this study
M. gryphiswaldense MSR-1 JH13	*ΔmamM* with inframe fusion of *egfp* to *cheW1*	this study
M. gryphiswaldense MSR-1 JH14	JH13 transposon mutant with inserted *mamC-maggbp-gbp* from $P_{mamDC45}$, Km^R	this study

3 DISCUSSION

3.1 Run-and-reverse motility is based on bidirectional motor output of *M. gryphiswaldense*

In this work, the tactic behavior and motility of bipolarly flagellated *M. gryphiswaldense* were studied in detail for the first time. In a set of behavioral experiments I first investigated the general swimming behavior of *M. gryphiswaldense* and found that cells display a run-and-reverse motility pattern, frequently swimming smoothly over large distances (> 1mm). In cells that were tethered to the cover slip bidirectional motor rotation was observed, suggesting changes in swimming direction were caused by motor reversals. At the genomic level a large number of putative sensory and signal transduction molecules were found that might play a role in magnetotaxis, hinting at a very complex chemosensory system. Apart from three CetAB-like gene pairs (Elliott et al. 2009), 56 genes encoding putative MCPs and 31 encoding single domain response regulators, I could identify four putative chemotaxis operons (*cheOp1-4)* that were located on nine different contigs in the draft genomic assembly. Of those only a single operon, *cheOp1*, was found to be essential for energy taxis of *M. gryphiswaldense*, while deletion of all three remaining operons only weakly affected chemotactic efficiency. *cheOp1* encodes the conserved chemotaxis genes *cheA*, *cheW*, *cheY*, *cheB* and *cheR*, and fluorescently labelled fusions of CheW and CheA were detected at both cell poles. In a strain that was deleted for *cheOp1* no swimming reversals were detected and cells were unable to navigate within oxygen gradients.

In contrast to some well investigated model organisms, many environmental isolates including the majority of marine bacteria swim similar to *M. gryphiswaldense* and employ the same run-and-reverse navigational strategy (Johansen et al. 2002). Cells with bipolar flagellation often move with equal probability in either direction and every reversal leads to reorientation angles close to 180 degrees. Assuming that motors at both poles rotate simultaneously, they have to turn in opposite directions at any given time to produce coordinated forward or reverse propulsion of the cell. Counter-rotating motors have been observed in *S. volutans*, marine spirilla and recently also in *M. magneticum*, a close relative of *M. gryphiswaldense* (Thar & Fenchel 2005; Krieg et al. 1967; Murat et al. 2014). Although one recent study has postulated motor activity alternating between the poles of *M. gryphiswaldense*, with reversible rotation of only a single flagellum at each time (Reufer et al. 2013), in my analysis of tethered cells I never detected extended rotation pauses. Together with the observation that motors turn CW and CCW with equal speed, we concluded that analogous to other bipolarly flagellated bacteria

M. gryphiswaldense most probably is propelled by simultaneous rotation of both its flagella with opposite rotational senses.

Bidirectional motor activity effecting symmetrical back-and-forth movements is in strong contrast to the well investigated run-and-tumble and other motility patterns. In the model organism *E. coli* smooth swimming is caused by collective CCW rotation of its 4-8 peritrichous flagella, while CW rotation of single or multiple flagella results in a tumble. In this motility regime, smooth swimming is clearly associated with motors turning in one specific direction, while motor rotation with the opposite sense leads to reorientation.

Despite the divergence from the swimming pattern of peritrichous *E. coli*, also in (mono-) polarly flagellated bacteria like *V. alginolyticus, A. brasilense* or *R. sphaeroides* the concentration of CheY~P is increased by repellent stimuli. This causes motors to switch from their default rotational motion to an alternative state, thereby randomly reorienting bacterial cells. In the case of counter-rotating motors, however, there is no obvious asymmetry between different motor states, since reversals of rotational sense from CCW to CW do not randomize swimming tracks to a greater extent than reversals in the opposite direction. This might imply that there is *per se* no default rotational state of flagellar motors (CCW or CW) in bipolarly flagellated bacteria, which would be altered after stimulation as in other bacteria for a characteristic time length (the duration of a stop or a tumble) before returning to the default condition.

In summary, according to the classical view of chemotaxis, the signal transduction cascade regulates how often the motor transiently deviates from its default state per time. In contrast, in bipolarly flagellated bacteria rather the frequency of switching between two equivalent modes might be regulated (like in gliding bacteria that show equally timed runs with each pole leading (Shi et al. 1996)). Instead of modulating the sheer number of uniform tumble events per time, in an analogous way bipolar swimmers might regulate the duration of both runs and reversals to control the degree of directional change per time.

The lack of clear phenotype in the *M. gryphiswaldense* Δ*cheOp2-4* mutant together with the smooth-swimming phenotype of the Δ*cheOp1* mutant suggested that CheA1 is the only essential histidine kinase involved in aerotaxis modulating CheY~P levels. Assuming that CheY~P is similarly produced at both poles and concentrations are more or less comparable, this implies that motors generate opposite output, although both polar complexes receive the same input. Therefore the question arises how such an asymmetric behavior might be implemented at the molecular level.

One hypothesis is that some kind of structural asymmetry is at the basis of opposite motor output generated at the two different poles (Fig. 3-1a). Structural asymmetry could be estab-

lished through expression of different homologs of motor proteins that are each exclusively localized to a single pole. For example, bipolarly flagellated bacteria like *P. molischianum*, *R. rubrum* or *M. gryphiswaldense* possess two pairs of stator genes *motAB*, whereas the genomes of model organisms *E. coli* and *Salmonella typhimurium* encode only a single pair of *motAB*. However, in other bacteria it is quite common that single flagellar motors are driven by different types of stator units and hybrid motors have been observed (Paulick et al. 2009; Toutain et al. 2005). *Bdellovibrio bacteriovorus* represents an extreme case and simultaneously expresses three pairs of stator genes *motAB*, although it possesses only a single polar flagellum (Morehouse et al. 2011). Having two variable stator proteins therefore *per se* is not a specific characteristic of bipolarly flagellated bacteria. Furthermore, both MotA proteins of *M. gryphiswaldense* contain the highly conserved charged residues involved in torque generation. Even in *B. subtilis*, where CW rotation is the default state of flagellar motors and CCW intervals are a consequence of CheY~P binding, there are no clear indications for a modified charge landscape on the cytoplasmic loop of MotA that might be responsible for the altered default rotational sense (Takahashi & Ito 2014). Nevertheless, the function and localization of individual stator proteins in *M. gryphiswaldense* should be investigated in future studies to gain better understanding of their role in counter-rotating motor behavior.

In the case of the rotor protein FliG, differential localization of two distinct homologs has been reported previously in the spirochete *Borellia burgdorferi* (Li et al. 2010). While one FliG homolog which shares a high degree of similarity with *E. coli* FliG is localized at both poles and is essential for flagella synthesis, the second homolog is less conserved and is localized at a single pole only. In contrast to deletion of the first homolog that leads to completely non-motile cells, deletion of the second homolog inactivates the flagella bundle only at one cell pole. The second FliG homolog therefore appears to be responsible for asymmetric motor output at the two cell poles in *B. burgdorferi*. In contrast to spirochetes, however, the genome of *M. gryphiswaldense* encodes only a single *fliG* copy. All the key charged residues needed for rotor-stator interaction and torque generation in *E. coli* and other bacteria (Lloyd et al. 1999) are well-conserved in *M. gryphiswaldense* FliG, which shares a high degree of conservation with *E. coli* FliG (28% identity, 52% similarity at the protein level).

Although structural asymmetry of motor components between opposite poles of bipolarly flagellated bacteria appears to be an attractive hypothesis for explaining counter-rotating motor output, in summary it has to be concluded that at least in *M. gryphiswaldense* so far there are no obvious candidates which are in possible support of such a theory. The genome of *M. gryphiswaldense* encodes only a single conserved copy each of rotor proteins FliG (*mgr0429*) (see above), FliM (*mgr0045*) and FliN (*mgr1042*), which holds also true for the closely related

M. magneticum (*amb0502*, *amb3498*, *amb0500*, respectively). Furthermore, there are no conspicuous features found in *M. gryphiswaldense* MotA homologs, and the number of different stator systems clearly does not correlate with the cellular pattern of flagellation or a putative structural asymmetry.

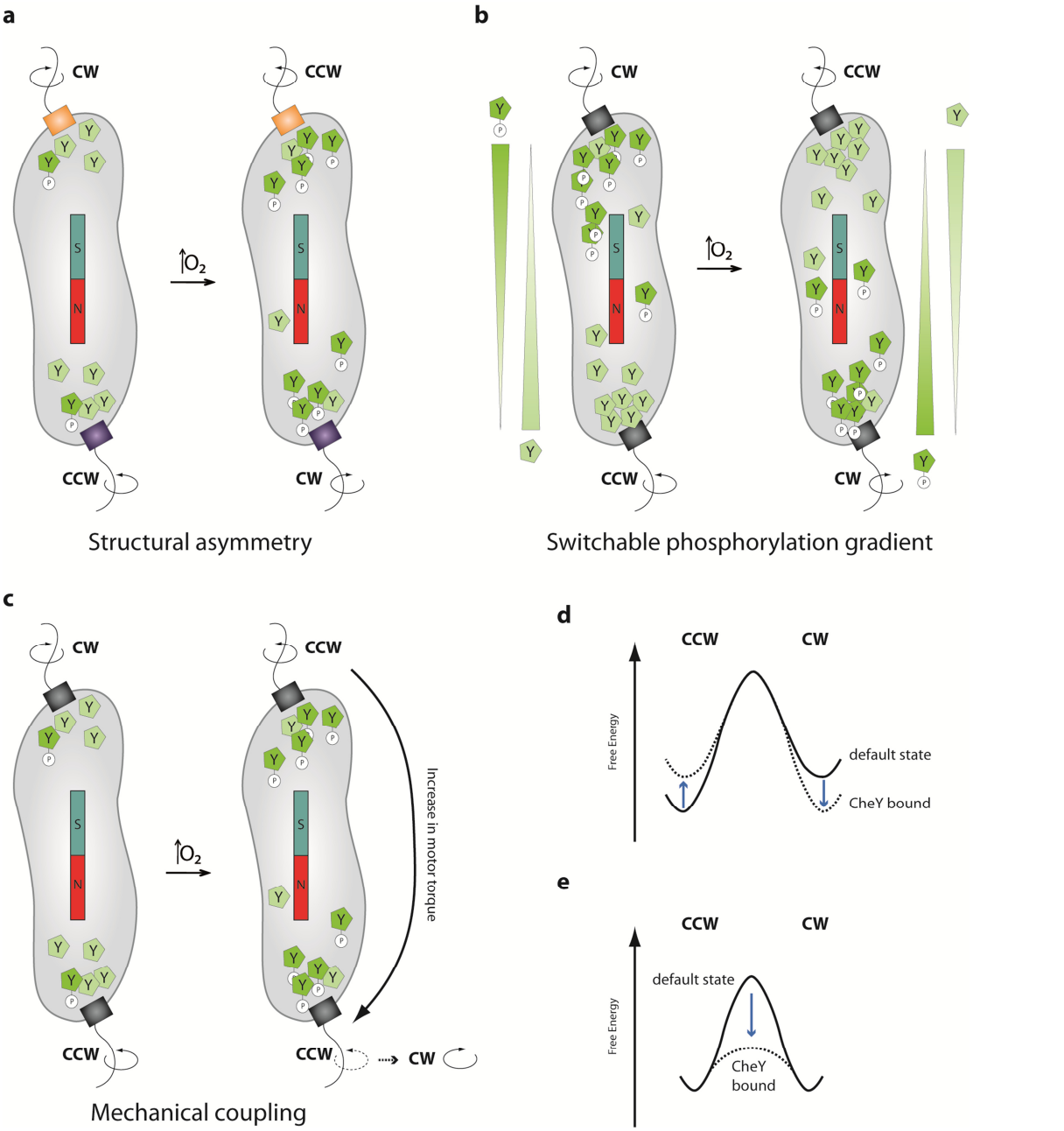

Fig. 3-1 Different models for motor coupling in bipolarly flagellated bacteria that might be based on: (a) structural asymmetry; (b) switchable phosphorylation gradients, or (c) mechanical coupling. For explanations see text. (d) Idealized free energy levels of CW and CCW states in motors of enteric bacteria. (e) Hypothetical free energy levels of CW and CCW states in motors with symmetrical output.

If the motors at both poles in principle are equivalent and their output is assumed to be determined by the level of CheY phosphorylation, then a CheY~P gradient would have to be established between opposite poles to explain counterrotating motor output (Fig. 3-1b). In such a model the phosphorylation gradient had to switch its relative orientation rapidly to enable swimming reversals. In order to achieve phosphorylation at one pole and concomitant dephosphorylation at the other pole, the action of a specific kinase/phosphatase pair at one pole had to be coordinated with the action of a corresponding pair of enzymes at the other pole in a timely fashion. In the early years of chemotaxis research it has been speculated that electrical signals might play a role in synchronizing motors separated by distances too large for diffusion (Berg 1975). However, to date no clear proof supporting such a hypothesis has been presented. Another point that argues against a switchable CheY~P gradient are reversals observed in *M. gryphiswaldense* under equilibrium conditions, since it does not seem plausible that the signal transduction chain produces strongly varying output, i.e. phosphorylation levels, at unchanged chemoeffector concentration.

For these reasons other mechanisms might be coordinating output of flagellar motors that are separated from each other by several micrometers. One possibility might be mechanical coupling between motors that have equal probability of being in either CW or CCW state. In the case of *E. coli* motors, the energy levels of CCW and CW states differ in that the CCW energy level is lower than the CW energy level as long as CheY~P is not bound to the switch complex (Fig. 3-1d) (Scharf et al. 1998; Sowa & Berry 2008). Upon binding of CheY~P the CCW state becomes less favorable and motors are inclined to switch to CW rotation. However, the example of *B. subtilis* motors (that switch from CW to CCW upon binding of CheY~P) proves that other energy landscapes are possible which most probably are due to the molecular architecture of the switch complex. By analogy, it therefore seems conceivable that bacteria with counter-rotating motors contain switch complexes with balanced CCW and CW energy levels that do not favor one direction over the other (Fig. 3-1e). Instead of specifically lowering the energy level of one particular rotational state, binding of CheY~P might lower the activation energy barrier of rotor unit flipping, which would increase the overall probability of motor reversals. Such a model is supported by recent findings in polarly flagellated cells of *Pseudomonas* spp., whose motors spend an equal amount of time in either CW or CCW rotation modes and therefore appear to be symmetric (Qian et al. 2013). As in classical chemotaxis systems, the frequency of motor reversals is controlled by CheY~P in *P. aeruginosa* and deletion of *cheY* leads to rare switching events and increased durations of both CW and CCW intervals. In the case of *M. gryphiswaldense* Δ*cheOp1* cells the activation energy for switching between CW and CCW might be too high, since virtually no reversals were observed in freely swimming cells in the absence of CheY~P.

Mechanical coupling between bipolar flagella, on the other hand, could be a direct effect of the torque-sensing capacity of flagellar motors. It has been recently found that apart from signals transduced via the CheY~P pathway, also mechanical load on the torque producing units affects the switching probability of flagellar motors (Yuan et al. 2009; Fahrner et al. 2003). When fast rotating motors are slowed down by a sudden increase in torque, e.g. due to neighboring motors that have reversed rotational sense, this results in a higher overall switching probability. It has therefore been hypothesized that the load-switching mechanism might be used to coordinate the switching of multiple flagellar motors within a single cell, which generally occurs in a very synchronous fashion and less frequent than isolated motors were measured to reverse (Bai et al. 2012; Hu & Tu 2013). In a similar way, such a mechanism could be the source of mechanical coupling between motors of *M. gryphiswaldense* that have equal probability of being in either state (switching of motor 1 to CW rotation would "force" motor 2 mechanically to rotate CCW and vice versa) (Fig. 3-1c). Mechanical effects on flagellar motors might also provide an alternative, more simple explanation for sensory behaviors that have recently been reported in MTB swimming in strong magnetic fields (Philippe & Wu 2010; Zhu et al. 2014; González et al. 2014). For example, the postulated ability of magnetospirilla to sense the degree of alignment of their cellular dipole with **B** possibly could be attributed to the drag forces that strong magnetic fields impose on flagellar motors, rather than representing effects of true signal transduction processes as has been claimed in these studies.

In conclusion, at the moment it cannot be decided which of the proposed models explains motor output coordination in *M. gryphiswaldense*. However, mechanical coupling of equivalent motors appears to be the most plausible hypothesis, because in this case increased CheY~P levels indeed would be reflected by increased swimming reversal rates, an effect that is hard to explain with the other two models.

3.2 Oxygen triggers an unusual tactic response in *M. gryphiswaldense* that is controlled by CheOp1

In this work aerotaxis was found to be the dominant tactic behavior of *M. gryphiswaldense*. In the presence of oxygen no other chemotactic response could be detected in chemical-in-plug assays. The sensory pathway CheOp1 was furthermore identified as being essential for tactic responses towards oxygen and nitrate, which are probably sensed through a common energy taxis mechanism. In the absence of CheOp1, no reaction towards oxygen was detected in flat capillaries, swim agar plates or temporal oxygen shift assays. Additionally, Δ*cheOp1* mutant cells did not form bands in gradients of nitrate under anoxic conditions.

In wild type cells the response to an up-shift from 0% to 2% oxygen was unusual in that it did not resemble a clear attractant or repellent response, because a short phase in which virtually every cell reversed was followed by a sustained drop in overall switching probability. Reversal frequency did not return to anoxic pre-stimulus levels for at least 80 s, resulting in long unidirectional swimming movements. Reversal frequency overshoot has been reported in other bacteria following a smooth swimming phase occurring in response to oxygen addition (Laszlo & Taylor 1981; Lindbeck et al. 1995). However, a repellent response towards high oxygen levels in other systems is terminated by a return to pre-stimulus reversal frequencies within 30 s (Shioi et al. 1987; Zhulin et al. 1996), and not by an extended phase of reversal suppression. In non-MTB a reduced reversal frequency is associated with preferred environments. However, in non-magnetic bacteria very long run intervals are not advantageous because cells quickly become disoriented due to Brownian motion. Therefore, reversals are not suppressed for extended time periods and cells return to baseline reversal frequencies through adaptation processes. In contrast, MTB are aligned to the geomagnetic field overruling random disorientation. Thus the straight, uninterrupted swimming tracks observed for MTB possibly may represent a form of "escape response" that is specific for these bacteria, swiftly guiding them to their preferred habitat. The steep gradient environments populated by MTB are typically located near the surface or within the first millimeters of sediments and are prone to strong temporal and spatial changes. The oxic-anoxic transition zone commonly is a very narrow layer, and few millimeters above or below the zone oxygen levels virtually are either completely oxic or anoxic (Flies, Jonkers, et al. 2005; Edwards et al. 2004). Under such near-equilibrium conditions at some distance to the OATZ, temporal gradient sensing cannot be very effective and the advantage of polar magnetotaxis might be its independency of sensing local gradients, which should prove beneficial after displacement into hyperoxic zones.

Oxygen can either be sensed directly (Szurmant & Ordal 2004) or indirectly by bacteria (Rebbapragada et al. 1997). Although the observed response of *M. gryphiswaldense* upon oxic shifts shows some characteristics that can be explained by a temporal sensing mechanism, the prominent difference clearly is the lack of adaptation, which points towards a different sensing mechanism or a specialized signal transduction pathway. The unusual reaction of *M. gryphiswaldense* could be explained by a form of two-step response. First, a "canonical" energy taxis mechanism might trigger multiple reversals as in other bacteria probably through increased phosphorylation of CheY. During prolonged exposure to elevated oxygen levels, however, the reversal frequency is reduced drastically below pre-stimulus levels by an as-yet unknown mechanism. Although the identification of relevant chemoreceptor(s) and CheY protein(s) which bind to the flagellar switch complex in *M. gryphiswaldense* was beyond the

scope of this work, it is possible to delineate several possible explanations for the shift of the chemotaxis signaling cascade and the motor components to a different state (Fig. 3-2):

1. The activity of chemoreceptors might be modulated.
2. The activity of the CheA kinase might be reduced.
3. The activity of CheY might be modulated or terminated.
4. Components of the motor switch complex might be directly targeted.

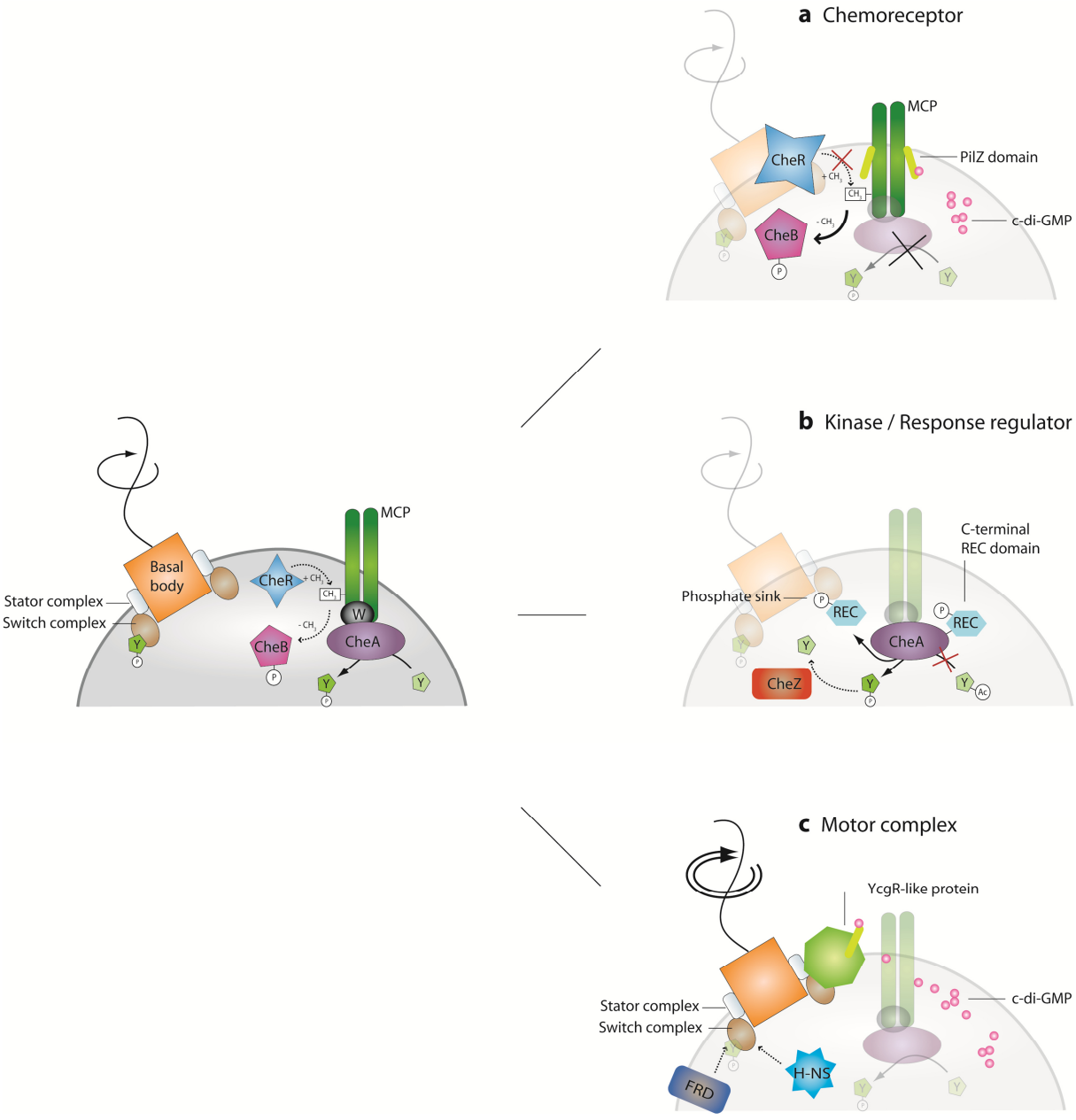

Fig. 3-2 Different models for swimming reversal suppression. (a) The activity of chemoreceptors could be modulated by adaptation proteins CheR/CheB or through binding of second messenger molecules. (b) The activity of the CheA kinase might be reduced, or the activity of CheY could be modulated or terminated by a dedicated phosphatase. (c) Components of the motor switch complex might be directly targeted by factors like FRD, H-NS or YcgR. For detailed explanations see text.

CheA1 is a hybrid histidine kinase that harbors a C-terminal response regulator receiver domain (REC). As commonly observed for such CheA proteins, no canonical P2 domain mediating binding of CheY is present (Wuichet et al. 2007). The C-terminal REC domain might possess an autoregulatory function, e.g. act as a phosphate sink or as attenuator of autophosphorylation (hypothesis 2; Fig 3-2b)(He et al. 2013; Inclán et al. 2008). Another possibility is that the signaling state of the kinase could be reset in the presence of repellent oxygen levels by an oxygen-sensitive allosteric factor directly binding CheA1.

At a later step of the signaling cascade downstream components could be modified such that overall fewer reversals are triggered during the escape response. The concentration of active CheY~P could be rapidly reduced through dephosphorylation mediated by a phosphatase (e.g. the CheZ homolog Mgr1070) or a phosphate sink (e.g. an alternative CheY species) (hypothesis 3; Fig 3-2b). The activity of CheY can also be modulated through acetylation, thereby inhibiting effective binding to both CheA and the switch complex (Liarzi et al. 2010).

Furthermore, the flagellar motor has been shown to interact with a growing list of identified proteins, and to be a direct target of factors modulating its output (hypothesis 4; Fig 3-2c) (Brown et al. 2011). In particular, there are several effectors that are supposed to interact with the rotor protein FliG. For instance, the metabolic state of the cell can be integrated by binding of fumarate reductase to FliG resulting in CW-biased motors. The *E. coli* transcriptional regulator H-NS stabilizes CCW motor rotation, while the *B. subtilis* protein EpsE functions as a clutch to promote biofilm formation (Brown et al. 2011; Blair et al. 2008). Another prominent example is the PilZ protein YcgR that is able to interact with motor components of *E. coli* (either FliG or MotA) depending on intracellular c-di-GMP levels, thereby slowing down rotation and simultaneously locking motors in the CCW mode (Paul et al. 2010; Boehm et al. 2010). Although no obvious homolog of YcgR exists in *M. gryphiswaldense*, factors influencing the conformation and activity of FliG might also be involved in magnetotaxis. However, it remains to be shown experimentally which of the many discussed mechanism is at the basis of reversal suppression in *M. gryphiswaldense*.

3.3 The magnetotaxis of *M. gryphiswaldense* is polar

The magnetic dipole moment resulting from intracellular magnetosome chains passively rotates MTB into alignment with **B** as they swim by means of flagella. This behavior was named magnetotaxis, although magnetic orientation is passive and MTB do not search for an ideal position within a magnetic field gradient. Nonetheless, magnetotaxis as observed in environmental bacteria has some intriguing features that justify the classification as a true adaptive and directed tactile behavior.

While related *Magnetospirilla* strains freshly isolated from the environment had been observed to display polar magnetotactic behavior (Schüler et al. 1999; Flies, Peplies, et al. 2005), this property apparently had been lost in the common *M. gryphiswaldense* lab strain during repeated subcultivation due to the absence of selective pressure, supposedly either through loss of the respective genes or, for instance, lack of expression of the necessary proteins. However, instead of the previously reported non-biased, axial magnetotactic behavior, in my experiments I found that polar responses can be elicited in individual cells through growth in magnetic fields that were superimposed on oxygen gradients. As has been proposed for axial magnetotaxis, *M. gryphiswaldense* indeed reverses motion at a relatively low frequency under both oxic and anoxic equilibrium conditions. However, my data provide strong evidence that contrary to previous assumptions it is feasible to gradually select polar swimming behavior in the *M. gryphiswaldense* lab strain, despite of the tendency of individual cells to reverse direction. Swimming polarity is an effect of preferred swimming with one cell pole leading, which automatically corresponds to a specific direction relative to **B** due to the magnetic alignment of the cell body (Fig. 3-3a). Cells that were grown under microoxic conditions in liquid culture agitated on a rotary shaker (i.e. in the absence of any gradients) swam equal distances in both directions (*pol*$^{-}$), while cells that were exposed to vertical magnetic fields and grown in non-agitated tubes gradually extended swim phases in one specific direction (*pol*$^{+}$), depending on the orientation of the oxygen gradient relative to **B** during selective growth. Strikingly, in the absence of CheOp1 (*aer*$^{-}$) no polarity selection occurred and no switch in swimming direction with respect to the magnetic field was detected upon oxic shifts, indicating that no additional dedicated sensory pathway is controlling magnetotactic swimming behavior.

The results of this study highlight the need to perform polarity assays under highly controlled atmospheric conditions to obtain conclusive results and avoid artefacts. Since all classical magnetotaxis assays used undefined oxic conditions, it cannot be excluded that at high local cell densities the oxygen levels vary considerably and thus might affect polarity behavior. My findings are supported by the results of another recent study which confirm the dependence of polar swimming behavior in *M. gryphiswaldense* on cultivation conditions (Lefèvre et al. 2014). We therefore suggest that the classical textbook distinction between polar and axial magneto-aerotaxis (possibly representing a lab artifact) has to be revised. Even though the swimming behaviors of magnetospirilla and other MTB (like e.g. monolophotrichous cocci) might be distinct regarding intermittent backwards excursions, and also might differ mechanistically at the molecular level, the resulting directed motion along **B** is comparable in all MTB and axial and polar behavior might "represent the endpoints of a continuum of responses" (Frankel et al. 2006).

Selection of swimming polarity during growth in microoxic culture tubes is probably explained by the cells with the appropriate bias being directed more efficiently towards favorable growth conditions in oxygen gradients, gradually outcompeting others more regularly exposed to more harmful oxygen concentrations. Compared to swimming polarity selection of *M. gryphiswaldense* cultures after only 2 passages (corresponding to less than 10 generations), 10 passages were needed to obtain SS bacteria in axenic cultures of the magnetotactic coccus strain MO-1 (Lefèvre, Song, et al. 2009), and very slow repolarization of mixed populations of uncultivated environmental MTB was reported by subjecting whole sediment microcosms to reversed magnetic fields over 3 weeks (Blakemore 1982). The observation that NS cells of strain MO-1 were unable to grow in magnetic fields mimicking a Southern hemisphere-like inclination (Zhang et al. 2010) might indicate that the output of the motor(s) of monopolarly flagellated MTB cannot readily be modulated through selection processes. In this case the composition of populations is changed only by the rare loss of magnetosome chains in a small number of cells, followed by randomly oriented *de novo* synthesis and outcompeting of cells with unfavorable polarity bias. Thus, swimming polarity in cocci might be determined in an *either-or* fashion by the relative orientation of the cell body to the magnetic dipole. This could be tested by visualization and analysis of the relative orientation of flagella in magnetically aligned swimming cells of the same swimming polarity.

Varying degrees of alignment with the external magnetic field indicate that cells of *M. gryphiswaldense* inherit variable numbers of magnetosomes during cell division, but from TEM analyses it is known that only a very small proportion of WT cells are devoid of a magnetosome chain. In contrast to magnetic cocci, polarity-selected (*pol*$^{+}$) *M. gryphiswaldense* cultures never displayed noticeable growth delays in magnetic fields of the opposite orientation and swimming polarity could be selected within few generations. This indicates that selection of swimming polarity in magnetospirilla was not caused by enrichment of pre-existing unidirectional NS or SS bacteria equally prevalent in non-selected populations, but is based on a gradual mechanism at the single cell level. This could be facilitated for example by redistribution of a hypothetical polarity determinant (Fig. 3-3b), which probably is no two-state phenomenon, but produces a wide array of relatively heterogeneous swimming patterns within a bacterial population. Despite the described relative ease of selection, swimming polarity is furthermore not lost after a single transfer under non-selective conditions. This implies that the cellular polarity axis determining swimming polarity is inherited quite confidently in the absence of selective pressure, maintaining its relative orientation in both daughter cells.

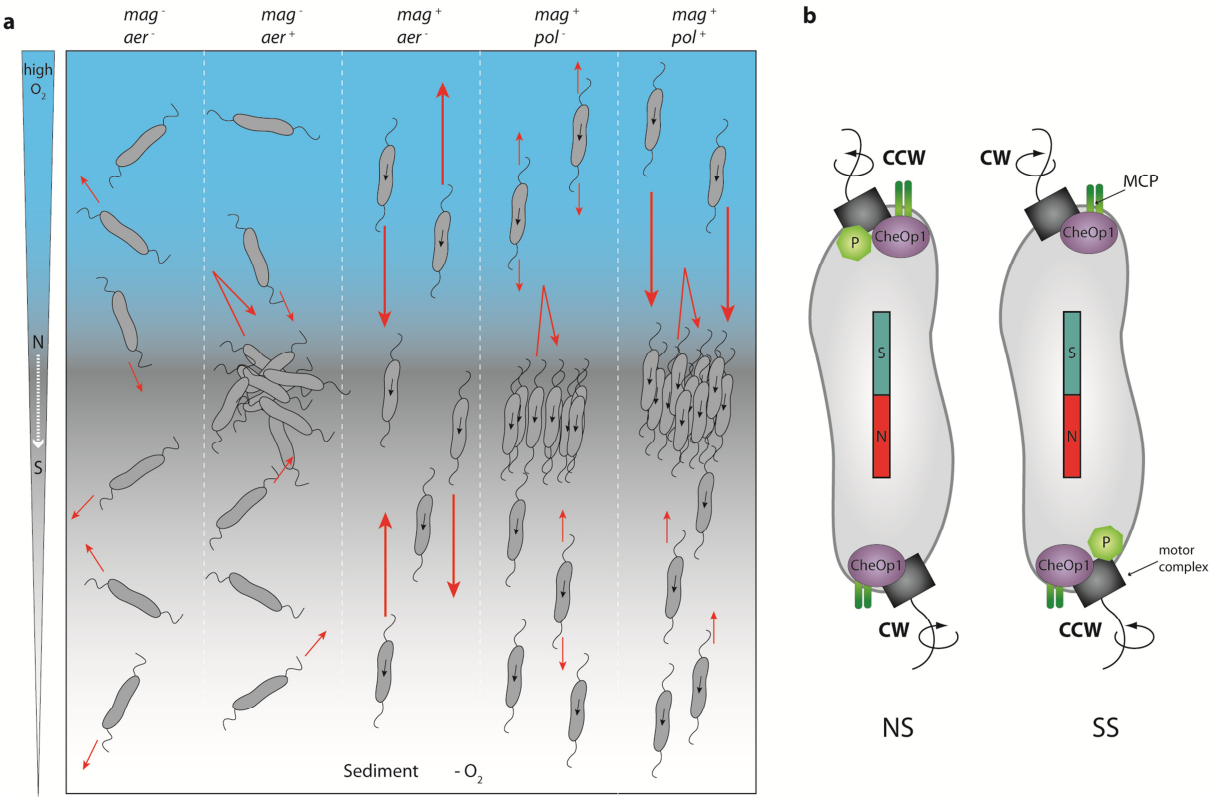

Fig. 3-3 (a) Schematic illustration of polar magnetotaxis in magnetospirilla compared to swimming phenotypes of mutants analyzed in this work. Representative, idealized swimming tracks of individual cells in a vertical O_2 gradient aligned to the magnetic field are shown as red arrows. Polar magnetotactic NS WT cells (*pol*$^+$) form an aerotactic band at the oxic-anoxic transition zone (OATZ). When displaced to hyper- or hypooxic zones, those cells avoid excursions into the "ecologically wrong" direction and directly swim back to the OATZ. In contrast, non-selected WT cells (*pol*$^-$) swim in either direction relative to **B** and therefore their return to the OATZ is slowed down. Non-aerotactic but magnetic (*mag*$^+$ *aer*$^-$) Δ*cheOp1* mutant cells swim aligned to **B**, but fail to reverse and accumulate at favorable O_2 levels, while aerotactic but non-magnetic (*mag*$^-$ *aer*$^+$) Δ*mamAB* mutant cells behave similar to other non-magnetotactic bacteria and only use temporal gradient sensing to steer towards the OATZ. (b) Model that shows how redistribution of a hypothetical polarity determinant (P) might cause NS and SS swimming behavior in *M. gryphiswaldense*.

In other motile bacteria (swimming or gliding), movement intervals with one pole leading are equivalent to those with the other pole in front (i.e. the time intervals have the same length) (Berg & Turner 1996; Shi, Zusman 1996). In contrast, I could demonstrate through long-term tracking of individual cells that *M. gryphiswaldense* is able to regulate the relative duration of swimming phases to achieve a net movement either parallel or anti-parallel to **B**. Although *M. gryphiswaldense* might employ some form of temporal sensing, this implies that reversal events are not fully randomized by adaptation processes under equilibrium conditions. To achieve this, motors have to be gradually locked into either CCW or CW rotation modes depending on polarity selection (Fig. 3-3b). However, suppression of reversal events after an oxic upshift is a general characteristic of *M. gryphiswaldense* that is not exclusively found in *pol*$^+$ cells, since overall reversal frequencies are similar in selected, non-selected and non-magnetic

cells. Therefore, less frequent motor reversals appear to be a prerequisite, but not a sufficient condition for the observed swimming polarity response.

To achieve distinct behaviors of NS and SS cells, swimming polarity in *Magnetospirilla* must be based on structural or distributional asymmetry introducing a second polarity axis (C polarity axis) parallel to the magnetic moment of the magnetosome chain (M polarity axis). Assuming the suppression of reversal events is mainly based on low or inactive CheY~P, or insensitive switch complexes, the predominant rotational sense of motors would depend on their inherent "default" sense determined by the C polarity axis. However, so far we can only speculate what causes symmetry breaking at the subcellular level and thereby determines swimming polarity.

Symmetry breaking could be established through (Fig. 3-4):

a) Hard-wired structural asymmetry of motor complexes
b) Asymmetric distribution (or activity) of chemotaxis clusters
c) A single (or multiple) polarity determinant(s), that modifies motor output

Adding to the reasons that argue against hardwired rotational asymmetry (Fig. 3-4a), it seems unlikely that C polarity is simply based on the relative arrangement of motor complexes with opposite default rotational senses, because this hypothesis can hardly explain how mixed hybrid motors could be functional without blocking motor rotation. However, in non-selected cells or during C polarity switching such intermediate states with hybrid motor compositions would have to be postulated.

The sensory pathway CheOp1 was found to control both aerotactic responses AND swimming polarity, thus providing a link for these two navigational mechanisms. Since in the absence of CheOp1 no polarity selection occurred, the CheOp1 signal transduction pathway possibly might function itself as a C polarity determinant through monopolar localization of chemotaxis clusters that could establish a CheY phosphorylation gradient. However, according to fluorescence microscopy experiments, in which we detected GFP-labelled CheW proteins at both poles, distributional asymmetry of CheOp1 components does not seem to play a direct role in introducing C polarity. Alternatively, CheA or another component might be modified at a single pole in a way that either silences kinase activity or inverts its output thereby creating a CheY phosphorylation gradient (Fig. 3-4b). However, if the kinase at one pole is silenced or modified, the corresponding motor had to be coupled to the output of the opposite motor for instance by mechanical means.

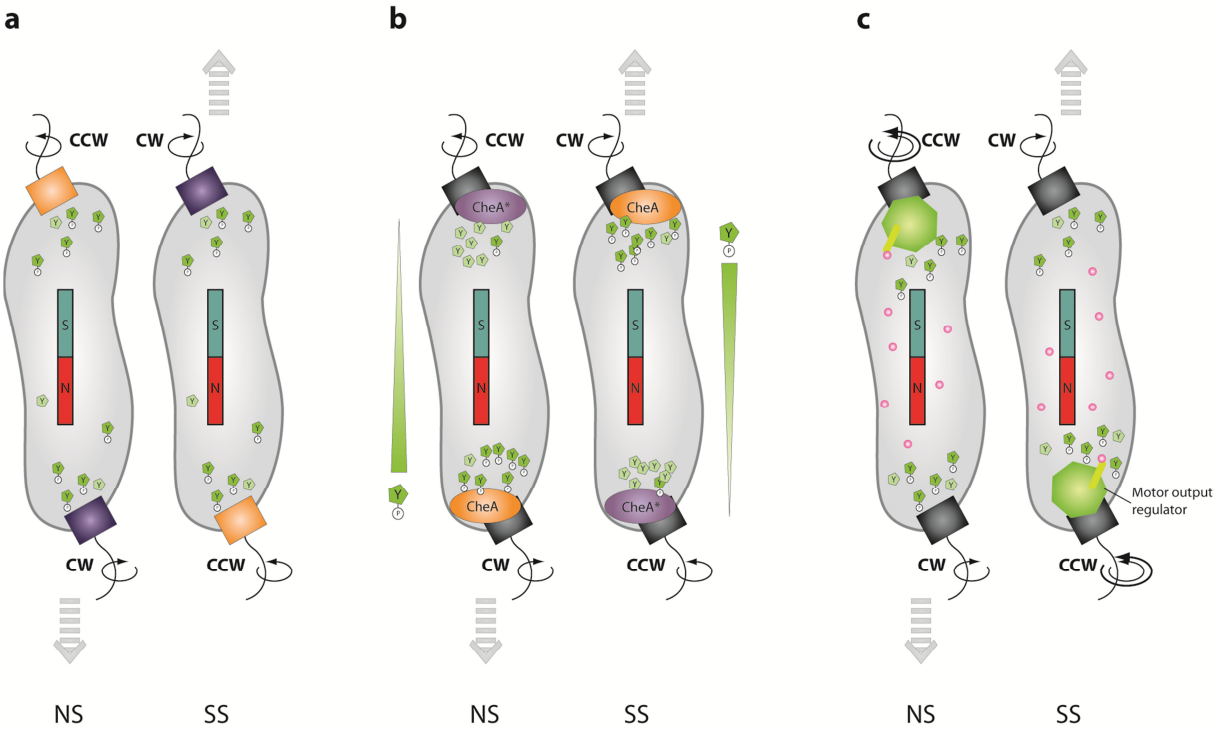

Fig. 3-4 Models for symmetry breaking at the subcellular level: (a) Hard-wired structural asymmetry of motor complexes; (b) Asymmetric distribution or activity of chemotaxis clusters; (c) A single (or multiple) polarity determinant(s), that modifies motor output. For explanations see text.

Clearly, one of the components defining C polarity has to be responsive to the oxygen level or an oxygen-dependent parameter, since exposure of *pol*$^+$ cells to repellent oxygen levels not only decreases the overall frequency of swimming reversals, but also leads to biased motor output. The major effect of the C polarity determinant therefore must be a specific shift of the motor rotational output from the default symmetric to asymmetric behavior favoring one rotational sense at a specific pole.

Among the many conceivable solutions to this problem, there seem to be two likely models. Either there is a single factor that specifically determines the rotational sense at one pole and the other motor is “overruled” through mechanical coupling, or there are two reciprocal hypothetical factors X and Y (one at each pole or a gradient of factors) that specifically lock the motors in opposite senses (Fig. 3-4c). A single hypothetical polarity factor could be bound to the switch complex of one pole and promote a particular sense of motor rotation in an oxygen- or second messenger-dependent manner, e.g. similar to YcgR in *E. coli*. In cells with opposite swimming polarity (NS vs. SS), in this scenario the polarity factor had to be localized to the opposite pole in each case. A rather parsimonious explanation involving only a single factor would be that a protein causing suppression of reversals in both non-selected and selected cells, at the same time is the basis of rotational bias.

However, in all these hypothetical scenarios two important questions remain: What happens in non-selected cells (no polarity determinant present, or a homogeneous distribution at both poles)? And how could asymmetric localization of polarity determinants be established during selection and how is it inherited? Repeated redefinition of polar identity is observed in dividing cells of *V. cholerae* and *C. crescentus* (Davis & Waldor 2013). However, in these organisms the development of polar identity follows a predefined course with a transition from new to old poles or the transition new – swarmer – stalked pole, respectively. Although reshaping through selection is likely, the C polarity axis of *M. gryphiswaldense* has to be relatively stable in the absence of selective pressure. For this reason the new poles formed during cell division cannot be equivalent, but will need to have opposite identities to maintain the relative alignment of the C and M polarity axis in both daughter cells. If the result of every division were daughter cells with opposing C polarity, every population consisted of approximately equal numbers of NS and SS bacteria. Therefore, the C polarity axis of the dividing cell has to be inherited by an unknown mechanism, maintaining its relative orientation with respect to the magnetic moment in both daughter cells.

The relatively fast selection of polar *M. gryphiswaldense* cells under selective growth conditions within 10 generations argues against a genetic, but for an epigenetic mode of swimming polarity determination. It furthermore suggests that reversals or at least gradual modifications of the C polarity axis might occur within the lifespan of individual cells. An example for such cell polarity reversals is the MglA/MglB system of *Myxoccoccus xanthus*, which defines a switchable polarity axis (Leonardy et al. 2010; Keilberg & Søgaard-Andersen 2014). Although the signal that is sensed and leads to pole switching currently is unknown, it has been found that reversals depend on the active response regulator phospo-FrzZ. Under standard conditions reversals occur on average every 8-9 minutes, without preference for movement with one pole in front. If an analogous mechanism was active in *M. gryphiswaldense* to switch between NS and SS polarity, it needed to be tightly controlled, and initiate polarity axis reversals only if redox configuration of the local habitat would be favorable for such a change.

3.4 Magnetic and aerotactic properties of *M. gryphiswaldense* cells can be modulated by nanobody-mediated magnetosome recruitment

In another study, we investigated the interaction between GFP-labelled CheW1 molecules and GFP-binding nanobodies (so-called green binding protein (GBP)) that were anchored to the magnetosome surface by fusion with the magnetosome membrane protein MamC. In wild type cells CheW1 was found to be localized to polar chemotaxis clusters. Through expression of intra-cellular nanotraps, however, we were able to recruit CheW-GFP to the magnetosome chain.

Although the soluble CheW protein in vitro forms complexes with its interaction partners (CheA and chemoreceptors) that were found to be stable over very long time scales (Erbse & Falke 2009), signaling complexes were shown to be subjected to slow turnover in vivo with dwelling times of approximately 10 min (Schulmeister et al. 2008). This is in line with findings that suggest that a small pool of unbound CheA might be permanently available in the cytoplasm (Briegel, Wong, et al. 2014). Therefore it seems likely that small numbers of free CheW present in the cytoplasm were bound by GBP expressed on the magnetosome surface, and that over time CheW previously bound to chemoreceptor clusters at the poles was successively released and trapped at the magnetosome chain.

The degree to which CheW was recruited to midcell depended on the relative concentration of GBP molecules on the magnetosome membranes and on the magnetosome chain configuration. In cells expressing the monovalent nanobody, we observed only partial recruitment, while over-expression of the bivalent nanobody completely depleted CheW from the poles. The observed equilibrium between polar and midcell localization indicated that turnover of the chemoreceptor-CheW complexes was comparable to the binding of $CheW_1$-GFP to the monovalent GBP, while the bivalent nanobody apparently had a much higher avidity and therefore completely abolished polar localization.

Ectopic recruitment of $CheW_1$-GFP gradually modulated chemotactic efficiency of *M. gryphiswaldense* cells. Although chemoreceptors cluster in the absence of other signal transduction factors, CheW is essential for stabilizing native interactions between receptors and CheA. Partial recruitment of $CheW_1$ to the midcell only gradually reduced chemotactic efficiency, while virtually complete depletion (>90%) of CheW1 from its native polar clusters that resulted from the expression of the bivalent nanobody abolished aerotactic responses nearly to the level of the ΔcheW deletion mutant. The observed aerotaxis defect was not due to GBP binding alone, since cytoplasmic expression of GBP alone did not have such an effect. Our findings provide further support to the view that although bacteria are not structured to the same degree as eukaryotic cells, the functionality of many of their proteins clearly depends on their localization. Our approach offers the possibility to investigate and manipulate protein function by subcellular retargeting even in very small prokaryotic cells.

Nanobody-mediated interaction between MamC and CheW also shifted magnetosome chains from their midcell position towards the cell poles and changed the chain configuration, i.e. magnetosome particles were less densely spaced and less well aligned. This effect impacted the magnetic alignment of swimming cells and possible applications of nanotrap technology therefore could include the generation of mutant strains with tailor-made magnetic or chemotactic properties, for example for the use as nanorobots. However, since nanotraps might be anchored

to various cellular structures, such as distinct subcellular locations (e. g. poles, midcell), specific protein complexes or compartments, nanotrap technology will not be restricted to MTB.

3.5 Open questions and further directions

The fascinating swimming behavior observed in polar MTB calls for further investigation of its apparently very complex molecular mechanism, its cellular determination and inheritance. This thesis was the first to experimentally analyze signal transduction components of MTB and disclosed several open questions in different areas of research that will need further attention in future studies:

- What is the role of the remaining three chemotaxis operons CheOp2-4? Although many of the proteins of these operons have been found expressed in proteomic analysis, as yet no clear phenotype was detected in the triple deletion strain with respect to chemotactic efficiency or selection of swimming polarity. Possibly these pathways fulfill roles in MTB that are completely different from those in other bacteria and that might be important for behaviors other than chemotaxis. Variation of experimental conditions might help reveal their function.
- Which CheY species is active at the motor switch complex, and which functions as a possible phosphate sink? So far it has remained unclear, which of the 31 putative CheY molecules controls motor behavior in *M. gryphiswaldense* and deletion of *cheY1* alone did not suppress motor reversals (own unpublished data). Furthermore, future studies will need to address the question which is the exact effect of CheY binding to the motor: a specific rotational sense that is being triggered as in well-characterized model organisms, or an increased probability of switching between two equivalent states as suggested in this work?
- Among the 56 MCP of *M. gryphiswaldense*, which is the chemoreceptor that is essential for energy taxis? At least 2 *aer*, 4 *cetAB* homologs, and 3 MCP-coding genes containing hemerythrin domains have been identified in the genome of *M. gryphiswaldense*. Deletion of a single *aer* homolog (*mgr3404*) did not impair aerotaxis (own unpublished data), and the other candidate proteins await further characterization. What is the overall function of this great sensory complexity (specific or redundant functions of individual components)?
- How is swimming polarity selected and can it be switched within the lifespan of a single cell? This could be tested with replication inhibitors (e.g. hydroxyurea). Is protein

synthesis needed for polarity reversals? This could be tested by applying translational inhibitors like chloramphenicol to the cells.

- How is swimming polarity inherited from individual cells to their offspring? Using single-cell-sorting the inheritance and clonality of polarity of single cell might be investigated.
- Are there factors interacting with chemotaxis/motor components that might determine C polarity and possibly could be identified by pull-down experiments?
- How exactly is CheOp1 involved in polarity selection? When CheOp1 is switched off in a polarity-selected population, do cells retain their swimming bias?
- Is there a direct link between polarity and metabolism/respiration? This could be investigated in a triple terminal oxidase mutant to test if swimming polarity can be selected when energy levels are not influenced by oxygen respiration.

There is growing interest in harnessing magnetotaxis in various applications. For example it has been suggested to exploit MTB as nanorobots to deliver drugs and microloads in microfluidic systems and even in the human body (Taherkhani et al. 2014; Martel et al. 2009; Martel et al. 2006). These future applications will rely on a thorough analysis and possibly manipulation of molecular mechanisms controlling motility, and will therefore greatly benefit from an improved understanding of this unique bacterial behavior.

4 References

Alexandre, G., Greer-Phillips, S. & Zhulin, I.B., 2004. Ecological role of energy taxis in microorganisms. *FEMS microbiology reviews*, 28(1), pp.113–26.

Attmannspacher, U., Scharf, B. & Schmitt, R., 2005. Control of speed modulation (chemokinesis) in the unidirectional rotary motor of Sinorhizobium meliloti. *Molecular Microbiology*, 56(3), pp.708–718.

Bai, F. et al., 2012. Coupling between switching regulation and torque generation in bacterial flagellar motor. *Physical Review Letters*, 108(17), pp.1–4.

Balkwill, D.L., Maratea, D. & Blakemore, R.P., 1980. Ultrastructure of a magnetotactic spirillum. *Journal of bacteriology*, 141(3), pp.1399–408.

Bazylinski, D. A. et al., 2000. N2-dependent growth and nitrogenase activity in the metal-metabolizing bacteria, Geobacter and Magnetospirillum species. *Environmental microbiology*, 2(3), pp.266–73.

Bazylinski, D. A.& Frankel, R.B., 2004. Magnetosome formation in prokaryotes. *Nature reviews. Microbiology*, 2(3), pp.217–30.

Bazylinski, D. & Lefèvre, C., 2013. Magnetotactic Bacteria from Extreme Environments. *Life*, 3(2), pp.295–307.

Bazylinski, D. & Williams, T., 2007. Ecophysiology of Magnetotactic Bacteria. In D. Schüler, ed. *Magnetoreception and Magnetosomes in Bacteria*. Microbiology Monographs. Springer Berlin Heidelberg, pp. 37–75.

Bazylinski, D.A. et al., 2013. Magnetovibrio blakemorei gen. nov., sp. nov., a magnetotactic bacterium (Alphaproteobacteria: Rhodospirillaceae) isolated from a salt marsh. *International journal of systematic and evolutionary microbiology*, 63(Pt 5), pp.1824–33.

Bellini, S., 2009a. Further studies on "magnetosensitive bacteria." *Chinese Journal of Oceanology and Limnology*, 27(1), pp.6–12.

Bellini, S., 2009b. On a unique behavior of freshwater bacteria. *Chinese Journal of Oceanology and Limnology*, 27(1), pp.3–5.

Berg, H.C., 1975. Chemotaxis in bacteria. *Annual review of biophysics and bioengineering*, 4(00), pp.119–36.

Blair, K.M. et al., 2008. A molecular clutch disables flagella in the Bacillus subtilis biofilm. *Science*, 320(5883), pp.1636–1638.

Blakemore, R., 1975. Magnetotactic bacteria. *Science (New York, N.Y.)*, 190(4212), pp.377–9.

Blakemore, R.P., 1982. Magnetotactic bacteria. *Annual review of microbiology*, 36(4212), pp.217–38.

Blakemore, R.P., Frankel, R.B. & Kalmijn, A.J., 1980. South-seeking magnetotactic bacteria in the Southern Hemisphere. *Nature*, 286(5771), pp.384–385.

Blakemore, R.P., Maratea, D. & Wolfe, R.S., 1979. Isolation and pure culture of a freshwater magnetic spirillum in chemically defined medium. *Journal of bacteriology*, 140(2), pp.720–9.

Boehm, A. et al., 2010. Second messenger-mediated adjustment of bacterial swimming velocity. *Cell*, 141(1), pp.107–16.

Briegel, A., Wong, M.L., et al., 2014. New insights into bacterial chemoreceptor array structure and assembly from electron cryotomography. *Biochemistry*, 53(10), pp.1575–85.

Briegel, A. et al., 2009. Universal architecture of bacterial chemoreceptor arrays. *Proceedings of the National Academy of Sciences of the United States of America*, 106(40), pp.17181–6.

Briegel, A., Ladinsky, M. & Oikonomou, C., 2014. Structure of bacterial cytoplasmic chemoreceptor arrays and implications for chemotactic signaling. *eLife*, pp.1–16.

Brown, M.T., Delalez, N.J. & Armitage, J.P., 2011. Protein dynamics and mechanisms controlling the rotational behaviour of the bacterial flagellar motor. *Current Opinion in Microbiology*, 14(6), pp.734–740.

Chen, C. et al., 2010. Phototaxis in the magnetotactic bacterium Magnetospirillum magneticum strain AMB-1 is independent of magnetic fields. *Applied microbiology and biotechnology*.

Davila, A.F. et al., 2003. A new model for a magnetoreceptor in homing pigeons based on interacting clusters of superparamagnetic magnetite. *Physics and Chemistry of the Earth, Parts A/B/C*, 28(16-19), pp.647–652.

Davis, B.M. & Waldor, M.K., 2013. Establishing polar identity in gram-negative rods. *Current opinion in microbiology*, 16(6), pp.752–9.

Edwards, K.J. et al., 2004. Spatiotemporal Distribution of Marine Magnetotactic Bacteria in a Seasonally Stratified Coastal Salt Pond Spatiotemporal Distribution of Marine Magnetotactic Bacteria in a Seasonally Stratified Coastal Salt Pond †. *Society*, 70(10), pp.6230–6239.

Elliott, K.T. et al., 2009. Conserved residues in the HAMP domain define a new family of proposed bipartite energy taxis receptors. *Journal of bacteriology*, 191(1), pp.375–87.

Engelmann, T.W., 1881. Neue Methode zur Untersuchung der Sauerstoffausscheidung pflanzlicher und thierischer Organismen. *Pflügers Archiv European Journal of Physiology*, 25(1), pp.285–292.

Erbse, A.H. & Falke, J.J., 2009. The core signaling proteins of bacterial chemotaxis assemble to form an ultrastable complex. *Biochemistry*, 48(29), pp.6975–87.

Fahrner, K.A., Ryu, W.S. & Berg, H.C., 2003. Biomechanics: bacterial flagellar switching under load. *Nature*, 423(6943), p.938.

Flies, C.B., Jonkers, H.M., et al., 2005. Diversity and vertical distribution of magnetotactic bacteria along chemical gradients in freshwater microcosms. *FEMS microbiology ecology*, 52(2), pp.185–95.

Flies, C.B., Peplies, J. & Schüler, D., 2005. Combined approach for characterization of uncultivated magnetotactic bacteria from various aquatic environments. *Applied and environmental microbiology*, 71(5), pp.2723–31.

Frankel, R., Williams, T. & Bazylinski, D., 2006. Magneto-Aerotaxis. In D. Schüler, ed. *Magnetoreception and Magnetosomes in Bacteria*. Microbiology Monographs. Springer Berlin / Heidelberg, pp. 1–24.

Frankel, R.B. et al., 1997. Magneto-aerotaxis in marine coccoid bacteria. *Biophysical journal*, 73(2), pp.994–1000.

Frankel, R.B. et al., 1981. Magnetotactic bacteria at the geomagnetic equator. *Science (New York, N.Y.)*, 212(4500), pp.1269–70.

Frankel, R.B., Blakemore, R.P. & Wolfe, R.S., 1979. Magnetite in freshwater magnetotactic bacteria. *Science (New York, N.Y.)*, 203(4387), pp.1355–1356.

Geelhoed, J.S. et al., 2010. Reduced inorganic sulfur oxidation supports autotrophic and mixotrophic growth of Magnetospirillum strain J10 and Magnetospirillum gryphiswaldense. *Environmental microbiology*, 12(4), pp.1031–40.

Gest, H., 1995. Phototaxis and other sensory phenomena in purple photosynthetic bacteria. *FEMS Microbiology Reviews*, 16(4), pp.287–294.

González, L.M. et al., 2014. Sudden motility reversal indicates sensing of magnetic field gradients in Magnetospirillum magneticum AMB-1 strain. *The ISME Journal*, pp.1–11.

Greenberg, M. et al., 2005. Observation of magnetoreceptive behavior in a multicellular magnetotactic prokaryote in higher than geomagnetic fields. *Biophysical journal*, 88(2), pp.1496–9.

Greene, S.E. & Komeili, A., 2012. Biogenesis and subcellular organization of the magnetosome organelles of magnetotactic bacteria. *Current opinion in cell biology*, 24(4), pp.490–5.

Hamer, R. et al., 2010. Deciphering chemotaxis pathways using cross species comparisons. *BMC systems biology*, 4, p.3.

He, K. et al., 2013. Phosphate Flow between Hybrid Histidine Kinases CheA 3 and CheS 3 Controls Rhodospirillum centenum Cyst Formation. , 9(12).

Heyen, U. & Schüler, D., 2003. Growth and magnetosome formation by microaerophilic Magnetospirillum strains in an oxygen-controlled fermentor. *Applied microbiology and biotechnology*, 61(5-6), pp.536–44.

Hu, B. & Tu, Y., 2013. Coordinated switching of bacterial flagellar motors: Evidence for direct motor-motor coupling? *Physical Review Letters*, 110(15), pp.1–5.

Inclán, Y.F., Laurent, S. & Zusman, D.R., 2008. The receiver domain of FrzE, a CheA-CheY fusion protein, regulates the CheA histidine kinase activity and downstream signalling to the A- and S-motility systems of Myxococcus xanthus. *Molecular Microbiology*, 68(5), pp.1328–1339.

Ji, B. et al., 2013. Comparative genomic analysis provides insights into the evolution and niche adaptation of marine Magnetospira sp. QH-2 strain. *Environmental microbiology*, p.n/a–n/a.

Jogler, C. et al., 2009. Comparative analysis of magnetosome gene clusters in magnetotactic bacteria provides further evidence for horizontal gene transfer. *Environmental microbiology*, 11(5), pp.1267–77.

Jogler, C. & Schüler, D., 2009. Genomics, genetics, and cell biology of magnetosome formation. *Annual review of microbiology*, 63, pp.501–21.

Johansen, J. et al., 2002. Variability in motility characteristics among marine bacteria. *Aquatic Microbial Ecology*, 28, pp.229–237.

Katzen, F. et al., 1999. New mobilizable vectors suitable for gene replacement in gram-negative bacteria and their use in mapping of the 3' end of the Xanthomonas campestris pv. campestris gum operon. *Applied and environmental microbiology*, 65(1), pp.278–82.

Katzmann, E. et al., 2013. Analysis of magnetosome chains in magnetotactic bacteria by magnetic measurements and automated image analysis of electron micrographs. *Applied and environmental microbiology*, 79(24), pp.7755–62.

Keilberg, D. & Søgaard-Andersen, L., 2014. Regulation of Bacterial Cell Polarity by Small GTPases. *Biochemistry*.

Kirschvink, J.L., 1997. Magnetoreception: Homing in on vertebrates. *Nature*, 390(6658), pp.339–340.

Kirschvink, J.L., Walker, M.M. & Diebel, C.E., 2001. Magnetite-based magnetoreception. *Current opinion in neurobiology*, 11(4), pp.462–7.

Kirschvink, J.L., Winklhofer, M. & Walker, M.M., 2010. Biophysics of magnetic orientation: strengthening the interface between theory and experimental design. *Journal of the Royal Society, Interface / the Royal Society*, 7 Suppl 2, pp.S179–91.

Kolinko, I. et al., 2014. Biosynthesis of magnetic nanostructures in a foreign organism by transfer of bacterial magnetosome gene clusters. *Nature Nanotechnology*, (February), pp.1–5.

Komeili, A., 2012. Molecular mechanisms of compartmentalization and biomineralization in magnetotactic bacteria. *FEMS microbiology reviews*, 36(1), pp.232–55.

Krell, T. et al., 2011. Diversity at its best: Bacterial taxis. *Environmental Microbiology*, 13, pp.1115–1124.

Krieg, N.R., Tomelty, J.P. & Wells, J.S., 1967. Inhibitio of flagellar coordination in Spirillum volutans. *Journal of bacteriology*, 94(5), pp.1431–6.

Laszlo, D.J. & Taylor, B.L., 1981. Aerotaxis in Salmonella typhimurium: Role of Electron Transport. *Journal of bacteriology*, 145(2), pp.990–1001.

Lefèvre, C.T., Song, T., et al., 2009. Characterization of bacterial magnetotactic behaviors by using a magnetospectrophotometry assay. *Applied and environmental microbiology*, 75(12), pp.3835–41.

Lefèvre, C.T. et al., 2014. Diversity of magneto-aerotactic behaviors and oxygen sensing mechanisms in cultured magnetotactic bacteria. *Biophysical journal*, 107(2), pp.527–38.

Lefèvre, C.T., Bernadac, A., et al., 2009. Isolation and characterization of a magnetotactic bacterial culture from the Mediterranean Sea. *Environmental microbiology*, 11(7), pp.1646–57.

Lefèvre, C.T. et al., 2013. Monophyletic origin of magnetotaxis and the first magnetosomes. *Environmental microbiology*, 1.

Lefèvre, C.T. & Bazylinski, D.A., 2013. Ecology, diversity, and evolution of magnetotactic bacteria. *Microbiology and molecular biology reviews : MMBR*, 77(3), pp.497–526.

Leonardy, S. et al., 2010. Regulation of dynamic polarity switching in bacteria by a Ras-like G-protein and its cognate GAP. *The EMBO journal*, 29(14), pp.2276–89.

Li, C. et al., 2010. Inactivation of a putative flagellar motor switch protein FliG1 prevents Borrelia burgdorferi from swimming in highly viscous media and blocks its infectivity. *Molecular microbiology*, 75(6), pp.1563–76.

Li, Y. et al., 2012. The Periplasmic Nitrate Reductase Nap Is Required for Anaerobic Growth and Involved in Redox Control of Magnetite Biomineralization in Magnetospirillum gryphiswaldense. *Journal of bacteriology*, 194(18), pp.4847–56.

Liarzi, O. et al., 2010. Acetylation represses the binding of CheY to its target proteins. *Molecular Microbiology*, 76(4), pp.932–943.

Lindbeck, J.C. et al., 1995. Aerotaxis in Halobacterium salinarium is methylation-dependent. *Microbiology (Reading, England)*, 141 (Pt 1, pp.2945–53.

Liu, J. et al., 2012. PNAS Plus: Molecular architecture of chemoreceptor arrays revealed by cryoelectron tomography of Escherichia coli minicells. *Proceedings of the National Academy of Sciences*, 109(23), pp.E1481–E1488.

Lloyd, S. A.et al., 1999. Structure of the C-terminal domain of FliG, a component of the rotor in the bacterial flagellar motor. *Nature*, 400(6743), pp.472–475.

Lohße, A. et al., 2011. Functional Analysis of the Magnetosome Island in Magnetospirillum gryphiswaldense: The mamAB Operon Is Sufficient for Magnetite Biomineralization. *PloS one*, 6(10), p.e25561.

Martel, S. et al., 2006. Controlled manipulation and actuation of micro-objects with magnetotactic bacteria. *Applied Physics Letters*, 89(23), p.233904.

Martel, S. et al., 2009. Flagellated Magnetotactic Bacteria as Controlled MRI-trackable Propulsion and Steering Systems for Medical Nanorobots Operating in the Human Microvasculature. *The International Journal of Robotics Research*, 28(4), pp.571–582.

Marx, C.J. & Lidstrom, M.E., 2002. Broad-host-range cre-lox system for antibiotic marker recycling in gram-negative bacteria. *BioTechniques*, 33(5), pp.1062–7.

Matsunaga, T. et al., 2005. Complete genome sequence of the facultative anaerobic magnetotactic bacterium Magnetospirillum sp. strain AMB-1. *DNA research : an international journal for rapid publication of reports on genes and genomes*, 12(3), pp.157–66.

Minamino, T. & Imada, K., 2015. The bacterial flagellar motor and its structural diversity. *Trends in Microbiology*, 23(5), pp.267–274.

Morehouse, K. A. et al., 2011. Three motAB stator gene products in Bdellovibrio bacteriovorus contribute to motility of a single flagellum during predatory and prey-independent growth. *Journal of bacteriology*, 193(4), pp.932–43.

Morimoto, Y. & Minamino, T., 2014. Structure and Function of the Bi-Directional Bacterial Flagellar Motor. *Biomolecules*, 4(1), pp.217–234.

Murat, D. et al., 2014. Flagella and motility of magnetotactic bacteria. In *4th International Meeting on Magnetotactic Bacteria - Meeting Program and Abstracts*. p. 25.

Nakamura, S. et al., 2010. Evidence for symmetry in the elementary process of bidirectional torque generation by the bacterial flagellar motor. *Proceedings of the National Academy of Sciences of the United States of America*, 107(41), pp.17616–20.

Parkinson, J.S., Hazelbauer, G.L. & Falke, J.J., 2015. Signaling and sensory adaptation in Escherichia coli chemoreceptors: 2015 update. *Trends in Microbiology*, 23(5), pp.257–266.

Paul, K. et al., 2010. The c-di-GMP binding protein YcgR controls flagellar motor direction and speed to affect chemotaxis by a "backstop brake" mechanism. *Molecular cell*, 38(1), pp.128–39.

Paulick, A. et al., 2009. Two different stator systems drive a single polar flagellum in Shewanella oneidensis MR-1. *Molecular microbiology*, 71(4), pp.836–50.

Pfeffer, W., 1888. Über chemotaktische Bewegungen von Bakterien, Flagellaten und Volvocineen. . *Untersuch. Bot. Inst. Tübingen*, 2, pp.582–661.

Philippe, N. & Wu, L.-F., 2010. An MCP-like protein interacts with the MamK cytoskeleton and is involved in magnetotaxis in Magnetospirillum magneticum AMB-1. *Journal of molecular biology*, 400(3), pp.309–22.

Pilizota, T. et al., 2009. A molecular brake, not a clutch, stops the Rhodobacter sphaeroides flagellar motor. *Proceedings of the National Academy of Sciences of the United States of America*, 106(28), pp.11582–7.

Porter, S.L., Wadhams, G.H. & Armitage, J.P., 2011. Signal processing in complex chemotaxis pathways. *Nature Reviews Microbiology*, 9(3), pp.153–65.

Qian, C. et al., 2013. Bacterial tethering analysis reveals a "run-reverse-turn" mechanism for Pseudomonas species motility. *Applied and environmental microbiology*, 79(15), pp.4734–43.

Rao, C. V., Glekas, G.D. & Ordal, G.W., 2008. The three adaptation systems of Bacillus subtilis chemotaxis. *Trends in Microbiology*, 16(10), pp.480–487.

Raschdorf, O. et al., 2013. The magnetosome proteins MamX, MamZ and MamH are involved in redox control of magnetite biomineralization in Magnetospirillum gryphiswaldense. *Molecular microbiology*, 89(5), pp.872–86.

Rebbapragada, A. et al., 1997. The Aer protein and the serine chemoreceptor Tsr independently sense intracellular energy levels and transduce oxygen, redox, and energy signals for Escherichia coli behavior. *Proceedings of the National Academy of Sciences of the United States of America*, 94(20), pp.10541–6.

Reufer, M. et al., 2013. Switching of swimming modes in Magnetospirillium gryphiswaldense. *arXiv preprint*, arXiv:1307, p.27.

Russell, M.H. et al., 2013. Integration of the Second Messenger c-di-GMP into the Chemotactic Signaling Pathway. *mBio*, 4(2).

Scharf, B.E. et al., 1998. Control of direction of flagellar rotation in bacterial chemotaxis. *Proceedings of the National Academy of Sciences of the United States of America*, 95(1), pp.201–206.

Schleifer, K.H. et al., 1991. The Genus Magnetospirillum gen. nov. Description of Magnetospirillum gryphiswaldense sp. nov. and Transfer of Aquaspirillum magnetotacticum to Magnetospirillum magnetotacticum comb. nov. *Systematic and Applied Microbiology*, 14(4), pp.379–385.

Schmitt, R., 2002. Sinorhizobial chemotaxis: a departure from the enterobacterial paradigm. *Microbiology (Reading, England)*, 148(Pt 3), pp.627–31.

Schüler, D. & Köhler, M., 1992. The isolation of a new magnetic spirillum. *Zentralblatt für Mikrobiologie*, 147(1-2), pp.150–151.

Schüler, D., Spring, S. & Bazylinski, D.A., 1999. Improved technique for the isolation of magnetotactic spirilla from a freshwater sediment and their phylogenetic characterization. *Systematic and applied microbiology*, 22(3), pp.466–71.

Schulmeister, S. et al., 2008. Protein exchange dynamics at chemoreceptor clusters in Escherichia coli. *Proceedings of the National Academy of Sciences of the United States of America*, 105(17), pp.6403–6408.

Schultheiss, D., Kube, M. & Schüler, D., 2004. Inactivation of the flagellin gene flaA in Magnetospirillum gryphiswaldense results in nonmagnetotactic mutants lacking flagellar filaments. *Applied and environmental microbiology*, 70(6), p.3624.

Schultheiss, D. & Schüler, D., 2003. Development of a genetic system for Magnetospirillum gryphiswaldense. *Archives of microbiology*, 179(2), pp.89–94.

Schweinitzer, T. & Josenhans, C., 2010. Bacterial energy taxis: a global strategy? *Archives of Microbiology*, 192(7), pp.507–520.

Shapiro, O.H. et al., 2011. Multicellular photo-magnetotactic bacteria. *Environmental Microbiology Reports*, 3(2), pp.233–238.

Shi, W., Ngok, F.K. & Zusman, D.R., 1996. Cell density regulates cellular reversal frequency in Myxococcus xanthus. *Proceedings of the National Academy of Sciences of the United States of America*, 93(9), pp.4142–6.

Shioi, J., Dang, C. V & Taylor, B.L., 1987. Oxygen as attractant and repellent in bacterial chemotaxis. *Journal of bacteriology*, 169(7), pp.3118–23.

Simmons, S.L., Bazylinski, D. A. & Edwards, K.J., 2006. South-seeking magnetotactic bacteria in the Northern Hemisphere. *Science (New York, N.Y.)*, 311(5759), pp.371–4.

Smith, M.J. et al., 2006. Quantifying the magnetic advantage in magnetotaxis. *Biophysical journal*, 91(3), pp.1098–107.

Sowa, Y. & Berry, R.M., 2008. Bacterial flagellar motor. *Quarterly reviews of biophysics*, 41(2), pp.103–32.

Spormann, A.M. & Wolfe, R.S., 1984. Chemotactic, magnetotactic and tactile behaviour in a magnetic spirillum. *FEMS Microbiology Letters*, 22(3), pp.171–177.

Spring, S. & Bazylinski, D.A., 2006. Magnetotactic Bacteria. In *The Prokaryotes*. New York, NY: Springer New York, pp. 842–862.

Steinberger, B. et al., 2006. Movement of magnetic bacteria in time-varying magnetic fields. *Journal of Fluid Mechanics*, 273(-1), p.189.

Szurmant, H. & Ordal, G.W., 2004. Diversity in Chemotaxis Mechanisms among the Bacteria and Archaea. *Society*, 68(2), pp.301–319.

Taherkhani, S. et al., 2014. Covalent Binding of Nanoliposomes to the Surface of Magnetotactic Bacteria for the Synthesis of Self Propelled Therapeutic Agents. *ACS nano*, (5), pp.5049–5060.

Takahashi, Y. & Ito, M., 2014. Mutational analysis of charged residues in the cytoplasmic loops of MotA and MotP in the Bacillus subtilis flagellar motor. *Journal of Biochemistry*, 156(4), p.mvu030.

Thar, R. & Fenchel, T., 2005. Survey of motile microaerophilic bacterial morphotypes in the oxygen gradient above a marine sulfidic sediment. *Applied and environmental microbiology*, 71(7), pp.3682–91.

Toutain, C.M., Zegans, M.E. & O'Toole, G. a., 2005. Evidence for two flagellar stators and their role in the motility of Pseudomonas aeruginosa. *Journal of Bacteriology*, 187(2), pp.771–777.

Turner, L., Ryu, W.S. & Berg, H.C., 2000. Real-Time Imaging of Fluorescent Flagellar Filaments. *Journal of Bacteriology*, 182(10), pp.2793–2801.

Uebe, R. et al., 2010. Deletion of a fur-like gene affects iron homeostasis and magnetosome formation in Magnetospirillum gryphiswaldense. *Journal of bacteriology*, 192(16), pp.4192–204.

Ullrich, S. & Schüler, D., 2010. Cre-lox-based method for generation of large deletions within the genomic magnetosome island of Magnetospirillum gryphiswaldense. *Applied and environmental microbiology*, 76(8), pp.2439–44.

Vladimirov, N. & Sourjik, V., 2009. Chemotaxis: how bacteria use memory. *Biological chemistry*, 390(11), pp.1097–104.

Wadhams, G.H. & Armitage, J.P., 2004. Making sense of it all: bacterial chemotaxis. *Nature reviews. Molecular cell biology*, 5(12), pp.1024–37.

Wisniewski-Dyé, F. et al., 2011. Azospirillum genomes reveal transition of bacteria from aquatic to terrestrial environments. *PLoS genetics*, 7(12), p.e1002430.

Wuichet, K., Alexander, R.P. & Zhulin, I.B., 2007. Comparative genomic and protein sequence analyses of a complex system controlling bacterial chemotaxis. *Methods in enzymology*, 422(06), pp.1–31.

Wuichet, K. & Zhulin, I.B., 2010. Origins and diversification of a complex signal transduction system in prokaryotes. *Science signaling*, 3(128), p.ra50.

Xie, L. et al., 2011. Bacterial flagellum as a propeller and as a rudder for efficient chemotaxis. *Proceedings of the National Academy of Sciences of the United States of America*, 108(6), pp.2246–51.

Xie, Z. et al., 2010. PAS domain containing chemoreceptor couples dynamic changes in metabolism with chemotaxis. *Proceedings of the National Academy of Sciences of the United States of America*, 107(5), pp.2235–40.

Yuan, J., Fahrner, K. A. & Berg, H.C., 2009. Switching of the Bacterial Flagellar Motor Near Zero Load. *Journal of Molecular Biology*, 390(3), pp.394–400.

Zhang, W.-J. et al., 2010. Configuration of redox gradient determines magnetotactic polarity of the marine bacteria MO-1. *Environmental Microbiology Reports*, 2(5), pp.646–650.

Zhu, K. et al., 2010. Isolation and characterization of a marine magnetotactic spirillum axenic culture QH-2 from an intertidal zone of the China Sea. *Research in microbiology*, 161(4), pp.276–83.

Zhu, X. et al., 2014. Angle sensing in magnetotaxis of Magnetospirillum magneticum AMB-1. *Integrative biology : quantitative biosciences from nano to macro*, 6(7), pp.706–13.

Zhulin, I.B. et al., 1996. Oxygen taxis and proton motive force in Azospirillum brasilense. *Journal of bacteriology*, 178(17), pp.5199–204.

Zhulin, I.B. & Armitage, J.P., 1993. Motility, chemokinesis, and methylation-independent chemotaxis in Azospirillum brasilense. *Journal of bacteriology*, 175(4), pp.952–8.

Danksagung

Ich möchte zunächst Prof. Schüler dafür danken, dass er mich für die Magnetotaxis begeistert und mir dieses extrem spannende, wie auch anspruchsvolle Thema anvertraut hat. Vielen Dank für die nötigen Freiräume, den Glauben an den Erfolg meines Projekts und die freundliche Betreuung.

Prof. Jung danke ich für das mir und meiner Arbeit entgegengebrachte Interesse und für die Anfertigung des Zweitgutachtens.

Prof. Armitage möchte ich für die fruchtbare Zusammenarbeit und die freundliche Aufnahme in ihrem Labor in Oxford danken. Prof. Petersen und den anderen Geophysikern gebührt Dank für die gute Kooperation beim Aufbau des Magnetodroms und Prof. Denis Bartolo für die Hilfe mit den mikrofluidischen Assays.

Prof. Mascher und Prof. Parniske danke ich für ihre Bereitschaft sich im Rahmen meines „Thesis Advisory Committee“ zu engagieren

Meine Büronachbarn Emanuel, René und Yingjie haben für eine unvergleichlich gute Arbeitsatmosphäre im Büro gesorgt, die auch immer wieder Raum für persönliches Kennenlernen ließ. Meinen Bachelorstudenten Julia und Chris danke ich für ihre große Motivation und ihren unermüdlichen Einsatz am Magnetotaxis-Projekt mitzuwirken

Dem ganzen Magnetolab und allen vergangenen Mitarbeitern möchte ich für das gute Arbeitsklima im Labor danken, und das unvergessliche Gesamterlebnis, dass mir diese Doktorarbeit beschert hat.

Sarah danke ich dafür, dass sie sich von uns hat adoptieren lassen und eine so gute Arbeitskollegin, verlässliche Kletterpartnerin und liebevolle Patentante unserer Kinder ist.

Meinen Eltern und meiner Familie danke ich dafür, dass sie mich immer in allem, was ich mir vorgenommen habe, unterstützt haben.

Meine eigene kleine Familie ist das Beste, was mir während der Doktorarbeit passieren konnte. Danke an Vitus und Clara, dass sie immer wussten, wo mein Lächeln zu finden war, wenn es im professionellen Leben einmal nicht so rund lief. Besonders danke ich meiner Frau Claudia für ihr Verständnis und ihre unermüdliche Unterstützung, und dafür, dass sie bis zum Schluss nie die Geduld mit mir verloren hat.

Eidesstattliche Erklärung

Ich erkläre hiermit an Eides statt, dass die vorgelegte Dissertation von mir selbständig und ohne unerlaubte Hilfe angefertigt ist. Des Weiteren erkläre ich, dass ich nicht anderweitig ohne Erfolg versucht habe, eine Dissertation einzureichen oder mich der Doktorprüfung zu unterziehen. Die vorliegende Dissertation liegt weder ganz, noch in wesentlichen Teilen einer anderen Prüfungskommission vor.

Felix Popp, München